ABSTRACT

Title of dissertation: NEW INSIGHTS FROM LARGE N_c QCD

Vojtech Krejcirik, Doctor of Philosophy, 2013

Dissertation directed by: Professor Thomas D. Cohen
Department of Physics

In this dissertation, three problems—one in meson physics, one in baryon physics, and one in nuclear physics—are analyzed in the large N_c limit of quantum chromodynamics. It is shown that a Hagedorn spectrum emerges naturally for mesons, i.e. that the number of mesons grows exponentially with mass; a new relation for the electromagnetic form factors of nucleon is derived in the combined large N_c and chiral limit of QCD; N_c scaling of the nucleon-nucleon scattering S-matrix is deduced as well as an exact formula for the nucleon-nucleon cross section in the leading order in $1/N_c$ expansion is derived.

NEW INSIGHTS FROM LARGE N_c QCD

by

Vojtech Krejcirik

Dissertation submitted to the Faculty of the Graduate School of the
University of Maryland, College Park in partial fulfillment
of the requirements for the degree of
Doctor of Philosophy
2013

Advisory Committee:
Professor Thomas D. Cohen, Chair/Advisor
Professor Paulo Bedaque
Professor Oscar W. Greenberg
Professor Carter Hall
Professor Alice Mignerey

Acknowledgments

I would like to express gratitude to my supervisor Tom Cohen for his guidance, patience and hours of valuable discussions. I also thank all other members of our group for plenty of advices and friendly atmosphere they create.

I am also very grateful to my parents and my wife Anička for their endless love and encouragement. I would never have accomplished anything without them.

This work was supported by DOE and the JSA/Jefferson Lab Fellowship.

Table of Contents

List of Figures

Chapter 1: Introduction

In the standard model of elementary particles, strong interactions are described by quantum chromodynamics (QCD). QCD is a gauge theory of quarks and gluons based on the $SU(N_c = 3)$ color group. Quantum chromodynamics is widely accepted as the theory that correctly captures the physics of strong interactions.

At high energies, where QCD can be treated perturbatively, predictions obtained from this theory agree very well with experimental data. In contrast to the high-energy regime, insight to low-energy phenomena is complicated by the fact that QCD at low energies is strongly coupled. Thus, the conventional perturbative expansion in powers of a coupling constant—i.e. around the non-interacting theory—is not applicable. In a way, this complication is not surprising since QCD must encode phenomena ranging from a parton distribution function in a single proton to energy levels in large nuclei.

A useful approach to bypass the issue of strong coupling is to construct an alternative expansion scheme. A plausible one is an expansion in the powers of $1/N_c$ around the limit of $N_c \to \infty$. This approach was suggested almost 40 years ago by Gerard 't Hooft [1], who pointed out that the number of colors, N_c, may serve as a parameter of QCD. Large N_c methods, which were originally applied to meson

physics, were later extended to the baryon sector by Edward Witten [2]. The reason why the large N_c limit is attractive is the following: in the limiting case of infinite number of colors, many aspects of QCD simplify substantially. Moreover, one can formally establish the expansion in powers of $1/N_c$ around the $N_c \to \infty$ world and thus include corrections systematically—similarly to the way the conventional perturbative expansion in powers of a coupling constant incorporates corrections to the non-interacting world. Naturally, one might worry whether the expansion parameter $1/N_c = 1/3$ is small enough to establish a phenomenologically reasonable expansion; yet, it is widely believed that many of the qualitative and sometimes semi-quantitative features of real-world QCD are well captured in the $1/N_c$ expansion scheme.

There are certain assumptions one must make in order for the large N_c approach to be of any phenomenological relevance. The most important assumption is that there is no phase transition between the physics at $N_c = 3$ and at $N_c = \infty$. Specifically, that QCD remains confined and that the chiral symmetry remains spontaneously broken.

In the remainder of Chapter 1, a general introduction to the physics in the large N_c world is presented. Particular attention is paid to the aspects of large N_c dynamics that have direct connection to problems discussed in this dissertation. In Chapters 2, 3, and 4, which compose the bulk of the dissertation, three different aspects of QCD are discussed from the point of view of large N_c dynamics—one from meson physics, one from baryon physics, and one from nuclear physics.

In Chapter 2, the existence of a Hagedorn spectrum for mesons—i.e. the

question whether the density of meson states grows exponentially with mass—is discussed. An argument is proposed that mesons must have a Hagedorn spectrum in the large N_c limit. The approach is based on the study of Euclidean-space correlation functions for composite operators constructed from quarks and gluons. The argument, however, relies on one critical assumption: that perturbation theory accurately describes the trace of the logarithm of a matrix of point-to-point correlation functions in the regime where the perturbative corrections to the asymptotically free values are small. On the other hand, no mention of string dynamics or broken center symmetry defining confinement is made. The fact that only very general assumptions about quantum chromodynamics at large N_c are required makes the argument of Chapter 2 particularly appealing.

In Chapter 3, a new relation for the electromagnetic form factors of nucleon is discussed. It holds for the long distance part of the Fourier transform of the electromagnetic form factors in the combined large N_c and chiral limit. The relation, which was previously derived in the Skyrme model, is shown to be truly model independent by calculating it directly in the large N_c variant of chiral perturbation theory.

In Chapter 4, the implications of the large N_c limit to the problem of nucleon-nucleon scattering are analyzed. It is found that the key quantity on which one should focus and which has a well-defined N_c scaling is the logarithm of the elastic S-matrix element—i.e. the phase shift. Several arguments are given for this scaling to hold not only for the real part but also for the imaginary part of the phase shift. Additionally, exact relations for the total cross section and for the inelastic cross

section are derived directly from the scaling of the S-matrix elements. An interesting result that determines the inelastic cross section to be exactly 1/8 of the total cross section in the $N_c \to \infty$ world emerges.

1.1 General aspects of large N_c limit of QCD

In this section, some general aspects of large N_c limit are discussed. The subject of large N_c QCD is very wide and presenting a complete description of the field is beyond the scope of this dissertation. Rather, only a few key aspects of large N_c dynamics that are essential for the problems analyzed in this dissertation are discussed in detail.

A crucial aspect in the large N_c analysis is counting. To be more formal, combinatoric properties of various Feynman diagrams distinguish contributions which are dominant and which are subleading. In this section, we closely follow the Witten's description [2] of 't Hooft's original idea [1].

The starting point of the discussion is the QCD Lagrangian:

$$\mathcal{L} = -\frac{1}{4} \operatorname{Tr} F_{\mu\nu} F^{\mu\nu} + \sum_{f=1}^{n_f} \bar{q}_f \left(i \not{D} - m_f \right) q_f \ . \tag{1.1}$$

In order to see how the $N_c \to \infty$ limit affects quantum chromodynamics, it is crucial to understand the group structure of individual objects.

With respect to the color group $SU(N_c)$, quarks and antiquarks are in the fundamental and antifundamental representation, respectively (recall that other variants of large N_c extensions with quarks in various representations of $SU(N_c)$ have been developed [3]; however, the analysis here is restricted to the most straightfor-

ward case of the fundamental representation). The dimension of both fundamental and antifundamental representations of $SU(N_c)$ is equal to N_c. Thus, one can say that there are N_c different quarks (and antiquarks) that one must consider when counting factors in Feynman diagrams. On the other hand, gluons are in the adjoint representation. The dimension of the adjoint representation of $SU(N_c)$ is equal to $N_c^2 - 1$. In the limit $N_c \to \infty$, one can neglect the 1 in the size of the dimension compared to N_c^2; essentially, there are N_c^2 different gluonic degrees of freedom—N_c times more than quark degrees of freedom.

In order to deduce the combinatoric factors for individual diagrams, it is necessary to understand the number of possibilities for color flow. For this purpose (and this purpose only), 't Hooft established a double-line notation for gluon fields. The quark field q^i has one upper index (from the color group viewpoint), which runs from 1 to N_c. The quark is represented by a line with the arrow pointing forward—as it is standard for fermion fields. Similarly, antiquark has one lower index $\bar{q}_j$ and is represented by a line with the arrow pointing backward. Gluons are conceptually different since they are in the adjoint representation of the color group—they have two color indices, one upper and one lower A^i_j, each running from 1 to N_c (recall that the diagonal element is neglected since its effect is suppressed when $N_c \to \infty$). Thus, from the color flow point of view, gluons are equivalent to a pair of quark (upper index i) and anti-quark (lower index j). The graphic representation of this statement is shown in Fig. 1.1.

Begin the analysis by looking at one of the simplest possible diagrams—a gluon self-energy. The diagram is shown in Fig. 1.2 both in the standard notation

Figure 1.1: At large N_c, gluons can be represented as a quark-antiquark pair—the so called double-line notation.

and in the double-line notation. From the color-flow point of view, the colors of incoming and outgoing gluon are given; in addition to that, there is a closed color line in the center of the loop that is contracted only with itself. The color running in this loop is not constrained and can be any of the N_c possibilities. From this, the combinatoric factor associated with diagrams in Fig. 1.2 is equal to N_c. At first sight, it is problematic; in order to have a well defined theory, the large N_c limit of the gluon self-energy correction should be smooth—or, in other words, of the same order in the N_c counting as the gluon propagator itself. Fortunately, there is a way to correct this undesired behavior. One can—and must—assign a specific N_c scaling also to the coupling constant of the three-gluon vertex. It is easy to see that in order to get a smooth large N_c limit, the coupling constant must be proportional to $1/\sqrt{N_c}$:

$$g \sim \frac{1}{\sqrt{N_c}}\,. \tag{1.2}$$

The large N_c limit with this scaling of the coupling constant is called the 't Hooft limit. It is easy to see from the analogous analysis of quark self-energy that the quark-quark-gluon coupling must obey the same large N_c scaling rule (1.2). It is natural since both the three-gluon and quark-quark-gluon couplings can be traced back to the gauge coupling, g, in the QCD Lagrangian (1.1), for which the relation

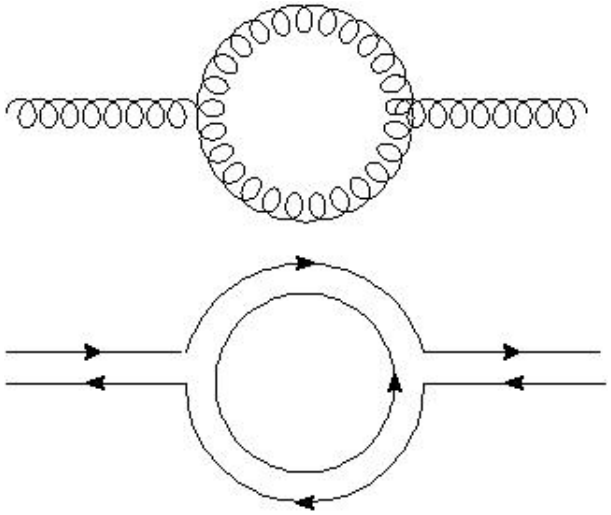

Figure 1.2: Feynman diagrams representing a first correction to the gluon propagator—i.e. the self-energy—in the standard (upper diagram) and in the double-line (lower diagram) notation.

(1.2) actually holds.

Knowing the N_c scaling of the coupling constant, one can immediately understand two important features that make the large N_c limit particularly attractive—the dominance of planar diagrams and the suppression of quark loops. In order to simplify the discussion in Sect. 1.2, it is useful to show these general features for one particular class of diagrams—a closed quark loop with a mesh of gluons inside. This class of diagrams plays a crucial role in the physics of mesons, as will be discussed more extensively later.

Naturally, a closed quark loop carries a combinatoric factor N_c by itself. First, look at the one-gluon correction to the simple quark loop, which is shown in Fig. 1.3. One immediately sees that there are two closed color loops yielding an overall factor

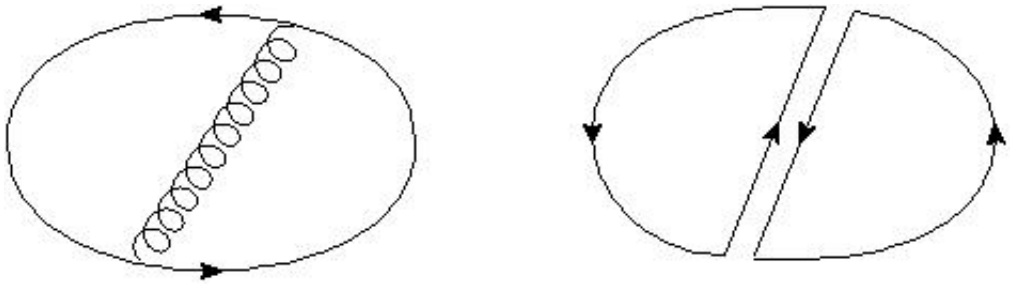

Figure 1.3: Closed quark loop with an intermediate gluon as an example of diagram whose combinatoric factor is equal to N_c.

N_c^2. In addition to this combinatoric factor, there are also two quark-quark-gluon vertices in the diagram. Each of these vertices carry an additional factor of $1/\sqrt{N_c}$. Together, they yield $N_c^2\,(1/\sqrt{N_c})^2 = N_c$. Thus, one-gluon correction diagram is of the same order in N_c as the original quark loop. It is easy to show that this behavior holds generically. Each addition of an internal gluon line adds one color loop and two vertices; powers of N_c coming from each of these two effects cancel exactly.

There is a caveat, however: the general statement presented above—that the addition of any number of internal gluon lines plays no role in the overall N_c scaling—holds only for the class of diagrams that are planar. To see the difference between planar and non-planar diagrams, look more closely at two diagrams in Fig. 1.4. Note, one is planar and the other one is not. The key difference is that in the upper diagram, gluon lines are connected in the center—i.e. there is an interaction vertex—whereas in the lower diagram they are not. The analysis of color flow in the planar case shows that there are four closed color loops and six factors of the coupling constant (since the four-gluon vertex scales as g^2). Putting the powers of

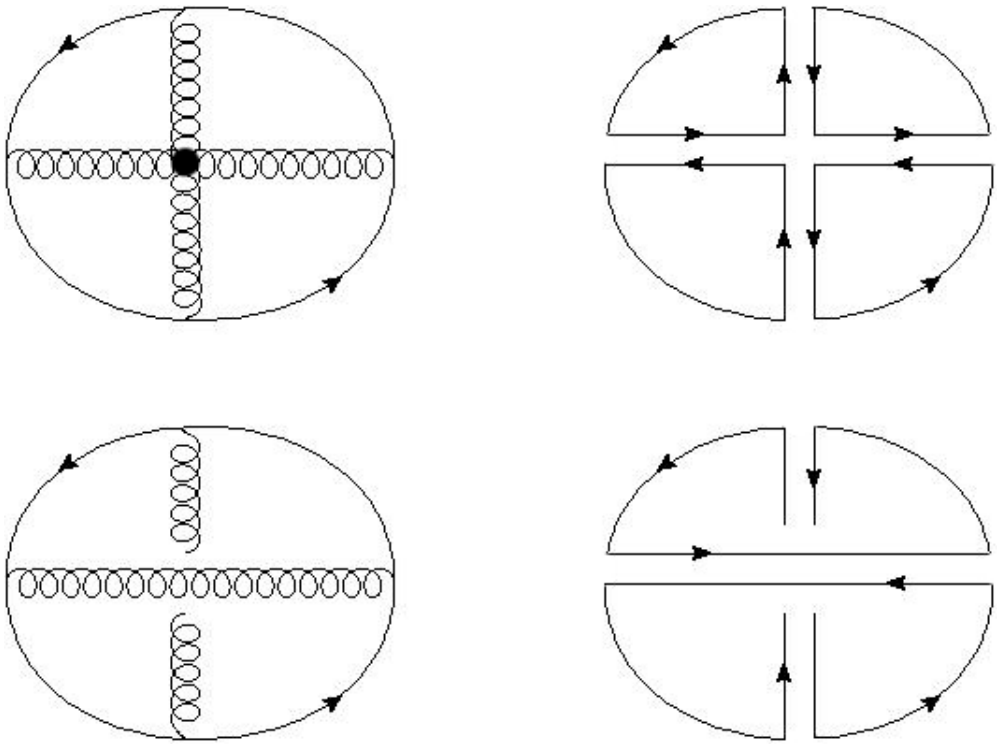

Figure 1.4: Comparison between planar diagrams (upper diagram, gluons couple in the center of the loop) and non-planar diagrams (lower diagram, gluons do not couple in the center).

N_c together, the planar diagram in Fig. 1.4 yields $N_c^4\,(1/\sqrt{N_c})^6 = N_c$ as anticipated. On the other hand, the non-planar diagram consists of one very tangled color loop. Doing the N_c counting, the non-planar diagram yields $N_c\,(1/\sqrt{N_c})^4 = 1/N_c$. One immediately sees that the non-planar diagram is suppressed by two powers of N_c compared to similar diagrams with a planar topology. It turns out that this is a general feature that holds for all types of diagrams at large N_c.

The second important feature of the large N_c limit is that diagrams with quark loops are suppressed. This is a straightforward consequence of the fact that there

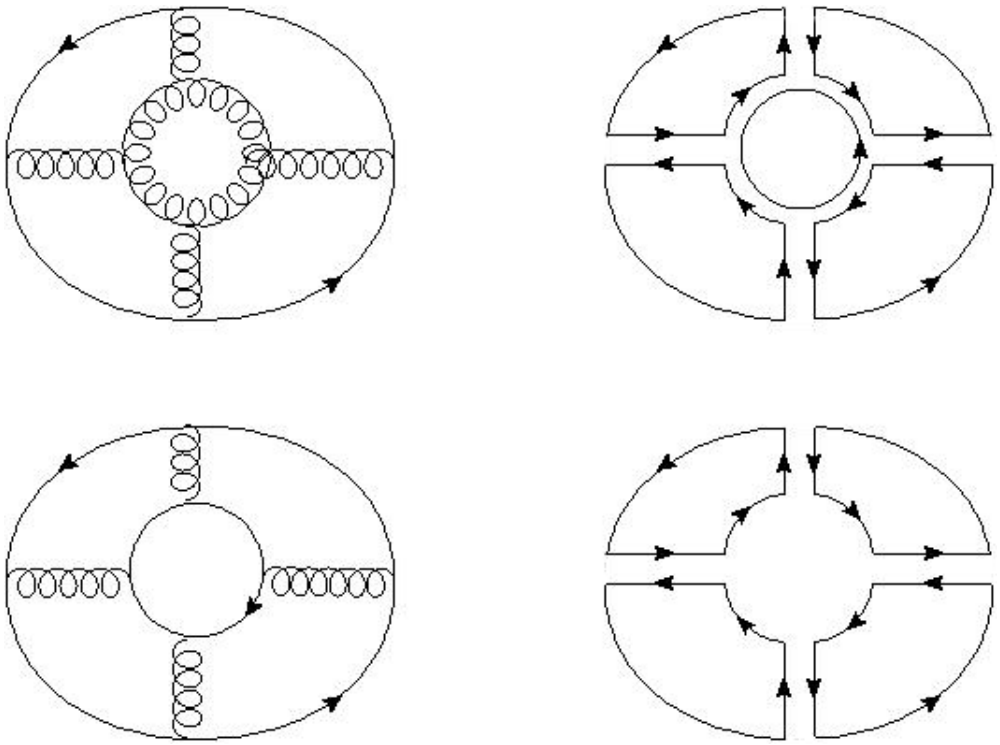

Figure 1.5: Comparison between diagrams with quark loop (upper diagram) and diagram with gluon loop (lower diagram).

are N_c different quarks but N_c^2 different gluons that can circulate in the loop. Two similar diagrams are shown in Fig. 1.5. One contains a quark loop whereas the other one contains a gluon loop. The extra color loop that is apparent in the center of the upper right diagram corresponds to an additional combinatoric factor N_c. It is this factor that explains why diagrams with gluon loops are enhanced in comparison to corresponding diagrams with quark loops instead.

In the following sections, the basic rules derived above are used to discuss some of the implications of the large N_c limit for meson, baryon, and nuclear physics.

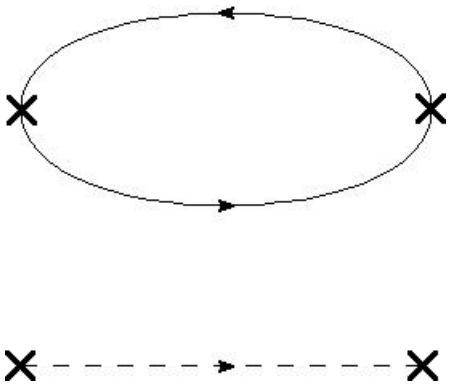

Figure 1.6: Relation between closed quark loop and a meson propagator.

1.2 Mesons at large N_c

In this section, some of the basic properties of mesons in the light of the large N_c limit of QCD are reviewed. According to a conventional wisdom at $N_c = 3$, mesons are hadrons with quantum numbers of a quark and an antiquark. The confining nature of QCD manifests itself in the fact that all physical states must be color singlets. Naively, for mesons, this is achieved when the quark and the antiquark carry the same color index (if quark color is c, antiquark color must be $\bar{c}$). A crucial assumption when extending the QCD analysis to the $N_c \to \infty$ world is that the theory remains confined—i.e. that physically observable states must be color singlets.

Mesons can be created and annihilated by quark bilinear currents—for example $\bar{q}q$ for scalar mesons, or $\bar{q}\gamma_5 q$ for pseudoscalar mesons, etc. Generically, these are denoted by $J(k)$ (for meson currents). One can show that, at large N_c, quark bilinear currents create only single-meson states (as opposed to multi-meson states).

Formally, this is equivalent to a statement:

$$\left\langle J^{\dagger}(-k)J(k)\right\rangle = \sum_{n} \frac{{a_n}^2}{k^2 - {m_n}^2} \ , \tag{1.3}$$

where m_n is the mass of the respective meson and a_n is the amplitude that the current $J(k)$ creates the respective meson $\langle 0|J|n\rangle = a_n$. Generally, the state of quark and antiquark can be diagrammatically represented as a closed quark loop. From this point view, one can identify the single quark loop and a meson propagator—the leading term in the QCD expansion (with no gluons in the loop) is shown in Fig. 1.6. Diagrams of this type (at the quark level) were introduced in the previous section. It was shown that combinatoric factor related to a closed quark loop is N_c; moreover, it was shown that diagrams with any number of gluons inside the quark loop (see Figs. 1.3, 1.4) are of the same order provided that they are of a planar topology. From the point of view of Eq. (1.3), it is crucial to show that all possible diagrams correspond to a single-meson state—i.e. they represent a color singlet regardless of how many gluons are inside the quark loop.

A typical planar diagram with many gluons is shown in Fig. 1.7. If this diagram were to be cut in any way (with the only constraint to cut both quark and antiquark just once) one immediately sees that the only color-singlet combination that one can create must contain all the gluons as well as both quarks on the boundaries. Indeed, the color index of a quark is contracted with the anti-color index of the nearest gluon, the color index of this gluon is contracted with the anti-color index of the next gluon until the lowest antiquark is reached. Generally, the

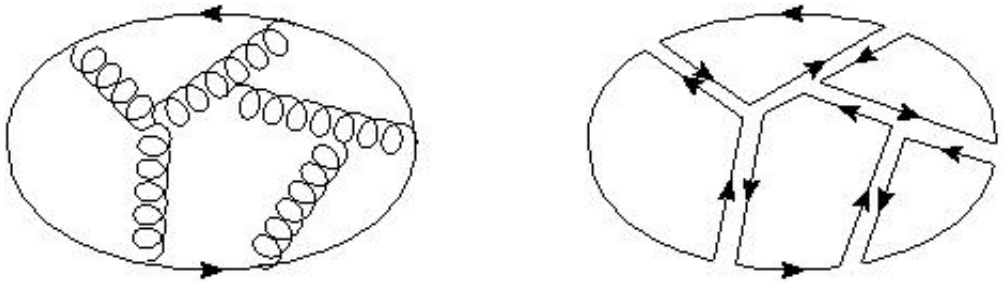

Figure 1.7: Color structure of a typical high order diagram with closed quark loop.

color structure of any cut in diagrams like the one in Fig. 1.7 is of the form:

$$\bar{q}_i \, A^i_j \, A^j_k \ldots A^l_m \, q^m \ . \tag{1.4}$$

It is easy to see that no subset in Eq. (1.4) can be a color singlet; all particles must be included in order to achieve a color singlet combination. Therefore, no other physical particle such as a glueball or an extra meson can be created in this process; all possible states created by quark bilinear currents $J(k)$ are single meson states.

Now, return to the current-current correlation function defined in Eq. (1.3) and diagrammatically represented in Fig. 1.6. The current insertions are represented by crosses on the left and on the right side of the diagrams. Looking at the N_c scaling properties, the combinatoric factor related to a closed quark loop is equal to N_c. Thus, in order to be consistent with N_c scaling, the matrix element a_n must be proportional to $\sqrt{N_c}$. It is an important feature of meson dynamics at large N_c; from this relation, the large N_c behavior of all possible n-meson coupling constants can be derived.

The next simplest example beyond the free propagation is the three-meson vertex. Schematic diagrams are shown in Fig. 1.8. Again, the combinatoric factor

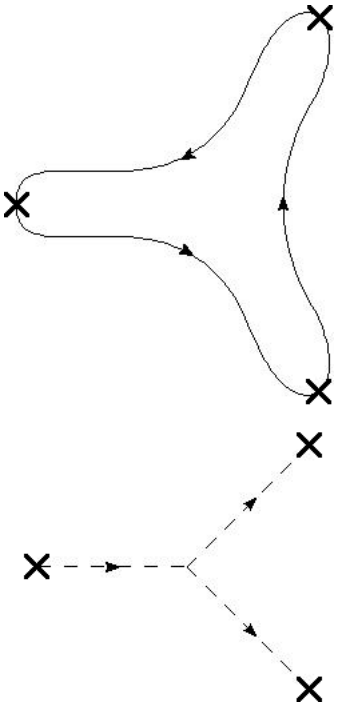

Figure 1.8: The derivation of scaling of three-meson vertex

coming from the quark loop is equal to N_c and so should be the counting in the meson sector. Recall that the inclusion of any number of gluons inside the quark loop does not alter the counting. There are three meson currents each carrying a factor of $\sqrt{N_c}$—together they yield $N_c^{3/2}$. In order to have a consistent N_c scaling, the three-meson vertex must be also N_c-dependent; specifically, it must go as $1/\sqrt{N_c}$. Following this line of argumentation, one can derive a general formula for the N_c scaling of any n-meson vertex:

$$\Gamma_{n-meson} \sim \frac{1}{N^{(n-2)/2}} \,. \tag{1.5}$$

From Eq. (1.5), one immediately sees that mesons are stable and non-interacting in the large N_c limit. Specifically, the amplitude for a meson to decay is given by diagrams containing three-meson vertices at tree level. The coupling constant for such

vertexes is proportional to $1/\sqrt{N_c}$ and therefore vanishes as $N_c \to \infty$. Similarly, the tree contribution to meson-meson scattering contains either one four-meson vertex or two three-meson vertices. In either cases, the scattering amplitude scales as $1/N_c$ and becomes negligible as $N_c \to \infty$.

1.3 Baryons at large N_c

In the previous section, the physics of mesons was discussed in the light of the large N_c limit. For mesons, the color-singlet nature is achieved by combining a quark with an antiquark. In the quark-antiquark sector, the structure of Feynman diagrams is the same for all $SU(N_c)$ groups, and the crucial thing for the N_c counting is to determine the combinatoric factor associated with each diagram. The nature of baryons, on the other hand, is conceptually different. Baryons originate in a fully antisymmetric color singlet representation of the respective gauge group, in our case $SU(N_c)$. From this, one immediately sees that the single baryon contains N_c quarks. When drawing Feynman diagrams, not only combinatoric factors play a role, but also diagrams themselves depend on the specific group; baryon correlators contain N_c quark lines (an illustration of a free baryon is shown in Fig. 1.9).

As was discussed by Witten [2], Feynman diagrams may not be a very useful framework to study the N_c properties of baryons. To see this, look at the one-gluon and two-gluon corrections to the free propagation of a baryon. They are shown in Fig. 1.10. The quark-quark-gluon coupling is of order $1/\sqrt{N_c}$. Thus, there is a factor $1/N_c$ coming from coupling constants contributing to the one-gluon exchange

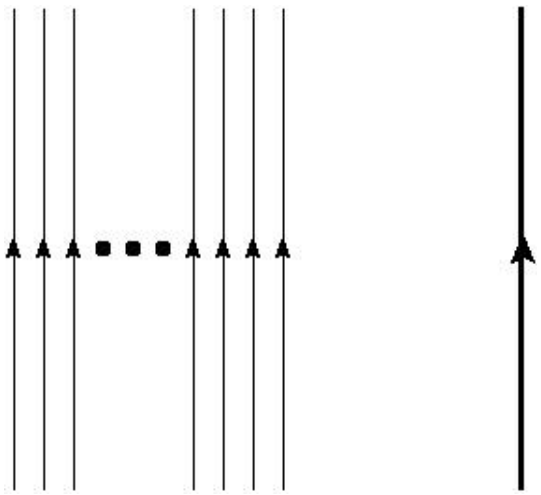

Figure 1.9: Schematic picture of a free baryon propagator consisting of N_c quarks.

correction to the free baryon propagator. However, there is more to the whole diagram; gluons can be exchanged between any two quarks in the baryon. There are $N_c(N_c-1)/2$ possible quark pairs in the baryon, which for large N_c effectively means a factor of N_c^2. Overall, the one-gluon exchange diagram is of order N_c and naively diverges in the large N_c limit. The situation is even more severe if one looks at a two-gluon exchange diagram. In this case, there are four coupling constants each bringing a factor $1/\sqrt{N_c}$, but there are N_c^4 ways how to choose four quark lines. Combined, the divergence of the two-gluon correction is of order N_c^2, more severe than of the previous one-gluon correction.

In order to see from where this undesirable behavior arises, it is helpful to study a simple observable first—the mass of the baryon. Mass of the baryon consists of contributions from masses of quarks, kinetic energies of quarks, and potential energies between quarks. Since there are N_c quarks in the baryon, the contribution of quark masses is simply $(N_c \times M_q)$, similarly, the effect of quark kinetic energies

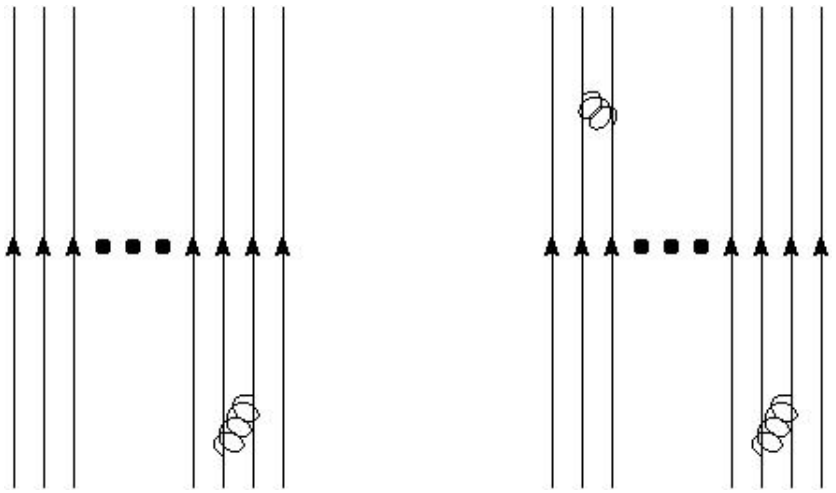

Figure 1.10: One-gluon (left) and two-gluon (right) corrections to the free propagation of baryon consisting of N_c quarks.

is $(N_c \times T_q)$ since the kinetic energy is also a single particle operator. The question of potential energy is more subtle. If the discussion is restricted only to two-body interactions, the potential between two quarks is of order $1/N_c$ (two quark-quark-gluon vertices are involved, carrying a factor $1/\sqrt{N_c}$ each); denote the two-body potential $(1/N_c \times V_{qq})$. On the other hand, that there are N_c^2 distinct pairs of quarks. Together, it yields:

$$M_B = N_c\, M_q + N_c\, T_q + \frac{1}{2} N_c^2 \left(\frac{1}{N_c} V_{qq}\right) = N_c \left(M_q + T_q + \frac{1}{2} V_{qq}\right) \ . \tag{1.6}$$

One sees that the mass of the baryon itself is of order N_c, since the N_c dependence factorizes equally from all contributing terms. It is a very important result with far reaching consequences. For example, one immediately sees why a naive perturbative expansion suggested above (i.e. drawing Feynman diagrams) leads to divergent results. The time evolution of a free baryon (i.e. the propagator) is proportional

to $e^{-iM_b t}$. If, for concreteness, one assumes that the specific form of the mass is $M_B = N_c M(1+g^2)$, where g^2 represents corrections due to the interaction, the exponential can be expanded as:

$$e^{-iM_b t} = e^{-iN_c M(1+g^2)t} = e^{-iN_c Mt}\left(1 - iN_c Mg^2 t - \frac{1}{2}N_c^2 M^2 g^4 t^2 \dots\right) . \qquad (1.7)$$

The two terms in the parentheses correspond to the two diagrams in Fig. 1.10. It is obvious that the higher order terms in the perturbative expansion are associated with higher powers of N_c.

Nevertheless, one can get some insight into the meson-baryon scattering at large N_c when doing the diagramatics carefully. The simplest diagram is shown in Fig. 1.11. As usual, there is a factor $1/N_c$ coming from the gluon exchange; however, there are N_c different quarks in the baryon that can participate in the exchange process. Therefore, the amplitude is proportional to $N_c^0 \sim 1$. Note that this result is natural. The meson mass is of order one and therefore the strength necessary to change its motion must be also of order one. Additionally, since the baryon is parametrically heavier it is not affected by the scattering with meson and can be treated as fully static.

The fact that the amplitude is independent of N_c is interesting by itself. When this observation is translated into the language of meson and baryon effective field theory, a new important feature of large N_c physics emerges—large N_c consistency relations and contracted $SU(2N_f)$ symmetry. This issue is addressed in the upcoming section.

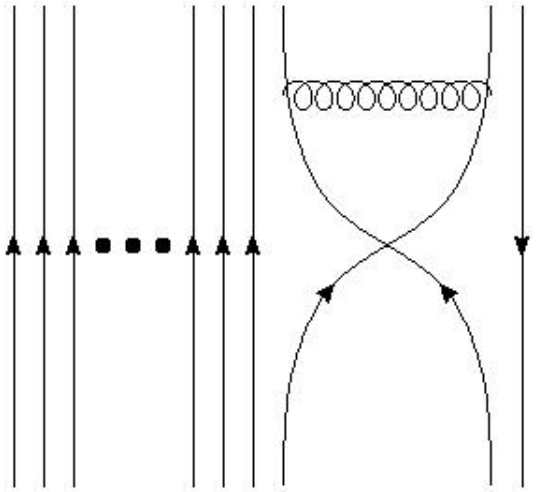

Figure 1.11: Color flow in the simple meson-baryon scattering.

1.3.1 Large N_c χPT and consistency relations

The focus of this section is on the interaction between nucleons and pions—the lightest available hadrons—in light of the large N_c limit. It was discussed in the previous section that the meson-baryon scattering amplitude must be of order one. If one assumes that the spontaneous chiral symmetry breaking pattern is preserved in the $N_c \to \infty$ world, then the coupling of pions—the Goldstone bosons of spontaneously broken chiral symmetry—to nucleons is known. The pion-nucleon-nucleon vertex is derivatively coupled and proportional to g_A/f_π. The large N_c counting rules tell us that the axial vector coupling constant g_A is proportional to N_c, and the pion decay constant f_π is proportional to $\sqrt{N_c}$. Combining these results, one obtains the pion-baryon-baryon vertex to carry the factor $\sqrt{N_c}$. From these two relations—scaling of the vertex and scaling of the amplitude—a consistency relations can be derived [4–9].

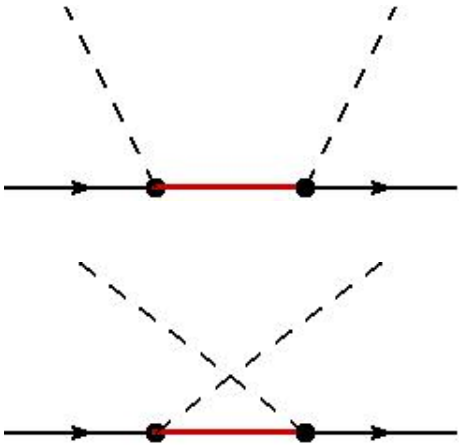

Figure 1.12: Direct and crossed diagrams contributing to the pion-nucleon scattering amplitude.

Start with the assumption that, at large N_c, QCD has a baryon state with spin $S = 1/2$ and isospin $I = 1/2$, which is called the nucleon. The mass of the nucleon is parametrically of order N_c, i.e. large, and therefore the nucleon can be treated as static. The axial-vector operator acting on the nucleon is $X_{ia} \sim \sigma_i \tau_a$. The pion-nucleon scattering is dominated by diagrams shown in Fig. 1.12. Thus, the scattering amplitude reads;

$$\mathcal{A} = i \left(\frac{g_A}{f_\pi} \right)^2 p_i \, p_j \left(\frac{\sigma_i \tau_a \ \sigma_j \tau_b}{-\omega} + \frac{\sigma_j \tau_b \ \sigma_i \tau_a}{\omega} \right) . \tag{1.8}$$

As discussed above, the coupling constants yield an overall factor of N_c. Such an amplitude clearly violates unitarity as $N_c \to \infty$; it is also in disagreement with the scaling rule for the meson-baryon scattering amplitude derived in the previous section.

In order to recapture the consistency, there must be a new baryon state that can be in the intermediate state that have a potential to cancel the leading N_c

dependence and preserve unitarity and scaling rules. In fact, the Δ resonance plays this role. Formally, one can generalize the spin-isospin operator X_{ia} to act in the extended space of all baryons and require this operator to satisfy the relation:

$$[X_{ia}\ ,\ X_{jb}] = 0. \tag{1.9}$$

Following this idea, it was derived that there must be a tower of degenerate baryons with $I = J$. The first member of this family is the nucleon with $I = J = 1/2$; the next one is the Δ with $I = J = 3/2$; and so on. In principle, one can continue to infinity, but all higher states are only artifacts of the large N_c limit since they have no counterparts in the $N_c = 3$ world.

The idea shown above can be represented in a group-theoretical language. Consider, for simplicity, the case of two flavors. Here, the original spin-flavor symmetry group is $SU(4)$ with generators:

$$J^i = J^i \otimes 1\ ,\quad I^a = 1 \otimes I^a\ ,\quad G^{ia} = J^i \otimes I^a\ . \tag{1.10}$$

The algebra of these generators is:

$$\begin{aligned}
\left[J^i\ ,\ J^j\right] &= i\epsilon_{ijk}J^k\ , \qquad \left[I^a\ ,\ I^b\right] = i\epsilon_{abc}I^c\ , \\
\left[J^i\ ,\ G^{jb}\right] &= i\epsilon_{ijk}G^{kb}\ , \quad \left[I^a\ ,\ G^{jb}\right] = i\epsilon_{abc}G^{jc}\ , \\
\left[J^i\ ,\ I^b\right] &= 0\ , \qquad \left[G^{ia}\ ,\ G^{jb}\right] = \frac{i}{4}\epsilon_{ijk}\delta_{ab}J^k + \frac{i}{4}\delta_{ij}\epsilon_{abc}I^c\ .
\end{aligned} \tag{1.11}$$

The desired algebra with vanishing commutator for spin-isospin generator is achieved by taking a limit:

$$X^{ia} \equiv \lim_{N_c\to\infty} \frac{G^{ia}}{N_c} \tag{1.12}$$

Thus, one sees that the baryon physics at large N_c is driven by a contracted $SU(4)$ (in general $SU(2N_f)$) symmetry. The specific matrices are determined by Clebsch-Gordan coefficients and their explicit representation will be shown in Chapter 3.

1.4 Nuclear physics at large N_c

Some aspects of meson and baryon physics were discussed earlier in this chapter. And actually, the large N_c limit proved to be useful in understanding many aspects of meson and baryon physics. However, its possible relevance and eventual phenomenological implications for nuclear physics are far less clear [10]. The key physical reason is that energy scales in nuclear physics are much smaller than in hadronic physics. A simple example is the binding energy of the deuteron—2.2 MeV—which is three orders of magnitude smaller than the masses of individual nucleons. However, in formal N_c counting, both nucleon mass and binding energy are of order N_c^1; i.e. they should be comparable—which is not the situation observed in nature. Currently, it is believed that the vast discrepancy between energy scales is caused by delicate cancellations which occur at $N_c = 3$ but do not hold in general. Regardless of the phenomenological (ir)relevance, it is still interesting to study nuclear phenomena in the large N_c limit. It may give insight into nuclear physics in a regime where there is no other control parameter; besides, the problem is interesting purely from a theoretical viewpoint.

The simplest problem in nuclear physics is nucleon-nucleon scattering. One might try to analyze the two baryon interaction in a way similar to meson-baryon

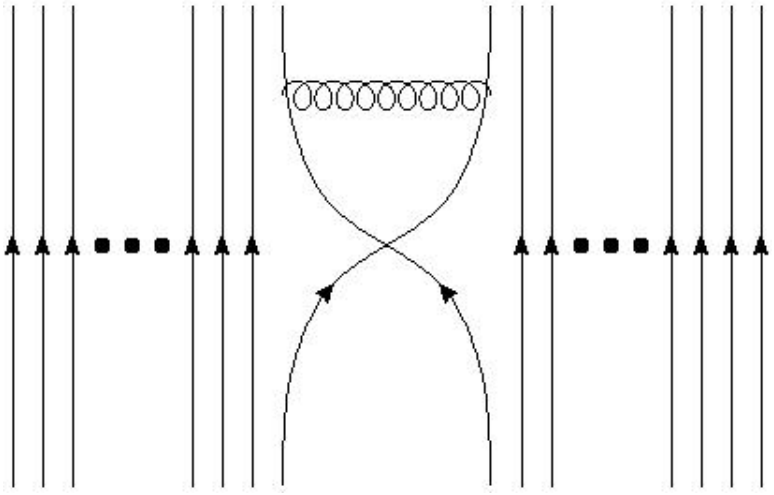

Figure 1.13: The simplest diagram contributing to the baryon-baryon scattering: the exchange of quarks with color and momentum conservation guaranteed by an additional gluon exchange.

interaction discussed in the previous section. It was shown in Sect. 1.3 that the mass of the baryon is of order N_c. From this, it is obvious that the overall one-baryon Hamiltonian must also be of order N_c to achieve self-consistency. The kinematic regime for this to be satisfied is for the fixed velocity of order N_c^0—so called Witten kinematics.

The simplest scattering process is shown in Fig. 1.13. According to the counting rules discussed above, there are N_c quarks in the first baryon and N_c quarks in the second baryon that can participate in the exchange—yielding a factor of N_c^2. Additionally, couplings coming from the gluon exchange contribute by a factor of $1/N_c$. Together, the diagram is of order N_c. Recall that the mass of the baryon itself as well as its kinetic energy is of order N_c. Thus, in order for the motion of baryon to be affected, the interaction must also be of order N_c. Combined, the Hamilto-

nian describing the physics of two baryons (in particular, the two body potential) is proportional to N_c.

Chapter 2: Hagedorn spectrum

In this chapter, the argument that mesons in large N_c QCD naturally have a Hagedorn spectrum—i.e. that the density of hadrons grows exponentially with mass of the hadron—is presented. This chapter is largely based on the analysis of Refs. [11, 12].

2.1 Motivation

One of the key tasks of particle and nuclear physics is to understand the spectrum of observed hadrons. Ideally, one should be able to predict the masses, widths, and all other relevant properties of any given hadron from the underlying theory—from quantum chromodynamics. The complete solution of this problem is beyond the scope of this dissertation; rather, this dissertation focuses on one of the aspects of hadronic spectrum, the density of meson states.

It was conjectured by Rolf Hagedorn almost 50 years ago that the density of hadrons (the concept of density will be discussed later) grew exponentially with mass for asymptotically large masses [13, 14]. Although the reasoning behind Hagedorn's original idea seems obscure from the point of view of today's physics, the idea itself played a very influential role in the development of various areas of particle

physics—ranging from QCD thermodynamics [15–17] to string theory [18]. For example in a simple model, where hadrons are treated as a noninteracting free gas, the exponential growth in the density of states implies the existence of an upper bound on the temperature of a hadronic phase. It was one of the first hints that there may exist various phases of strongly interacting matter—and as such it was an extremely influential notion. Even today, the concept of exponentially growing spectrum is involved in an analysis of ultrarelativistic heavy ion collisions in the context of resonance gas models [19, 20].

Traditionally, a Hagedorn spectrum was specified in terms of a density of hadron states as a function of mass, $\rho(m)$. However, the precise definition of density requires some type of smearing, which can be, in principle, arbitrary. The Hagedorn spectrum is the one for which the density of states asymptotes at large m to:

$$\rho_{\text{Hagedorn}}(m) = f(m) \exp\left(\frac{m}{T_H}\right) , \tag{2.1}$$

where T_H is the Hagedorn temperature; it is a parameter controlling the exponential growth; $f(m)$ is a sub-exponential prefactor. The prefactor $f(m)$ determines the thermodynamic behavior of strongly interacting matter as T_H is approached [17]; it also plays a crucial role in attempts to fit the Hagedorn spectrum from data [12, 21].

However, a more useful quantity with which one should work and which is more rigorously defined is the so-called accumulated spectrum $N(m)$ [22, 23]:

$$N(m) = \int_0^m \mathrm{d}m' \rho(m') = \sum_{i=\text{hadrons}} \theta(m - m_i) , \tag{2.2}$$

where $\theta(x)$ is a Heaviside step function. $N(m)$ represents the total number of hadrons with mass less than m. The Hagedorn conjecture can be reformulated

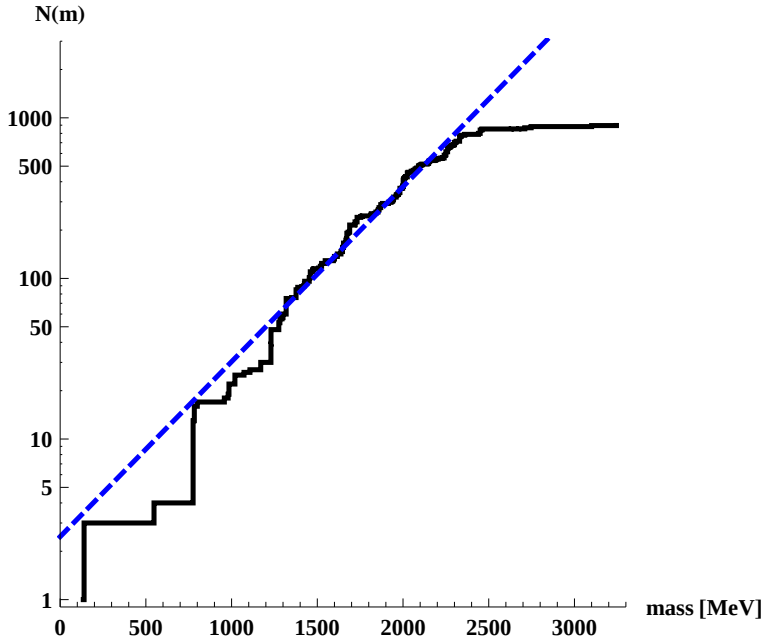

Figure 2.1: Accumulated spectrum $N(m)$ of non-strange mesons using masses of mesons reported by the Particle Data Group [24]. The fit is of the form $N(m) = ae^{m/T_H}$ and yields a Hagedorn temperature of 369 MeV [12]. The fit was done for mesons with masses up to 2.3 GeV.

using the accumulated spectrum: at large m, $N(m)$ asymptotes to:

$$N_{\text{Hagedorn}}(m) = g(m) \exp\left(\frac{m}{T_H}\right) , \tag{2.3}$$

where $g(m)$ is a new prefactor satisfying $f(m) = g'(m) + g(m)/T_h$.

The empirical spectrum of non-strange mesons is shown in Fig. 2.1. Indeed, the number of mesons does grow very rapidly up to a point around 2.3 GeV, where it sharply bends towards a constant. The apparent reason for this is that it becomes extremely difficult to extract the resonance properties from the scattering data so high in the spectrum. Although the graph appears to be consistent with the idea

that QCD has a Hagedorn spectrum (assuming the saturation at high mass is due to difficulty in extracting meson masses rather than to the non-existence of high-mass mesons), it was extensively discussed by Cohen and Krejčiřík [12] that it is not possible to convincingly establish the presence of a Hagedorn spectrum just from data. In part this is due to a practical issue; the range of known hadron masses is limited and one would need to have access to much higher masses to get compelling evidence for exponential growth. Note also that a Hagedorn spectrum is supposed to hold for asymptotically large masses—the question whether the observed data reaches an asymptotic regime cannot be answered, even in principle.

Moreover, there is an important conceptual issue underlying the practical one: highly excited hadrons are not particles but resonances. Resonances have widths and therefore their mass—the key parameter when it comes to the definition of the spectrum—is not well defined.

The mass parameters of hadronic resonances are extracted from complicated partial wave analyses of various scattering experiments. The extraction of data from scattering cross sections often includes some model dependent assumptions. The model-dependence is relatively weak for resonances that are narrow and isolated; for these, one can state their mass with some level of confidence. However, as resonances become wide or close to each other, it becomes more and more difficult to isolate a resonant state in a meaningful way and the dependence on the uncontrolled modeling grows. Sometimes, even the existence of a resonance itself is not absolutely clear. The model-dependence, which affects the very notion of the existence of a single hadron as well as its mass, makes the concept of a density of hadrons intellectually

problematic.

Before the issue of ill-defined hadron masses will be addressed, it is useful to understand why a Hagedorn spectrum is expected to emerge in QCD. From today's physics point of view, the motivation comes from the similarities between QCD and string theories. It is worth noting that, originally, the string theory was formulated to describe strong interactions. The key observation is that a Hagedorn spectrum arises automatically in simple string theories [18]. When strings are unbreakable and noninteracting, the exponentially growing spectrum appears naturally due to the effect of degeneracy. On the QCD side, there is strong evidence from lattice QCD calculations [25] that widely separated static quarks have a linearly rising potential—it is known as the area law for Wilson loops. The linearly rising potential arises from the fact that the gluon flux arranges itself into a tube connecting two quarks for widely separated sources. This flux tube has a characteristic width and energy per unit length [25]. Thus, it is plausible to expect that QCD should act stringy under certain conditions. A key condition is for the length of a respective flux tube to be much longer than its width and thus for the flux tube to resemble a string. Note that this is precisely what one expects for highly excited mesonic states. Naively, relative motion of quark and antiquark in a highly excited system means that they are further apart for a significant fraction of time; thus the fluxtube connecting them is long. If highly excited mesons can be viewed as an effective string theory, it is natural to expect them to have a Hagedorn spectrum.

However, there is a problem with this simple picture. The reasoning presented above is based on a pure gauge theory with static quark sources. In this case,

confinement directly implies that strings are unbreakable. In real QCD, however, flux tubes can break—or equivalently, mesons can decay. Note that this is merely a reformulation of the issue discussed earlier; the fact that mesons decay imply that they can only be seen as resonances with nonzero widths.

The resonant nature of states in a spectrum causes problems and it is unclear how to deal with this issue in an unambiguous way in the physical world—the fact that mesons decay is unquestionable. However, there is a clear way how to bypass this problem in theory—that is to work in the large N_c limit of QCD [1, 2]. It follows directly from the standard counting rules of the large N_c limit that meson decay amplitudes behave as $1/N_c$ as the large N_c limit is approached. Thus, mesons become stable and the flux tubes do not break. The fact that mesons are stable at large N_c was discussed more extensively in Chapter 1. In this chapter, this fact is used as a starting point allowing one to formulate the question of a Hagedorn spectrum in a more rigorous manner.

In conclusion, the concept of particle's mass is well defined in large N_c QCD and questions about spectrum of mesons are well posed—at least theoretically. Of course, one might argue about the phenomenological relevance of this analysis, since it is far from obvious how close the $N_c = 3$ world is to the $N_c \to \infty$ world. However, it is a problem with all large N_c calculations and is beyond the scope of this work.

A Hagedorn spectrum in some variant of large N_c QCD was first obtained by Kogan and Zhitnitsky [26]. Given certain assumptions, they explicitly computed the spectrum of large N_c QCD in 1+1 dimensions with fermions in adjoint representation. Ideally, the spectrum for large N_c QCD for any spatial dimension

should be calculated. However, it is not clear how to proceed directly beyond 1+1 dimensions. An alternative indirect way to demonstrate a Hagedorn spectrum in 2+1 and 3+1 dimensions is presented here. The argument relies only on standard and generally accepted properties of QCD—confinement which manifests itself in its very basic sense, that all physical states are color singlets; QCD at high momenta (or equivalently, at short distances) is asymptotically free and corrections can be accommodated using perturbation theory (as long as the perturbative expansion is valid). However, no explicit use is made of stringy dynamics for the flux tube or an unbroken center symmetry defining confinement. The fact that no stringy dynamics is explicitly needed is of great importance from the broader perspective. There is, as mentioned earlier, a strong belief that there is an equivalence between large N_c QCD and certain class of string models. Naturally, the fact that two different theories—large N_c QCD and string models—share the same features (in this case, a Hagedorn spectrum) is obviously far from being a proof of equivalence, yet it is a strong hint that there is an underlying connection between them.

The core of the argument for a Hagedorn spectrum given here is the fact that the number of independent local operators with a given set of quantum numbers grows exponentially with the mass dimension of these operators. The presented approach was published by Cohen and Krejčiřík [11]. It is similar in spirit to the ideas of Kogan and Zhitnitski [26]; it has elements which can be traced to Refs. [27–29].

2.2 Mathematical argument for a Hagedorn spectrum

In this section, the argument for the existence of a Hagedorn spectrum at large N_c is presented. First, the outline of the procedure and the main ideas behind it are discussed. The technical details are left for the remainder of the chapter.

First, recall that $N(M)$ is defined as the number of hadrons with mass less than M (2.3). It turns out that it is useful to introduce a related quantity $W(M)$ defined as a sum of the masses of particles with mass less than M:

$$W(M) = \sum_{i}^{N_M} m_i = MN(M) - \int_0^M \mathrm{d}\mu N(\mu) \ . \tag{2.4}$$

From their relation (2.4), it is clear that if one of them grows exponentially so does the other.

The argument starts with the explicit construction of a sequence of sets of local operators with fixed mass dimension (labeled by n). Sets are constructed in such a way that the number of operators in each set grows exponentially:

$$N = A^n. \tag{2.5}$$

The crucial part of the argument is to demonstrate that at sufficiently large n the following inequalities are true for all n,

$$\mathrm{A}: \quad N(an+b) \geq V \ ; \tag{2.6}$$

$$\mathrm{B}: \quad V \geq W(m_N) \ , \tag{2.7}$$

where V is the negative logarithmic derivative of the trace of a matrix of Euclidean space correlators. It is an auxiliary quantity designed to be of use in the derivation

of inequalities. a and b are constants with dimension of mass. The key feature of inequalities A (2.6) and B (2.7) is that the very left hand side is linear in n and does not grow faster.

From Eq. (2.4-2.7), it can be shown that consistency requires the number of hadrons $N(m)$ to grow exponentially with mass. To see this, assume that the number of hadrons is bounded from above $N(M) \leq \exp(\alpha M)$, i.e. it is in the form of an exponential. Taking a logarithm of Eqs. (2.6-2.7) yields:

$$a\alpha \log_A(e) M + b \geq M - \frac{1}{\alpha} \,. \tag{2.8}$$

One sees, that there is a contradiction if $M \to \infty$ unless $\alpha \geq \frac{1}{a \log_A(e)}$. Thus, α cannot be infinitesimally small and the statement that the function $N(M)$ is bound by an exponential is false. Formally:

$$N(M) \geq \exp\left(\frac{1}{a \log_A(e)} m\right) \,, \tag{2.9}$$

thus the condition defining a Hagedorn spectrum is obtained.

Alternatively—in a sense that will be formalized later in the chapter—one can set the number of operators $N = A^n$ (on the left-hand side of inequality A (2.6)) equal to the number of particles $N(m)$. Thus one gets $n = \log N(m)/\log(A)$. The inequalities in the limit of large m reads:

$$a \log N(m)/\log A \geq m \,. \tag{2.10}$$

This equation can be satisfied only if number of particles grows at least exponentially $\log N(m) \geq m \log A/a$, which is equivalent to the equation (2.9).

It is obvious that the crucial step in a pursuit of the Hagedorn spectrum is to prove the inequalities A (2.6) and B (2.7). Their derivation, which is somewhat subtle, will be presented together with all other technical details in the following subsections.

2.2.1 Local operators and current correlators

To begin, sets of composite single-color-trace color-singlet local operators are constructed. The auxiliary quantity V in Eqs. (2.6, 2.7), which lies at the core of the whole argument, is the matrix of correlators of operators in these sets.

If one assumes confinement in its most basic sense, that all particles are color singlets, it is guaranteed by the single-color-trace nature of the operators that they make only single-hadron states when acting on the vacuum state at large N_c [2]. Another property these operators must satisfy at large N_c is that the correlator between two distinct operators in the set must vanish when the distance between the operators goes to zero, i.e. they are in a sense orthogonal. For simplicity, only operators transforming as Lorentz scalars are considered; they produce spinless hadrons when acting on the vacuum. This restriction, however, does not alter the overall conclusion made about the existence of the Hagedorn spectrum; naturally, if the number of spinless hadrons grows exponentially, so does the number of all hadrons. Moreover, a simple generalization of the argument yields exponential growth for mesons of any spin.

The operators need to be different for 2+1 and 3+1 dimensions. The following

basic building blocks are used in the construction of sets of operators. In 3+1 dimensions, they are:

$$O_1 = \text{const} \cdot F_{\mu\nu}F^{\mu\nu} \ , \quad O_2 = \text{const} \cdot F_{\mu\nu}\widetilde{F}^{\mu\nu} \ , \tag{2.11}$$

and in 2+1 dimensions, they are:

$$\begin{aligned} O_1 &= \text{const} \cdot F_{\alpha\beta}F^{\alpha\beta}\, F_{\alpha'\beta'}F^{\alpha'\beta'}\, F_{\alpha''\beta''}F^{\alpha''\beta''} \ , \\ O_2 &= \text{const} \cdot \left[\epsilon^{\alpha\mu\nu}F_{\mu\nu}\, \epsilon^{\beta\mu'\nu'}F_{\mu'\nu'}\, \epsilon^{\gamma\mu''\nu''}F_{\mu''\nu''}\, \epsilon_{\alpha\beta\gamma}\right]^2 \ . \end{aligned} \tag{2.12}$$

The constants in (2.11, 2.12) do not affect any results and may be chosen arbitrarily. Note also that these operators are not traced over color. Thus, they become pure color adjoint operators in the large N_c limit. It is easy to see that operators O_1 and O_2 are linearly independent—one is a scalar (parity even) and one is a pseudoscalar (parity odd).

Individual color-singlet operators are built in the following way:

$$J_{l_1,l_2,\ldots,l_n} = \bar{q}O_{l_1}O_{l_2}\ldots O_{l_n}q \ , \tag{2.13}$$

where l_i is either 1 or 2 and n is the total number of the operators O placed between quark operators. Sets of operators having the same value of n create a sequence. The first few sets are:

$$\begin{aligned} \mathcal{S}_1 &= \{J_1, J_2\} = \{\overline{q}O_1q, \overline{q}O_2q\} \ , \\ \mathcal{S}_2 &= \{J_{11}, J_{12}, J_{21}, J_{22}\} = \{\overline{q}O_1O_1q, \overline{q}O_1O_2q, \cdots\} \ , \\ \mathcal{S}_3 &= \{J_{111}, J_{112}, J_{121}, J_{122}, J_{211}, J_{212}, \cdots\} \ , \\ &\cdots \ . \end{aligned} \tag{2.14}$$

The n^{th} element of the sequence is labeled $\mathcal{S}_n$. Eventually, the behavior as n becomes large will be discussed. The number of operators J in the nth set of the sequence is, by construction, $N = 2^n$. Additionally, all currents in a given set, $\mathcal{S}_n$, have the same (naive) mass dimension. The dimension is $4n+3$ for 3+1 dimensions and $9n+2$ for 2+1 dimensions, respectively.

Within each set in the sequence, one can define a correlator matrix between two space-time points $\mathbf{\Pi}^{(n)}$. The matrix elements read:

$$\Pi^{(n)}_{ab}(x-y) = \left\langle J^{\dagger}_a(x) J_b(y) \right\rangle \ , \tag{2.15}$$

where currents $J_{a,b} \in \mathcal{S}_n$. The dimension of a correlator matrix is equal to the number of currents in the respective set—2^n.

The following notation will be used throughout this chapter: matrix elements are written down with explicit indices, the matrices themselves are indicated by boldface ($\Pi_{ab} \leftrightarrow \mathbf{\Pi}$).

Since currents can create only single particle states (a consequence of large N_c limit and confinement) the spectral decomposition of the current is given by

$$J_a(t,\vec{x})|0\rangle = \sum_k \int \frac{\mathrm{d}^3\vec{p}}{(2\pi)^{3/2}} \ c_{ak} \ \frac{1}{\sqrt{2E_k}} \ e^{i(E_k t - \vec{p}\cdot\vec{x})} \ |k,\vec{p}\rangle \ , \tag{2.16}$$

where c_{ak} is the amplitude that the current a creates the particle k.

Using Eq. (2.16) the matrix $\mathbf{\Pi}^{(n)}$ can be rewritten (without loss of generality, take $y = 0$):

$$\Pi^{(n)}_{ab}(t,\vec{x}) = \sum_k \int \frac{\mathrm{d}^3\vec{p}}{(2\pi)^3} \ C_{ab,k} \ \Delta(t,\vec{x};m_k) \ , \tag{2.17}$$

where $C_{ab,k} = c^*_{ak}c_{bk}$ is the matrix of coefficients and $\Delta(t,\vec{x};m_k)$ is the propagator for a noninteracting scalar of mass m_k . The correlator matrix (2.17) can be viewed as

a Kallen-Lehmann spectral representation with the spectral function ρ proportional to the sum of Dirac delta functions. An analytic continuation to an imaginary time ($\tau = it$) reads (with $x = 0$):

$$\Pi_{ab}^{(n)}(\tau) = \sum_k \int \frac{\mathrm{d}^3\vec{p}}{(2\pi)^3}\, C_{ab,k}\;\; \Delta(\tau; m_k)\ . \tag{2.18}$$

In Eq. (2.18), the matrix of Euclidean correlators is defined; the negative logarithmic derivative of the trace of this matrix is a crucial element in the derivation of the Hagedorn spectrum.

2.2.2 Inequality B

In this section, Eq. (2.7)—inequality B—is derived. It is one of two crucial inequalities which are necessary to demonstrate a Hagedorn spectrum.

$$-\frac{d}{d\tau}\mathrm{Tr}\log\mathbf{\Pi} \geq W(m_{2^n})\ .$$

Recall that an equation similar to Eq. (2.7) is widely used in the context of lattice QCD. There, current-current correlation functions in Euclidean space are used to extract the hadronic states in a given channel [25]. Specifically:

$$\begin{aligned} \lim_{\tau\to\infty} -\frac{\mathrm{d}}{\mathrm{d}\tau}\log\langle J(\tau)J(0)\rangle &= m_0\ , \\ -\frac{\mathrm{d}}{\mathrm{d}\tau}\log\langle J(\tau)J(0)\rangle &> m_0\ , \end{aligned} \tag{2.19}$$

where m_0 is a state with the lowest mass (ground state). Eq. (2.7) is a generalization of the relation (2.19) to the case of the matrix of correlators $\mathbf{\Pi}^{(n)}$.

The matrix elements of Eq. (2.18) are

$$\Pi_{ab}^{(n)}(\tau) = \left\langle J_a^\dagger(\tau)J_b(0)\right\rangle = \sum_k \int \frac{\mathrm{d}^3\vec{p}}{(2\pi)^3}\, C_{ab,k}\;\frac{1}{2E_k}\;e^{-E_k\tau}\ , \tag{2.20}$$

where $a, b = 1 \ldots 2^n$. The key quantity of interest is the negative derivative of the trace of the logarithm of the correlator matrix:

$$V^{(n)} \equiv -\frac{\mathrm{d}}{\mathrm{d}\tau} \mathrm{Tr} \log \mathbf{\Pi}^{(n)} = \mathrm{Tr} \left(-\dot{\mathbf{\Pi}}^{(n)} {\mathbf{\Pi}^{(n)}}^{-1} \right) \ , \tag{2.21}$$

where a dot above a symbol denotes the derivative with respect to Euclidean time τ. It will be proven that this expression is greater than the sum of the lowest $N = 2^n$ masses with scalar quantum numbers.

First, define the following quantity:

$$-\check{\Pi}^{(n)}_{ab}(\tau) \equiv \sum_k \int \frac{\mathrm{d}^3\vec{p}}{(2\pi)^3} \ C_{ab,k} \ \frac{1}{2E_k} \ e^{-E_k \tau} \ m_k \ . \tag{2.22}$$

If one compares "hooked" quantity of Eq. (2.22) with the derivative with respect to τ:

$$-\dot{\Pi}^{(n)}_{ab}(\tau) = \sum_k \int \frac{\mathrm{d}^3\vec{p}}{(2\pi)^3} \ C_{ab,k} \ \frac{1}{2E_k} \ e^{-E_k \tau} \ \sqrt{p^2 + m_k^2} \ , \tag{2.23}$$

it is straightforward to see that the trace (2.21) with $\check{\mathbf{\Pi}}$ matrix is always smaller than the trace with $\dot{\mathbf{\Pi}}$ matrix. The proof is the following:

$$\begin{aligned} \mathrm{Tr} \left(-\dot{\mathbf{\Pi}} \right) \mathbf{\Pi}^{-1} &\geq \mathrm{Tr} \left(-\check{\mathbf{\Pi}} \right) \mathbf{\Pi}^{-1} \ , \\ \sum_c \langle \psi_c | - \dot{\mathbf{\Pi}} | \psi_c \rangle \lambda_c^{-1} &\geq \sum_c \langle \psi_c | - \check{\mathbf{\Pi}} | \psi_c \rangle \lambda_c^{-1} \ , \end{aligned} \tag{2.24}$$

where $|\psi_c\rangle$ are eigenvectors of matrix $\mathbf{\Pi}$ and λ_c are corresponding eigenvalues. All eigenvalues, λ_c, are positive since $\mathbf{\Pi}$ is a positive definite matrix. On the left-hand side, there is an average of the energy (recall that energy includes momentum) in certain states. The energy on the left-hand side is always greater than the mass on the right-hand side of the inequality (2.24). Since the average is taken with positive weights λ_c^{-1}, the inequality holds.

The next step is to split the matrix $\mathbf{\Pi}$ into two parts, $\mathbf{A}$ and $\mathbf{B}$, where the part $\mathbf{A}$ couples only to the first 2^n masses and the part $\mathbf{B}$ couples to the rest:

$$\begin{aligned} A_{ab}^{(n)}(\tau) &\equiv \sum_{k=1}^{2^n} \int \frac{\mathrm{d}^3\vec{p}}{(2\pi)^3}\, C_{ab,k}\, \frac{1}{2E_k}\, e^{-E_k\tau}\ , \\ B_{ab}^{(n)}(\tau) &\equiv \sum_{k=2^n+1}^{\infty} \int \frac{\mathrm{d}^3\vec{p}}{(2\pi)^3}\, C_{ab,k}\, \frac{1}{2E_k}\, e^{-E_k\tau}\ . \end{aligned} \tag{2.25}$$

Obviously, such splitting can be done for the matrix itself $\mathbf{\Pi} = \mathbf{A} + \mathbf{B}$, for the derivative $\dot{\mathbf{\Pi}} = \dot{\mathbf{A}} + \dot{\mathbf{B}}$ of the matrix, as well as for the "hooked" matrix $\check{\mathbf{\Pi}} = \check{\mathbf{A}} + \check{\mathbf{B}}$.

Recall that the goal is to relate the $\mathbf{\Pi}$ matrix to the meson masses. The following matrix identity, which is valid for every n, holds:

$$\begin{aligned} \mathrm{Tr}\left(\left(-\check{\mathbf{A}} - \check{\mathbf{B}}\right)(\mathbf{A}+\mathbf{B})^{-1}\right) = \mathrm{Tr}&\left(\frac{1}{\sqrt{\mathbf{A}+\mathbf{B}}}\sqrt{\mathbf{A}}\left(\frac{1}{\sqrt{\mathbf{A}}}(-\check{\mathbf{A}})\frac{1}{\sqrt{\mathbf{A}}}\right)\sqrt{\mathbf{A}}\frac{1}{\sqrt{\mathbf{A}+\mathbf{B}}}\right) \\ &+ \mathrm{Tr}\left(\frac{1}{\sqrt{\mathbf{A}+\mathbf{B}}}\sqrt{\mathbf{B}}\left(\frac{1}{\sqrt{\mathbf{B}}}(-\check{\mathbf{B}})\frac{1}{\sqrt{\mathbf{B}}}\right)\sqrt{\mathbf{B}}\frac{1}{\sqrt{\mathbf{A}+\mathbf{B}}}\right)\ . \end{aligned} \tag{2.26}$$

Next, introduce the definitions:

$$\begin{aligned} \mathbf{X} &\equiv \sqrt{\mathbf{A}}\frac{1}{\sqrt{\mathbf{A}+\mathbf{B}}}\ , \quad \mathbf{Y} \equiv \sqrt{\mathbf{B}}\frac{1}{\sqrt{\mathbf{A}+\mathbf{B}}}\ , \\ \underline{\mathbf{A}} &\equiv \frac{1}{\sqrt{\mathbf{A}}}(-\check{\mathbf{A}})\frac{1}{\sqrt{\mathbf{A}}}\ , \quad \underline{\mathbf{B}} \equiv \frac{1}{\sqrt{\mathbf{B}}}(-\check{\mathbf{B}})\frac{1}{\sqrt{\mathbf{B}}}\ , \end{aligned} \tag{2.27}$$

which allow one to rewrite the Eq. (2.26) in the following way:

$$\mathrm{Tr}\left(\left(-\check{\mathbf{A}} - \check{\mathbf{B}}\right)(\mathbf{A}+\mathbf{B})^{-1}\right) = \mathrm{Tr}\left(\mathbf{X}^\dagger\underline{\mathbf{A}}\mathbf{X} + \mathbf{Y}^\dagger\underline{\mathbf{B}}\mathbf{Y}\right)\ . \tag{2.28}$$

Since the operators $\mathbf{X}$ and $\mathbf{Y}$ satisfy the relation $\mathbf{X}^\dagger\mathbf{X} + \mathbf{Y}^\dagger\mathbf{Y} = 1$, they can be simultaneously diagonalized. Moreover, their eigenvalues are related:

$$\mathbf{X}^\dagger\mathbf{X}|\psi_i\rangle = p_i|\psi_i\rangle\ , \quad \mathbf{Y}^\dagger\mathbf{Y}|\psi_i\rangle = (1-p_i)|\psi_i\rangle\ , \tag{2.29}$$

with $0 \leq p_i \leq 1$.

The states $|\chi_i\rangle$ defined using X matrix as $|\chi_i\rangle \equiv 1/\sqrt{p_i}\, X|\psi_i\rangle$ form an orthonormal basis of states; similarly, states $|\Upsilon_i\rangle$ defined with the Y matrix $|\Upsilon_i\rangle \equiv 1/\sqrt{1-p_i}\, Y|\psi_i\rangle$ also form an orthonormal basis. Thus, the trace can be rewritten into the following form:

$$\begin{aligned}\mathrm{Tr}\left(\mathbf{X}^\dagger \underline{\mathbf{A}} \mathbf{X} + \mathbf{Y}^\dagger \underline{\mathbf{B}} \mathbf{Y}\right) &= \sum_i \langle\psi_i|\mathbf{X}^\dagger \underline{\mathbf{A}} \mathbf{X} + \mathbf{Y}^\dagger \underline{\mathbf{B}} \mathbf{Y}|\psi_i\rangle \\ &= \sum_i \langle\chi_i|\underline{\mathbf{A}}|\chi_i\rangle + (1-p_i)\left(\langle\Upsilon_i|\underline{\mathbf{B}}|\Upsilon_i\rangle - \langle\chi_i|\underline{\mathbf{A}}|\chi_i\rangle\right) \\ &\geq \mathrm{Tr}\underline{\mathbf{A}} = \mathrm{Tr}\frac{-\check{\mathbf{A}}}{\mathbf{A}}\ .\end{aligned} \tag{2.30}$$

The second term on the right-hand side of Eq. (2.30) is always positive. It is due to the fact that the highest possible eigenvalue of operator $\underline{\mathbf{A}}$ is less than or equal to m_{2^n} (m_j represents the mass of the j^{th} state), while the smallest possible eigenvalue of $\underline{\mathbf{B}}$ is always greater or equal to m_{2^n+1}. These relations follow directly from Eqs. (2.22), (2.25), and (2.27).

In Eq. (2.30), currents in operator $\mathbf{A}$ can be reorganized in a way similar to Gram-Schmidt orthogonalization. Specifically, that the first current couples only to the first (lightest) meson, second current only to the second meson, etc. This process will lead to the diagonal matrix. Moreover, the nth diagonal element is equal to the mass of the nth particle. Consequently:

$$\mathrm{Tr}\frac{-\check{\mathbf{A}}^{(n)}}{\mathbf{A}^{(n)}} = \sum_k^{2^n} m_k\ . \tag{2.31}$$

The quantity on the right hand side is exactly the function $W(m_{2^n})$, which was defined by equation (2.4). Thus, the inequality B (2.7) follows:

$$V = -\frac{\mathrm{d}}{\mathrm{d}\tau}\mathrm{Tr}\log\mathbf{\Pi} \geq \sum_k^{2^n} m_k = W(m_{2^n})\ . \tag{2.32}$$

2.2.3 Inequality A

Having demonstrated inequality B (2.7), the existence of a Hagedorn spectrum at large N_c will have been demonstrated if the inequality A (2.6) can be shown to be true. It states that the trace of the logarithm of correlator matrix grows at most linearly in n (where n is the step in the sequence):

$$N(an+b) \geq -\frac{d}{d\tau}\mathrm{Tr}\log\mathbf{\Pi}\ .$$

First, look at the situation at sufficiently small times. In this region, asymptotic freedom allows one to treat fields inside currents as non-interacting. Thus, the correlator of a single operator J_a can be decomposed to a product of free single particle propagators for each of its constituents. Additionally, in the large N_c limit, the matrix of correlators is diagonal (a consequence of single-color-trace nature of currents which guarantees that operators are orthogonal at infinitesimal times). Doing the trace of the matrix, one obtains 2^n terms with the same structure. Thus, as a consequence of asymptotic freedom, the investigation of one current-current correlator and its logarithmic derivative gives the full information. Schematically:

$$\mathbf{\Pi}^{(n)} = \begin{pmatrix} \Pi^{(n)}_{00} & & & \\ & \Pi^{(n)}_{11} & & \\ & & \ddots & \\ & & & \Pi^{(n)}_{2^n 2^n} \end{pmatrix}\ .$$

In the asymptotically free regime, the time scale is the only dimensional parameter available. Thus, the structure of the correlator is fully given by dimensional

analysis. The mass dimensions of elementary currents J is known; it is $4n+3$ for 3+1 dimensions, and $9n+2$ for 2+1 dimensions. Thus:

$$\Pi_{ab}^{(n)} = \begin{cases} \delta_{ab}\,\text{const}\ \tau^{-(8n+6)} & \text{for} \quad 3+1\,\text{dimensions} \\ \delta_{ab}\,\text{const}\ \tau^{-(18n+4)} & \text{for} \quad 2+1\,\text{dimensions} \end{cases} . \tag{2.33}$$

The trace of the logarithmic derivative equals

$$-\frac{\mathrm{d}}{\mathrm{d}\tau}\mathrm{Tr}\log\mathbf{\Pi}^{(n)} = \begin{cases} (2^n)\frac{8n+6}{\tau} & \text{for} \quad 3+1\,\text{dimensions} \\ (2^n)\frac{18n+4}{\tau} & \text{for} \quad 2+1\,\text{dimensions} \end{cases} \tag{2.34}$$

The inequality condition (2.6) necessary for establishing the Hagedorn spectrum is thus reproduced—provided that the value of τ, for which one reaches to good approximation an asymptotically free regime, is independent of n.

Following the argument in Sect. 2.2.1, not only the existence of a Hagedorn spectrum was shown, but also an estimate for a bound on the Hagedorn temperature corresponding to our sets of currents was obtained:

$$T_H \leq \begin{cases} \frac{8\log_2(e)}{\tau_0} & \text{for} \quad 3+1\,\text{dimensions} \\ \frac{24\log_2(e)}{\tau_0} & \text{for} \quad 2+1\,\text{dimensions} \end{cases} \tag{2.35}$$

On the previous lines, QCD has been shown to have a Hagedorn spectrum, provided that the QCD is in a nearly asymptotically free regime for short times. If that is the case, all possible interaction between gluons can be neglected and calculation is vastly simplified. A critical question to investigate is the circumstances under which the corrections to the asymptotically free result are small, such that statements made earlier are valid.

The standard approach to incorporate these effects of interaction is via perturbation theory. However, as the time increases and one moves further away from the

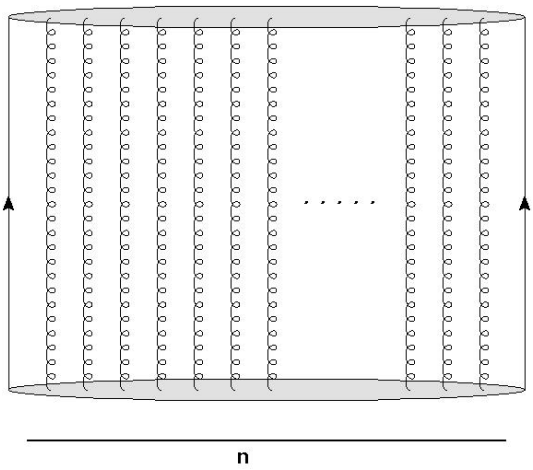

Figure 2.2: The Feynman diagram for a current-current correlator in the asymptotically free regime.

asymptotic region, the perturbative corrections keep growing and eventually push the system outside the region of validity of perturbation theory. Thus, the region where perturbation theory is applicable in QCD is limited. In the analysis, the standard assumption about the perturbative expansion are assumed: provided that the corrections are small, perturbation theory accurately describes correlation functions. Note that this is not a rigorous mathematical theorem. Note also that this formulation is widely used as a basis of analysis of correlation functions in QCD [30].

Given the assumption about smallness of perturbative corrections, the critical question one needs to address is the following: how do pertrubative corrections scale with n? More formally, the goal here is to show that at fixed τ, at any fixed order, the perturbative corrections to the quantity $2^{-n}\frac{\mathrm{d}}{\mathrm{d}\tau}\mathrm{Tr}\log\mathbf{\Pi}^{(n)}$ are at most linear in n. If that is true, the inequality A (2.6) is satisfied and QCD at large N_c has a Hagedorn spectrum given the assumptions above.

In order to get more insight into the properties of correlation functions, it is useful to look at a situation where interactions among gluons are neglected first. A typical Feynman diagram is shown in Fig. 2.2. Analysis of the non-interacting case will allow one to extract certain important features of correlation functions that will be generalized later to a case where interactions are present.

Due to the large N_c limit, the correlator matrix is diagonal for non-interacting fields. Thus, each gluonic operator O_l (2.11, 2.12) inside the current contributes in the same way to the final propagator:

$$\Pi^1_{ij\,\mathrm{free}}(\tau) = \langle O_i(\tau)\, O_j(0)\rangle_{\mathrm{free}} = \delta_{ij}\, \pi^1_{\mathrm{free}}(\tau)\ . \tag{2.36}$$

The superscript one in Π^1 indicates that this quantity represents the propagation of one gluonic operator. The δ_{ij} is a consequence of the form of operators (2.11, 2.12), which were defined to satisfy this property in the first place. The fact that the non-interacting propagator is the same for both operators O_1 and O_2 comes from a dimensional analysis; they must be proportional to each other (the proportionality constant in their definitions (2.11, 2.12) is chosen accordingly). It needs to be emphasized that the single-operator propagator is not gauge invariant, however it is only a part of the full correlator which is gauge invariant. The small letter π on the right-hand side of Eq. (2.36) indicates a function, not a matrix. This convention will be applied from now on. Recall the convention used to distinguish matrix and matrix elements: the matrix elements have explicit indices, whereas the respective matrices are denoted in boldface. The correlation function of the full current has two parts: n propagators of single gluonic operator O_i, and two quark propagators.

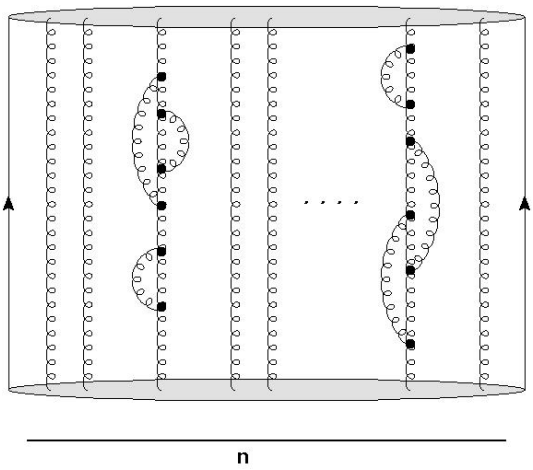

Figure 2.3: An example of a Feynman diagram, where interactions do not couple distinct gluon lines connected to the sources.

The matrix element of a correlator matrix reads:

$$\Pi^{(n)}_{ab}(\tau) = \delta_{ab}\, \pi^q_{\rm free}(\tau) \left[\pi^1_{\rm free}(\tau)\right]^n \pi^q_{\rm free}(\tau)\ , \tag{2.37}$$

where $\pi^q_{\rm free}(\tau)$ is the free quark propagator.

Recall that indices a, b run from 1 to 2^n (the dimension of the matrix which is equal to the number of elements in the respective set). The quantity of interested is the derivative of trace of the logarithm:

$$2^{-n}\frac{\rm d}{{\rm d}\tau}{\rm Tr}\,\log \mathbf{\Pi}^{(n)} = 2\frac{\rm d}{{\rm d}\tau}\log \pi^q_{\rm free} + n\frac{\rm d}{{\rm d}\tau}\log \pi^1_{\rm free}\ . \tag{2.38}$$

It is easy to see that the first term is independent of n (it comes for 2 quarks on the boundaries), and the second term is linearly proportional to n (comes from n gluonic operators that form the current). This result, which is based on the analysis of the respective Feynman diagram, is in agreement with the result obtained above.

The analysis of diagrams with interactions is more complicated. Consider the

case, when the interaction up to order α^l is included following the standard logic of perturbative expansion.

First, consider only a small set of all possible diagrams, namely those where all the interactions act on single gluonic propagators (see Fig. 2.3) and there are no interactions between gluons. Effectively, these interactions only modify the gluonic free propagators, similarly as self-energy modifies the free particle propagators.

$$\pi^1_{\text{free}}(\tau) \to \pi^1_{\text{free}}(\tau)\ (1 + c\,(\tau))\ . \tag{2.39}$$

A perturbative correction is denoted by $(1 + c(\tau))$. Note that the function $c(\tau)$ depends on the order in perturbation theory, but it is well defined at any given order l. Naturally, corrections of this type can appear on any internal line. Thus, if one restricts oneself only to this particular class of diagrams, the total correlator can be written as:

$$\Pi^{(n)}_{ab}(\tau) = \delta_{ab}\ \pi^q_{\text{free}}(\tau)\left[\pi^1_{\text{free}}(\tau)\,(1 + c(\tau))\right]^n \pi^q_{\text{free}}(\tau)\ . \tag{2.40}$$

The structure certainly contains more information (interaction of higher order in α) than necessary. However, it certainly contains all possible combinations that are required to a desired order α^l. The trace of the logarithm reads:

$$2^{-n}\frac{\mathrm{d}}{\mathrm{d}\tau}\mathrm{Tr}\,\log\mathbf{\Pi}^{(n)} = 2\frac{\mathrm{d}}{\mathrm{d}\tau}\log\pi^q_{\text{free}} + n\frac{\mathrm{d}}{\mathrm{d}\tau}\log\pi^1_{\text{free}} + n\frac{\mathrm{d}}{\mathrm{d}\tau}\log(1 + c)\ . \tag{2.41}$$

The specific form of the self-energy-like correction $c(\tau)$ is unknown. However, it is clearly independent of n. Thus, the expression on the right-hand side of Eq. (2.41) grows, again, linearly with n.

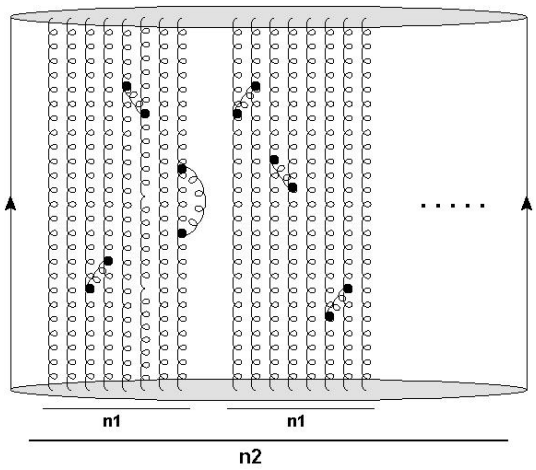

Figure 2.4: Division of gluon lines into n_2 clusters each containing n_1 lines.

This result clearly does not correspond to the full perturbative result, since it is based on the analysis of an artificial subset of all possible diagrams. Nevertheless, it illustrates the basic idea: the logarithmic structure and factorizing point-to-point correlators for the individual lines yields overall perturbative corrections that grow at most linearly with n. The next step is to include inter-gluonic interactions.

In order to deal with the possible interactions between gluonic lines, one can artificially divide the total number of internal gluon lines n into n_2 clusters with each cluster containing n_1 gluon lines. That is $n = n_1 n_2$. Since the work is done in the large n limit, following conditions on n_1 and n_2 are also imposed: $n_1 \gg 1$, $n_2 \gg 1$, and $n_1 \gg l$ (the order in perturbation theory which is considered). For the beginning, assume there are no interactions between clusters (or clusters and quarks on the boundary), i.e. that all couplings occur within clusters. This is illustrated in Fig. 2.4. Obviously, certain classes of diagrams are still neglected, but it will be shown later that corrections due to their presence do not affect the leading behavior

in n.

The generalized propagator of one cluster is given by

$$\mathbf{\Pi}^C(\tau) = \left[\pi^1_{\text{free}}(\tau)\right]^{n_1} \left[\mathbf{1} + \mathbf{C}'(\tau, n_1)\right] \ , \tag{2.42}$$

where $[\mathbf{1} + \mathbf{C}'(\tau, n_1)]$ is the effect of interactions within one cluster. One can see it as a self-energy of the whole cluster of n_1 gluonic lines. The dimension of the matrix $\mathbf{\Pi}^C$ is $2^{n_1} \times 2^{n_1}$. $\mathbf{C}'(\tau, n_1)$ depends not only on the order in perturbation theory, but also on the size of the cluster—the number of internal lines n_1.

To proceed, one needs to formally define a mapping from the "cluster" space (matrices of the dimension 2^{n_1}) to the "overall correlator" space (matrices of the dimension 2^n). Call this mapping $\mathbf{D}(\mathbf{M})$. To be precise, one needs to define n_2 different mappings $\mathbf{D}^{(k)}(\mathbf{M})$, each corresponding to a different cluster.

The mapping is a $2^n \times 2^n$ matrix $D^{(k)}_{ab}$. The indices a and b can be represented by a sequence of n numbers $a = (a_1 a_2 \dots a_n)$, $b = (b_1 b_2 \dots b_n)$, where $a_i, b_i = 0, 1$, It follows from the original definition of currents (2.13), since each of them is constructed from n building block operators O_1 and O_2.

Since n lines were divided into n_2 clusters of n_1 elements and interactions between clusters are neglected, each of the clusters can be treated independently. The mappings $\mathbf{D}^{(k)}$ are defined in such a way, that the first one, $\mathbf{D}^{(1)}$, affects only first n_1 subindices within indices a and b, the mapping corresponding to second cluster, $\mathbf{D}^{(2)}$, affects subindices $n_1 + 1$ to $2n_1$, etc. All n_2 mappings corresponding

to all n_2 clusters are defined this way. Specifically:

$$D^{(1)}_{(a_1a_2\ldots a_n)(b_1b_2\ldots b_n)}(\mathbf{M}) = M_{(a_1\ldots a_{n_1})(b_1\ldots b_{n_1})} \prod_{l=n_1+1}^{n} \delta_{a_l b_l} \ ,$$

$$D^{(2)}_{(a_1a_2\ldots a_n)(b_1b_2\ldots b_n)}(\mathbf{M}) = M_{(a_{n_1+1}\ldots a_{2n_1})(b_{n_1+1}\ldots b_{2n_1})} \prod_{l=1}^{n_1} \delta_{a_l b_l} \prod_{l'=2n_1+1}^{n} \delta_{a_{l'} b_{l'}} \ .$$

The general form reads:

$$D^{(k)}_{(a_1a_2\ldots a_n)(b_1b_2\ldots b_n)}(\mathbf{M}) = M_{(a_{(k-1)n_1+1}\ldots a_{kn_1})(b_{(k-1)n_1+1}\ldots b_{kn_1})} \prod_{l=1}^{(k-1)n_1} \delta_{a_l b_l} \prod_{l'=kn_1+1}^{n} \delta_{a_{l'} b_{l'}} \ . \tag{2.43}$$

The dimension of matrix $\mathbf{M}$ is $n_1 \times n_1$.

Matrix $\mathbf{M}$ is a straightforward generalization of the single gluon propagator discussed earlier. There, $\mathbf{\Pi^C}$ was just a number (matrix 1×1) and the matrix $\mathbf{D}$ was diagonal.

Formally, the 2^n dimensional space of overall matrices is factorized as a product of n_2 subspaces of dimension 2^{n_1}. Each subspace corresponds to one cluster. The vectors in this space have the form:

$$|V\rangle = |v^{(1)}\rangle \otimes |v^{(2)}\rangle \otimes \cdots \otimes |v^{(n_2)}\rangle \ , \tag{2.44}$$

and the spirit of the mapping $\mathbf{D}^{(k)}$ is:

$$\mathbf{D}^{(k)}(\mathbf{M}) = \mathbf{1}^{(1)} \otimes \mathbf{1}^{(2)} \otimes \cdots \otimes \mathbf{M}^{(k)} \otimes \cdots \otimes \mathbf{1}^{(n_2)} \ . \tag{2.45}$$

It follows directly from the construction of $\mathbf{D}^{(k)}(\mathbf{M})$, that $\mathrm{Tr}\,\log \mathbf{D}^{(k)}(\mathbf{M}) = \mathrm{Tr}\,\log \mathbf{M}$.

Using the notation of mappings $\mathbf{D}^{(k)}$, the overall correlator contains a product of n_2 matrices $\mathbf{D}^{(k)}$ corresponding to the respective clusters (note that the inter-cluster interactions are still neglected):

$$\mathbf{\Pi}^{(n)} = \pi^q_{\mathrm{free}}(\tau) \ \mathbf{D}^{(1)}(\mathbf{\Pi}^C) \ \times \ \mathbf{D}^{(2)}(\mathbf{\Pi}^C) \ \ldots \ \mathbf{D}^{(n_2)}(\mathbf{\Pi}^C) \ \pi^q_{\mathrm{free}}(\tau) \ . \tag{2.46}$$

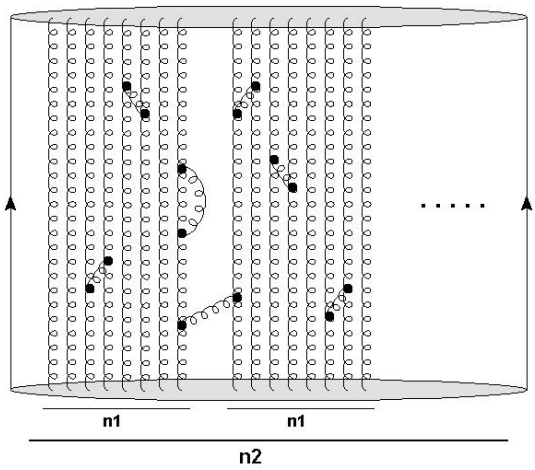

Figure 2.5: A typical diagram with interaction between two clusters

Using the standard linear algebra relation, Tr $\log(\mathbf{AB}) = \text{Tr} \log \mathbf{A} + \text{Tr} \log \mathbf{B}$, and the property that Tr $\log \mathbf{D}^{(k)}(\mathbf{M}) = \text{Tr} \log \mathbf{M}$, it is straightforward to show that

$$2^{-n} \frac{\mathrm{d}}{\mathrm{d}\tau} \text{Tr} \log \mathbf{\Pi}^{(n)} = 2 \frac{\mathrm{d}}{\mathrm{d}\tau} \log \pi^{q}_{\text{free}} + n_1 n_2 \frac{\mathrm{d}}{\mathrm{d}\tau} \log \pi^{1}_{\text{free}} + n_2 \frac{\mathrm{d}}{\mathrm{d}\tau} \log(1 + c'(n_1)) \ , \quad (2.47)$$

where $c'(n_1) \equiv \exp\left(\text{Tr} \log\left(\mathbf{1} + \mathbf{C}'\right)\right) - 1$.

The first two terms on the right-hand side of Eq. (2.47) were discussed earlier, after equation (2.38) (note that $n_1 n_2 = n$). The third term, however, requires a little more attention. The expression $\frac{\mathrm{d}}{\mathrm{d}\tau} \log(1 + c'(n_1))$ is clearly some function of n_1, formally $f(n_1)$. The specific form of the functional dependence is unknown. Recall, however, that the clusters were chosen completely arbitrarily. Thus, one can switch the meaning of n_1 and n_2 and the result must remain unchanged. This requires $n_2 f(n_1) = n_1 f(n_2)$ and consequently the functional dependence of $f(m)$ must be a linear function of m. Thus, the third term on the right-hand side of Eq. (2.47) is also proportional to $n = n_1 n_2$.

In order to complete the demonstration of the Hagedorn spectrum, it needs to

be shown that the effect of diagrams with interactions between clusters is subleading, i.e. it does not affect the leading n behavior. An example of a typical diagram is shown in Fig. 2.5.

The way to account for these effects is by including a correction matrix $(\mathbf{1}+\mathbf{C}'')$ between the matrices corresponding to clusters. Additionally, the interaction between the quarks on the boundary and the clusters next to them can be accommodated in a similar manner $(\mathbf{1}+\mathbf{C}^q)$. The total correlator matrix reads:

$$\begin{aligned}\mathbf{\Pi}^{(n)}(\tau) = \pi^q_{\text{free}}(\tau)\ (\mathbf{1}+\mathbf{C}^q)\ \times\ \mathbf{D}^{(1)}(\mathbf{\Pi}^C)\ \times\ (\mathbf{1}+\mathbf{C}'')\ \times\ \mathbf{D}^{(2)}(\mathbf{\Pi}^C)\ \ldots \\ (\mathbf{1}+\mathbf{C}'')\ \times\ \mathbf{D}^{(n_2)}(\mathbf{\Pi}^C)\ \times\ \mathbf{D}^{(1)}(\mathbf{\Pi}^C)\ (\mathbf{1}+\mathbf{C}^q)\ \pi^q_{\text{free}}(\tau)\ .\end{aligned} \tag{2.48}$$

The key point in the analysis of the above expression is that the matrices $\mathbf{C}''$ and $\mathbf{C}^q$ must be independent of n_1. This condition is satisfied due to the following reason. By construction, n_1 is much larger than the order in perturbation theory being considered. Additionally, only planar diagrams contribute at large N_c limit. Thus, at order α^l, a diagram connecting two clusters can go $l-1$ gluon lines deep into the cluster—at most. Since l is much smaller than n_1, it cannot go across the cluster. Therefore $\mathbf{C}''$ cannot, in principle, know how large the cluster is and must therefore be independent of n_1. The fact that it is also independent of n_2, the total number of clusters, is obvious.

Following the same argument as before, the trace of the logarithm reads:

$$\begin{aligned}2^{-n}\frac{\mathrm{d}}{\mathrm{d}\tau}\mathrm{Tr}\,\log\mathbf{\Pi}^{(n)} = 2\frac{\mathrm{d}}{\mathrm{d}\tau}\log\left(\pi^q_{\text{free}}(1+c^q)\right) + n_1 n_2\frac{\mathrm{d}}{\mathrm{d}\tau}\log\pi^1_{\text{free}} \\ + n_2\frac{\mathrm{d}}{\mathrm{d}\tau}\log(1+c'(n_1)) + (n_2-1)\frac{\mathrm{d}}{\mathrm{d}\tau}\log(1+c'')\ .\end{aligned} \tag{2.49}$$

where $c^q(\tau)$ and $c''(\tau)$ are defined analogously to $c'(\tau)$ and are ordinary functions.

On the right-hand side, the first term is independent of n, the second term is linear in n. The last two terms can be rewritten as $n_2(f(n_1)+g)-g$, using the natural definitions $f(n_1) \equiv \frac{\mathrm{d}}{\mathrm{d}\tau}\log(1+c'(n_1))$ and $g \equiv \frac{\mathrm{d}}{\mathrm{d}\tau}\log(1+c'')$. Similarly as before, one uses the fact that switching n_1 and n_2 cannot affect the result (provided that the order in perturbation theory is less than both n_1 and n_2). The consistency condition reads:

$$n_2(f(n_1)+g) = n_1(f(n_2)+g) \ , \tag{2.50}$$

which yields $f(m) = bm - g$ where b is a constant.

Thus, including the interactions between the clusters only modifies the subleading behavior in $f(n)$. Taking the last two terms together and exploiting the fact that $n = n_1 n_2$, one sees the right-hand side of Eq. (2.49) grows at most linearly with n. Completing the analysis, the inequality A (2.6) is satisfied even if the interactions are included via perturbation theory.

This completes our argument that the Hagedorn spectrum naturally emerges for mesons in the large N_c world.

2.3 Summary

In this chapter, it was shown that a Hagedorn spectrum emerges naturally for mesons in large N_c QCD—i.e. that the density of meson states grows exponentially with mass. A rather involved mathematical argument was presented in Sect. 2.2. Conceptually, a crucial part of the argument is the explicit construction of independent local operators is such a way that their number grows exponentially with

the mass dimension. The analysis of Euclidean space correlators led to inequalities which directly imply a Hagedorn spectrum.

Chapter 3: Form factor ratio

In this chapter, the following new theorem in QCD is proven:

$$\lim_{r\to\infty}\lim_{m_\pi\to 0}\lim_{N_c\to\infty}\frac{r^2\,\widetilde{G}_E^{I=0}\,\widetilde{G}_E^{I=1}}{\widetilde{G}_M^{I=0}\,\widetilde{G}_M^{I=1}} \;=\; 18\,. \tag{3.1}$$

In the ratio (3.1), $\widetilde{G}_{E,M}$ are position-space isoscalar and isovector electric and magnetic nucleon form factors. The position-space form factors are the Fourier-transformed counterparts of the standard momentum-space form factors $G_{E,M}$ [31]. This theorem holds in a combined limit $N_c \to \infty$ and $m_\pi \to 0$ with the large N_c limit taken first and exploit the longest distance nucleon physics. The analysis presented in this chapter is based on Ref. [32].

3.1 Motivation

It was discussed more extensively in Chapter 1 that QCD becomes weakly interacting theory of mesons in the large N_c limit. From this, Witten argued [2] that baryons emerge as soliton-like configurations of meson fields. Based on this observation, a new class of baryon models has been developed—chiral soliton models treated semiclassically. In the design of these models, not only the large N_c limit but also the approximate chiral limit has been taken into account. More specifically, the degrees of freedom in these models are weakly interacting mesons; baryons are

identified with soliton-like solutions constructed from meson fields. In these models, the large N_c physics is encoded in the very core—in the semiclassical treatment. The issue of chiral limit (and following chiral symmetry) is a little more subtle; it is imposed as a constraint on the dynamics of meson fields at a later stage effectively limiting the possible forms of the Lagrangian.

The observation stated in the previous paragraph can be reformulated more rigorously: chiral soliton models when treated semiclassically are models of baryons based on large N_c and chiral limits of QCD with $N_c \to \infty$ taken first. A famous example of such a model is the Skyrme model [33, 34]. In the Skyrme model, meson fields form hedgehog configurations—Skyrmions—and baryons are identified with the quantum states of collective motion of these configurations.

Chiral soliton models played an influential role in the development of hadronic physics for decades. Recently, there has been a broad interest in a different class of baryon models that share certain features with chiral soliton models—baryon models based on gauge/gravity duality (holographic models) [35–43]. The key similarity is the large N_c limit, which stands at the very core of the formulation of holographic models as well as of soliton models. Undoubtedly, these models look very different from the traditional 4D soliton-based models—if for no other reason, they are formulated in five dimensions instead of four. Nevertheless, one can use the understanding of old and (relatively) simple chiral soliton models to get some insights into new and complicated holographic models since they are expected to share certain features—indeed, they are based on the same limiting structure of QCD.

To give a broader perspective, one of the key undesirable features of building

models needs to be stressed. While constructing a model, one often has only few theoretical constraints. Certainly, assumptions of large N_c and chiral limit place some constraints on the structure of the model. Yet, there is in principle an infinite number of constructions that can be formulated. Naturally, getting the correct large N_c and chiral behavior is only one piece of the model building; and even then the individual models can differ substantially in details of the dynamics as well as in the physical predictions. However, the implications of large N_c and chiral physics are both constraining and "simple" to implement. Considering the vast knowledge and intuition obtained in the analysis of soliton models, it seems plausible that one can develop checks that establish whether the large N_c and chiral limits are encoded correctly in holographic models. Additionally, holographic models are so different from conventional models and are rather nontrivial to implement that having a simple litmus test as to whether they are implemented correctly is highly desirable.

Since the test should be applicable to a wide array of models (of a particular type), the obvious tools to use are model-independent relations. A large class of model-independent constraints was derived from consistency relations for the large N_c limit [4–9]. Particularly, the chiral behavior associated with the longest distance properties of the system [44–46] is greatly constrained. It is worth noting that all known model-independent relations of this type are reproduced in chiral soliton models; they are reproduced regardless of the specifics of the individual model's dynamics. Indeed, it was pointed out long ago by Adkins and Nappi [47] that, in the Skyrme model, certain class of relations holds independently of all model parameters. This observation led to a discovery of many new model-independent

relations. The theorem (3.1) discussed in this chapter is one of them.

However, to test whether holographic models (in addition to soliton models) have correctly encoded the chiral and large N_c scaling behavior, a new class of model-independent relations needs to be formulated. The reason for this is that the typical model-independent relation fixes how certain quantities diverge as $m_\pi \to 0$ (for example charge radius). However, many of the calculations in holographic models have only been done for $m_\pi = 0$ up to date. Thus the relations using behavior associated with deviations from $m_\pi = 0$ as probes cannot be used to analyze holographic models. Based on the analysis of the Skyrme model, Cherman et. al. [48] proposed to use the long distance behavior of the position-space electromagnetic form factors as a model-independent probe instead of the m_π dependence. A particularly useful relation of this type is for a long distance limit of a ratio of the product of the isovector and isoscalar position-space electric form factors to the product of the magnetic nucleon form factors (3.1):

$$\lim_{r\to\infty} \frac{r^2\, \widetilde{G}_E^{I=0}\, \widetilde{G}_E^{I=1}}{\widetilde{G}_M^{I=0}\, \widetilde{G}_M^{I=1}} \;=\; 18\,.$$

One of the remarkable things about this ratio (3.1) is that all low-energy constants, normalization of currents, and various sign or Fourier transform conventions cancel. The final result contains only a power of radius r, which can be deduced from dimensional analysis, and a constant. This constant—18—is a universal model-independent quantity that must be reproduced in all models formulated in the combined large N_c and chiral limit.

This particular model-independent relation has already proven its value in

analyzing holographic baryon models. It was shown that the treatment of solitons as instantons [38–43] in the Sakai and Sugimoto [38] "top down" model lead to nucleon form factors that failed to satisfy the relation (3.1). It indicates that something is wrong with such an approach. It was recently shown by Cherman and Ishii [49] that the reason for this is due to a failure of the flat-space instanton approximation—a calculational method widely used to extract physical predictions from the "top-down" holographic models. On the other hand, nucleon form factors derived in a "bottom up" phenomenological model [35–37] were shown to satisfy the model-independent relation (3.1). Thus one can claim that the "bottom-up" holographic model had correctly incorporated the large N_c and chiral behavior.

Equation (3.1) was originally [48] derived in the context of the Skyrme model, and it was proposed to be model independent. The indirect, yet strong, argument for its model-independence is in the same spirit as an argument of Adkins and Nappi [47]. Specifically, that Eq. (3.1) holds in any Skyrme model independently of the details (i.e. the form of the Lagrangian, the number of degrees of freedom, low energy constants, ...). Note that in the past, whenever a result derived in the Skyrme model was completely independent of model details, it also turned out to be the result of large N_c chiral perturbation theory. And large N_c χPT is known to correctly describe the longest distance physics in QCD. Although it may seem to be a convincing argument that the result (3.1) is truly model independent, it is important to verify it directly in large N_c chiral perturbation theory. The calculations doing so are presented in this chapter.

Some of the general features of large N_c chiral perturbation theory were briefly

discussed in Chapter 1; a particular attention was paid to the consistency relations and the emergent spin-flavor symmetry, which are the main difference from the conventional χPT. Here, some other details of this formalism specific to the analysis of long-distance behavior of electromagnetic form factors are discussed.

Since the pion is the lightest particle available in the system, the pion cloud is what dominates the long distance hadronic physics in QCD. Moreover, pion loops contribute at the leading order in the $1/N_c$ expansion [50] in the baryon sector. Thus, the dominant diagrams contributing to the longest distance physics will consist of currents connected to the pion loops with the number of pions running in loops being the smallest possible for the given current quantum numbers. Note, additionally, that, according to the standard large N_c counting rules, baryon mass is parametrically large compared to the pion mass—of order N_c . It leads to another simplification since it allows one to treat baryons non-relativistically and neglect their recoil. In summary, the heavy baryon large N_c χPT is the formalism in which the work is done.

Formally, the large N_c physics enters χPT in two different places. First, it eliminates some diagrams, those that are suppressed by factors of $1/N_c$. Second, it forces one to include Δ-isobar in the calculation. The reason for this is that, in the large N_c limit, Δ and nucleons are degenerate due to the consistency relations discussed earlier (in general the whole tower of $I = J$ isobars must be degenerate forming the ground state multiplet). More formally, in order to keep track of $1/N_c$ corrections, one introduces an N-Δ mass difference $\Delta = m_\Delta - m_N$, which is of order $1/N_c$. It serves as a new low-energy constant of the theory. It makes the total

number of low energy constants in the large N_c variant of χPT to be four—g_A, f_π, m_π and Δ. The need to include the Δ increases the number of Feynman diagrams one must consider and this operation has far-reaching consequences.

It was shown by Cohen and Broniowski [44, 45] that the effect of Δ isobar is different for different isospin-spin channels. For isoscalar-scalar ($\widetilde{G}_E^{I=0}$) and isovector-vector ($\widetilde{G}_M^{I=1}$) channels, it only leads to a multiplicative factor. On the other hand, in the isoscalar-vector ($\widetilde{G}_M^{I=0}$) and isovector-scalar ($\widetilde{G}_E^{I=1}$) channels, the amplitudes corresponding to individual diagrams cancel exactly in the leading order in $1/N_c$ expansion (where $\Delta = 0$). Thus, the N-Δ mass splitting must be taken into account, and $\widetilde{G}_M^{I=0}$ and $\widetilde{G}_E^{I=1}$ become proportional to Δ (and is thus of order $1/N_c$). Recall the form of the relation (3.1)—in this ratio, one of these quantities ($\widetilde{G}_E^{I=1}$) is in the numerator and the other ($\widetilde{G}_M^{I=0}$) in the denominator, so that the dependence on Δ cancels exactly.

The analysis presented in this chapter is done in the combined large N_c and chiral limit. In this case, a problem may arise for observables sensitive to pion dynamics. Generally, these two limits do not commute and the specific ordering of limits matter [44,45]. The main discussion here is done using the following ordering: $N_c \to \infty$ limit first, $m_\pi \to 0$ limit second. The motivation for this particular choice is that this ordering is what both soliton and holographic models of baryons use implicitly. The large N_c limit is encoded in the very core of the baryon model formulation (semiclassical treatment for soliton models, holographic principle for holographic models) and chiral limit is imposed later as a constraint on the model dynamics.

3.2 Model independent relation and the role of the limits

The longest distance behavior of the position space form factors will be calculated in the context of large N_c chiral perturbation theory. The relevant Feynman diagrams are summarized in Fig. 3.1. Keeping the technical details aside for now—they will be thoroughly discussed in the next section—the final results for the Fourier transformed form factors are given here:

$$\lim_{r\to\infty} \widetilde{G}_E^{I=0} = \frac{3^3}{2^9\pi^5}\,\frac{1}{f_\pi^3}\left(\frac{g_A}{f_\pi}\right)^3\,\frac{1}{r^9}, \tag{3.2}$$

$$\lim_{r\to\infty} \widetilde{G}_M^{I=0} = \frac{3}{2^9\pi^5}\,\frac{1}{f_\pi^3}\left(\frac{g_A}{f_\pi}\right)^3\,\frac{\Delta}{r^7}, \tag{3.3}$$

$$\lim_{r\to\infty} \widetilde{G}_E^{I=1} = \frac{1}{2^4\pi^2}\,\left(\frac{g_A}{f_\pi}\right)^2\,\frac{\Delta}{r^4}, \tag{3.4}$$

$$\lim_{r\to\infty} \widetilde{G}_M^{I=1} = \frac{1}{2^5\pi^2}\,\left(\frac{g_A}{f_\pi}\right)^2\,\frac{1}{r^4}. \tag{3.5}$$

The first thing to realize looking at Eqs. (3.2-3.5) is that they are identical to those derived in the Skyrme model [48]. The fact that Eqs. (3.2-3.5) were calculated in the large N_c variant of chiral perturbation theory, however, shows that these results are truly model-independent. This was expected and is in agreement with the observation of Adkins and Nappi [47] discussed above that the Skyrme model correctly captures the longest distance behavior of the large N_c physics.

The results of (3.2-3.5) lead trivially to the theorem proposed at the beginning of this chapter (3.1):

$$\lim_{r\to\infty} \frac{r^2\,\widetilde{G}_E^{I=0}\,\widetilde{G}_E^{I=1}}{\widetilde{G}_M^{I=0}\,\widetilde{G}_M^{I=1}} = 18. \tag{3.6}$$

As advertised earlier, all low energy constants cancel in the ratio and only the

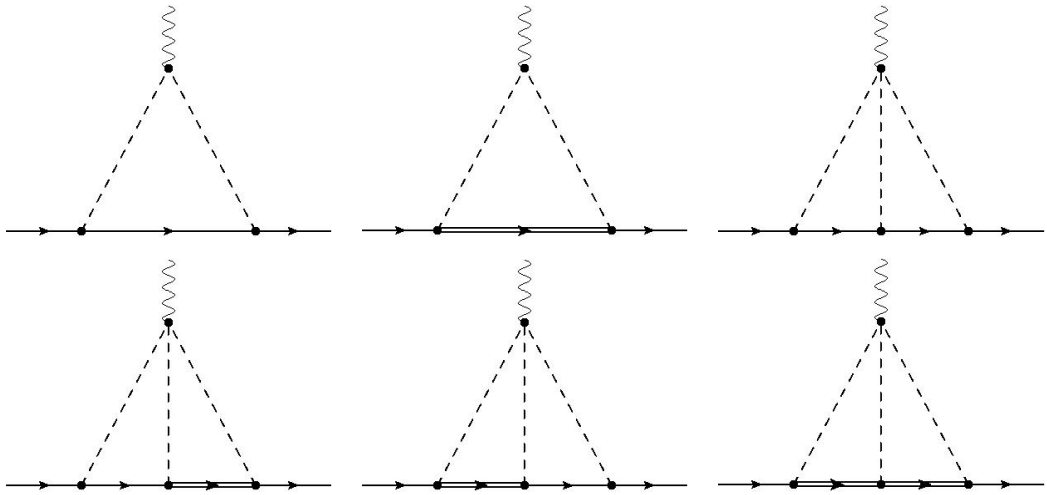

Figure 3.1: Feynman diagrams contributing to the long distance part of the isovector (first two diagrams starting from top-left corner) and isoscalar form factors. Double lines in the intermediate states represent the Δ-isobar.

universal number 18 survives.

The discussion of the new model-independent relation (3.1) could end here, since its model independence was proven. However, in order to understand the underlying dynamics, it is useful to analyze the effect of each of the three limits involved in the calculation—$\lim N_c \to \infty$, $\lim m_\pi \to 0$, $\lim r \to \infty$. Recall that the calculation leading to Eqs. (3.2-3.5) was done with large N_c limit taken first, chiral limit second, and long-distance probe last.

The first interesting question that arises is what happens when m_π remains finite. A semi-rigorous argument gives that the value of the ratio remains 18 even away from the chiral limit. The key observation is that the amplitude for finding a pion far away from the baryon is of Yuakawa type, i.e. exponential $\exp(-m_\pi r)$ that can be modified by a power law. The longest-range isovector part of the cur-

rent is dominated by loops containing two pions, therefore one expects the longest range behavior of isovector form factors (both electric and magnetic) to be proportional to $\exp(-2m_\pi r)$. Similarly, isoscalar form factors should be proportional to $\exp(-3m_\pi r)$, since three-pion contribution dominates the isoscalar physics. In the ratio (3.1), both terms (one electric and one magnetic) proportional to exponentials cancel; one is always in the numerator and one in the denominator. Thus, they do not affect the result.

The ratio Eq. (3.6) was calculated by taking the $N_c \to \infty$ limit at the outset. This particular choice is motivated by the the fact that it is equivalent to the limit structure of soliton models as well as holographic models. It is clearly an interesting question to ask what happens if the $N_c \to \infty$ is left to the end of the calculation.

The presence of the Δ-isobar is the key issue one must address. In the large N_c limit, the Δ is degenerate with the nucleon, and diagrams with Δ in the intermediate state contribute to the longest distance physics. However, for any finite N_c, the degeneracy is lifted and the energy difference between nucleon and Δ emerges. Thus, diagrams with Δ contribute at a shorter range than analogous diagrams containing only nucleons. The following cartoon picture will clarify the argument. In diagrams containing only nucleons, there is only one intrinsic mass scale—m_π. However, the presence of the Δ isobar brings another mass scale to the diagram, the mass difference Δ. It effectively enhances the suppression factor by $\exp(-\Delta r)$. The flow

of the limits can be sketched as:

$$\begin{aligned}
&\approx\ e^{-m_\pi r} + e^{-m_\pi r} e^{-\Delta r} && \approx\ e^{-m_\pi r} + e^{-m_\pi r} e^{-\Delta r} \\
&\text{limit } N_c \to \infty && \text{limit } m_\pi \to 0 \\
&\approx\ e^{-m_\pi r} + e^{-m_\pi r} && \approx\ 1 + e^{-\Delta r} \\
&\text{limit } m_\pi \to 0 && \text{limit } r \to \infty \\
&\approx\ 1 + 1 && \approx\ 1 + 0 \\
&\text{limit } r \to \infty && \text{limit } N_c \to \infty \\
&\approx\ 1 + 1 && \approx\ 1 + 0
\end{aligned}$$

One sees that taking $\Delta \to 0$ (i.e. $N_c \to \infty$) first eliminates the difference between amplitudes with and without Δs. This is the reason why diagrams with Δ in the intermediate state must be included if $N_c \to \infty$ is taken at the outset of the problem. On the other hand, if one switches the order of limits ($m_\pi \to 0$ first, $r \to \infty$, $N_c \to \infty$ last), the amplitude derived from diagrams with Δ remains suppressed making only diagrams with nucleons in the intermediate state to contribute.

It was discussed earlier, that amplitudes add up for isoscalar electric and isovector magnetic form factors. Thus the difference coming from a reversed ordering of limits is only a multiplicative factor. A deeper analysis shows that:

$$\lim_{N_c\to\infty} \lim_{r\to\infty} \lim_{m_\pi\to 0} \widetilde{G}_E^{I=0} = \frac{2}{9} \cdot \lim_{r\to\infty} \lim_{m_\pi\to 0} \lim_{N_c\to\infty} \widetilde{G}_E^{I=0}, \tag{3.7}$$

$$\lim_{N_c\to\infty} \lim_{r\to\infty} \lim_{m_\pi\to 0} \widetilde{G}_M^{I=1} = \frac{2}{3} \cdot \lim_{r\to\infty} \lim_{m_\pi\to 0} \lim_{N_c\to\infty} \widetilde{G}_M^{I=1}. \tag{3.8}$$

On the other hand, the situation is more complex for isoscalar magnetic and isovector electric form factors, where amplitudes subtracted exactly in the leading order and

form factors were proportional to Δ. In this case, the difference is not only in the multiplicative factor but also in the dimensionless number $1/(\Delta r)$ eliminating the Δ-dependence:

$$\lim_{N_c\to\infty}\lim_{r\to\infty}\lim_{m_\pi\to 0}\widetilde{G}_M^{I=0} = \frac{1}{\Delta r}\frac{2}{3\pi}\cdot\lim_{r\to\infty}\lim_{m_\pi\to 0}\lim_{N_c\to\infty}\widetilde{G}_M^{I=0}, \tag{3.9}$$

$$\lim_{N_c\to\infty}\lim_{r\to\infty}\lim_{m_\pi\to 0}\widetilde{G}_E^{I=1} = \frac{1}{\Delta r}\frac{1}{\pi}\cdot\lim_{r\to\infty}\lim_{m_\pi\to 0}\lim_{N_c\to\infty}\widetilde{G}_E^{I=1}. \tag{3.10}$$

Combining the results of Eqs. (3.7-3.10), reversing the order of large N_c and chiral limits changes the result by one half:

$$\lim_{N_c\to\infty}\lim_{r\to\infty}\frac{r^2\,\widetilde{G}_E^{I=0}\,\widetilde{G}_E^{I=1}}{\widetilde{G}_M^{I=0}\,\widetilde{G}_M^{I=1}} = 9. \tag{3.11}$$

3.3 Calculation of position-space form factors

In this section, the position space form factors $\widetilde{G}_E^{I=0}$, $\widetilde{G}_E^{I=I}$, $\widetilde{G}_M^{I=0}$, and $\widetilde{G}_M^{I=1}$ are calculated in the framework of large N_c chiral perturbation theory. The electric and magnetic form factors can be derived from the interaction of a nucleon with a photon, since the electromagnetic field couples to the vector current. The following convection for indices is used: Latin indices a, b, ... label isospin, Latin indices i, j, ... indicate 3-vector components, and Greek indices μ, ν, ... denote components of Lorentz 4-vectors.

In the fully relativistic form, baryon current reads:

$$\langle\vec{p}'|J_\mu(q^2)|\vec{p}\rangle = \bar{u}(\vec{p}')\left(\gamma_\mu F_1(q^2) + \frac{i}{2M}\sigma_{\mu\nu}q^\nu F_2(q^2)\right)u(\vec{p}), \tag{3.12}$$

where $\vec{p}' = \vec{p} + \vec{q}$ and both incoming and outgoing nucleons are on-shell. F_1 and F_2 are Dirac and Pauli form factors. In the non-relativistic limit, Eq. (3.12) simplifies

substantially. Note that the use of the non-relativistic reduction is justified by the fact that the work is done in the large N_c limit where the mass of the nucleon is parametrically large. The new form factors—electric and magnetic—can be defined in a way that the time (0^{th}) component of the vector current depends entirely on the electric form factor G_E, and the spatial (i^{th}) components depend entirely on the magnetic form factor G_M:

$$\begin{aligned} \langle \vec{p}' | J_0(q^2) | \vec{p} \rangle &= U^\dagger \; G_E(q^2) \; U, \\ \langle \vec{p}' | \vec{J}_i(q^2) | \vec{p} \rangle &= U^\dagger \; \frac{-i}{2M} \epsilon_{ijk} \, \vec{q}_j \, \sigma_k \, G_M(q^2) \; U; \end{aligned} \tag{3.13}$$

The electric and magnetic form factors G_E and G_M are a linear combination of the original Dirac and Pauli form factors F_1 and F_2:

$$\begin{aligned} G_E(q^2) &= F_1(q^2) + F_2(q^2) \frac{q^2}{4M^2}, \\ G_M(q^2) &= F_1(q^2) + F_2(q^2). \end{aligned}$$

The nucleon wave function U is a two-component spinor in the spin space as well as a two-component spinor in the isospin space. Since the incoming and outgoing baryons are the same, only terms proportional to the diagonal matrix in isospin space are non-zero. The most general diagonal matrix in isospin space is a linear combination of the identity matrix $\mathbf{I}_\tau$ and the third Pauli matrix τ_3. The definitions of current matrix elements (3.13) allows one to distinguish and define the isoscalar and the isovector current. The term proportional to the identity matrix, $U^\dagger \, \mathbf{I}_\tau \, U$, is defined to be the isoscalar current (proton plus neutron) and the term proportional to the third Pauli matrix, $U^\dagger \, \tau_3 \, U$, is defined to be the isovector current (proton minus neutron). Note that this definition is identical to the definitions used in [34, 48].

Additionally, the particular normalization convection adopted for isoscalars and isovectors is irrelevant from the point of view of the model-independent relation (3.1). There, one isoscalar (isovector) quantity is in the numerator and one in the denominator and thus any normalization factor cancels.

To extract the position-space form factors from the momentum-space currents, the following convention [48] is adopted:

$$\begin{aligned} \widetilde{G}_E(r) &= \int \frac{\mathrm{d}\Omega_x}{4\pi} \int \frac{\mathrm{d}^3 q}{(2\pi)^3}\, e^{i\vec{q}\cdot\vec{x}}\, \langle \vec{p}' |\, J^0\, | \vec{p} \rangle, \\ \widetilde{G}_M(r) &= \int \frac{\mathrm{d}\Omega_x}{4\pi} \int \frac{\mathrm{d}^3 q}{(2\pi)^3}\, e^{i\vec{q}\cdot\vec{x}}\, \frac{1}{2}\epsilon_{ij3}\, \vec{x}_j\, \langle \vec{p}' |\, \vec{J}_i\, | \vec{p} \rangle. \end{aligned} \tag{3.14}$$

Note, again, that the exact normalization factors used in (3.14) play no role in the model-independent relation (3.1) since one quantity of the same type is always in the numerator and one in the denominator.

3.3.1 Feynman rules

The form factors are extracted from the nucleon currents which are extracted from the amplitudes corresponding to the nucleon-photon interaction. Amplitudes are calculated in the language of quantum field theory. In order to proceed, one needs the Feynman rules for the following vertices: photon and two pions, photon and three pions, pion with baryons in all four possible combinations of incoming and outgoing nucleon and Δ. One also needs propagators for intermediate pions, nucleons, and Δs.

The Feynman rules are obtained from the conventional χPT Lagrangian [51] enriched with the effects of large N_c physics [6,7]. The Feynman rule for the photon-

two pions vertex reads:

$$\epsilon_{a3b}\, A_\mu\, (p_a^\mu + p_b^\mu)\ , \tag{3.15}$$

where p_a and p_b are the incoming and outgoing pion 4-momenta, respectively. This interaction is crucial for the isovector form factor (see the factor ϵ_{a3b}, which eventually transforms into a τ_3 matrix entering the nucleon current). The coupling of photon to three pions is derived from the QCD anomaly [52]. This vertex plays a central role in the isoscalar piece of the baryon current (see the factor ϵ_{abc}, which eventually transforms into an identity matrix, $\mathbf{I}_\tau$, entering the nucleon current). The Feynman rule reads:

$$\frac{1}{12\pi^2 f_\pi^3}\, \epsilon_{abc}\, \epsilon^{\mu\nu\kappa\lambda} A_\mu\, p_{a\nu}\, p_{b\kappa}\, p_{c\lambda}\ . \tag{3.16}$$

The pion-baryon-baryon$'$ coupling is of the vector-isovector form and is derivatively coupled. Note that the outgoing baryon (labeled B') may differ from the incoming one (labeled B), since both nucleon and Δ (and eventually higher states) may be involved. The Feynman rule reads:

$$\frac{g_A}{2f_\pi}\, \sqrt{\frac{2J^{(B')}+1}{2J^{(B)}+1}}\, \tau_a^{(BB')}\ \sigma_i^{(BB')}\, \vec{p}_i\ , \tag{3.17}$$

where $\vec{p}_i$ stands for the outgoing 3-momentum of a pion with isospin a. In (3.17), $\tau^{BB'}$ and $\sigma^{BB'}$ are operators in isospin and in spin space respectively. They are a generalization of Pauli matrices that stand in the well-known pion-nucleon-nucleon vertex. The coupling is derived from the consistency relations of large N_c QCD [6,7] and follows directly from the contracted $SU(4)$ spin-flavor symmetry emerging at large N_c. From these relations, one derives not only the degeneracy of baryons with $I = J$ (nucleon with $I = J = 1/2$, Δ with $I = J = 3/2$, ...), but also the specific

Table 3.1: Coupling matrices for pion-nucleon-nucleon (left column) and pion-Δ-nucleon (right column) vertices.

$$\tau_1, \sigma_1^{(NN)} = \tau_1, \sigma_1 = \begin{pmatrix} 0 & 1 \\ 1 & 0 \end{pmatrix} \qquad \tau_1, \sigma_1^{(\Delta N)} = \begin{pmatrix} \frac{\sqrt{3}}{2} & 0 & -\frac{1}{2} & 0 \\ 0 & \frac{1}{2} & 0 & -\frac{\sqrt{3}}{2} \end{pmatrix}$$

$$\tau_2, \sigma_2^{(NN)} = \tau_2, \sigma_2 = i \begin{pmatrix} 0 & -1 \\ 1 & 0 \end{pmatrix} \qquad \tau_2, \sigma_2^{(\Delta N)} = i \begin{pmatrix} \frac{\sqrt{3}}{2} & 0 & \frac{1}{2} & 0 \\ 0 & \frac{1}{2} & 0 & \frac{\sqrt{3}}{2} \end{pmatrix}$$

$$\tau_3, \sigma_3^{(NN)} = \tau_3, \sigma_3 = \begin{pmatrix} 1 & 0 \\ 0 & -1 \end{pmatrix} \qquad \tau_3, \sigma_3^{(\Delta N)} = \begin{pmatrix} 0 & -1 & 0 & 0 \\ 0 & 0 & -1 & 0 \end{pmatrix}$$

form of the pion-baryon-baryon$'$ vertex, which is given by an appropriate Clebsch-Gordan coefficient of the contracted $SU(4)$ symmetry. For example, the isospin part of the coupling for incoming nucleon with isospin projection α and outgoing delta with isospin projection α' is:

$$\left(\tau_a^{(N\Delta)}\right)_{\alpha\alpha'} = \sqrt{3} \left(\frac{1}{2}\,\alpha \ , \ 1\,a \,|\, \frac{3}{2}\,\alpha'\right).$$

Generally, all combinations can be summarized in the form of matrices, which are shown in Tables 3.1 and 3.2. Recall that the matrices for the pion-nucleon-nucleon vertex are ordinary Pauli matrices reproducing the standard χPT [51].

The next key ingredient in the field-theoretical calculation are propagators for particles in intermediate states. One needs propagators for pion, nucleon, and Δ. For pions, the full relativistic propagator must be employed since the chiral limit

Table 3.2: Coupling matrices for pion-nucleon-Δ (left column) and pion-Δ-Δ (right column) vertices.

$$\tau_1, \sigma_1^{(N\Delta)} = \begin{pmatrix} -\sqrt{\frac{3}{2}} & 0 \\ 0 & -\sqrt{\frac{1}{2}} \\ \sqrt{\frac{1}{2}} & 0 \\ 0 & \sqrt{\frac{3}{2}} \end{pmatrix} \qquad \tau_1, \sigma_1^{(\Delta\Delta)} = \begin{pmatrix} 0 & \sqrt{\frac{3}{5}} & 0 & 0 \\ \sqrt{\frac{3}{5}} & 0 & \frac{2}{\sqrt{5}} & 0 \\ 0 & \frac{2}{\sqrt{5}} & 0 & \sqrt{\frac{3}{5}} \\ 0 & 0 & \sqrt{\frac{3}{5}} & 0 \end{pmatrix}$$

$$\tau_2, \sigma_2^{(N\Delta)} = i \begin{pmatrix} \sqrt{\frac{3}{2}} & 0 \\ 0 & \sqrt{\frac{1}{2}} \\ \sqrt{\frac{1}{2}} & 0 \\ 0 & \sqrt{\frac{3}{2}} \end{pmatrix} \qquad \tau_2, \sigma_2^{(\Delta\Delta)} = i \begin{pmatrix} 0 & -\sqrt{\frac{3}{5}} & 0 & 0 \\ \sqrt{\frac{3}{5}} & 0 & -\frac{2}{\sqrt{5}} & 0 \\ 0 & \frac{2}{\sqrt{5}} & 0 & -\sqrt{\frac{3}{5}} \\ 0 & 0 & \sqrt{\frac{3}{5}} & 0 \end{pmatrix}$$

$$\tau_3, \sigma_3^{(N\Delta)} = \begin{pmatrix} 0 & 0 \\ \sqrt{2} & 0 \\ 0 & \sqrt{2} \\ 0 & 0 \end{pmatrix} \qquad \tau_3, \sigma_3^{(\Delta\Delta)} = \begin{pmatrix} \frac{3}{\sqrt{5}} & 0 & 0 & 0 \\ 0 & \frac{1}{\sqrt{5}} & 0 & 0 \\ 0 & 0 & -\frac{1}{\sqrt{5}} & 0 \\ 0 & 0 & 0 & -\frac{3}{\sqrt{5}} \end{pmatrix}$$

($m_\pi \to 0$) is eventually taken. The pion propagator reads:

$$\Delta^\pi(k) = \frac{i}{k^2 - m_\pi^2 + i\epsilon}, \tag{3.18}$$

where k is the propagating 4-momentum.

For the nucleon and the Δ, the heavy baryon approximation allows one to use non-relativistic variants of the propagators:

$$\Delta^N(k) = \frac{i}{k^0 + i\epsilon}\,, \quad \Delta^\Delta(k) = \frac{i}{k^0 - \Delta + i\epsilon}. \tag{3.19}$$

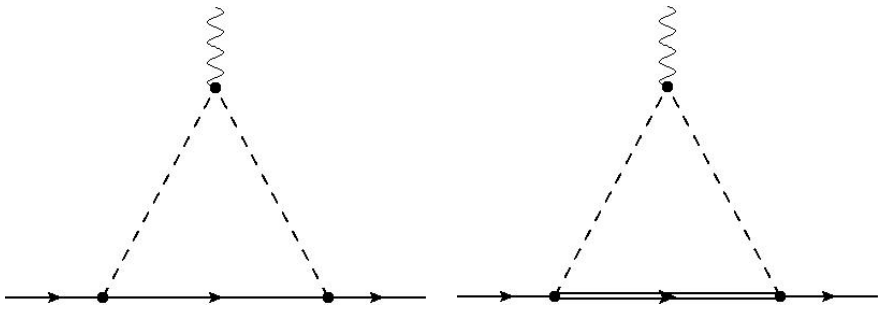

Figure 3.2: Feynman diagrams contributing to the long distance part of the isovector form factors (double line represents the Δ-isobar).

Note that the difference between nucleon and Δ propagators lies in the presence of $\Delta = M_\Delta - M_N$ in the denominator. This is exactly the $1/N_c$-order difference that plays a crucial role in the isoscalar-vector and isovector-scalar currents.

3.3.2 Isovector form factors

Start with the analysis of isovector form factors; their calculation is simpler and easier to follow than that of isoscalar form factors. The isovector currents are determined from Feynman diagrams containing one loop, which are summarized in Fig. 3.2. Recall that two pions are needed for the photon-two pions vertex (3.15) which governs the isovector physics.

The amplitudes corresponding to the diagrams in Fig. 3.2 consist of two parts: one that is the same for both diagrams, and one that is different. The difference can be traced back to two distinct factors: vertex matrices and intermediate baryon propagators. The total isovector amplitude (with the combinatoric factor 2! included) is evaluated using Feynman rules for vertices (3.15, 3.17) and propagators

(3.18, 3.19). It reads:

$$
\begin{aligned}
M_{fi} = eA_\mu J^\mu_{I=1} = eA_\mu \; 4i \left(\frac{g_A}{2f_\pi}\right)^2 \epsilon_{ab3} \int \frac{\mathrm{d}^4k}{(2\pi)^4} k^\mu \left(\frac{\vec{q}}{2}+\vec{k}\right)_l \left(\frac{\vec{q}}{2}-\vec{k}\right)_n \\
\Delta^\pi\left(k+\frac{q}{2}\right)\; \Delta^\pi\left(k-\frac{q}{2}\right) \\
U^\dagger \Big(\tau_b^{(NN)} \tau_a^{(NN)} \; \sigma_n^{(NN)} \sigma_l^{(NN)} \; \Delta^N(k) \\
+ \; \tau_b^{(\Delta N)} \tau_a^{(N\Delta)} \; \sigma_n^{(\Delta N)} \sigma_l^{(N\Delta)} \; \Delta^\Delta(k) \Big) U.
\end{aligned}
\tag{3.20}
$$

The product of two matrices in (3.20) (either the product of two isospin-space matrices τ or the product of two spin-space matrices σ—recall that they are the same but act in different Hilbert spaces) is a two dimensional matrix. Thus, it can be decomposed into two parts: the part proportional to the identity matrix, and the part proportional to the Pauli matrix. The products of two isospin matrices (note that the same expressions hold also for spin matrices σ) read:

$$
\begin{aligned}
\tau_a^{(NN)} \tau_b^{(NN)} &= \delta_{ab}\, \mathbf{I}_\tau + i\, \epsilon_{abc}\, \tau_c \;, \\
\tau_a^{(\Delta N)} \tau_b^{(N\Delta)} &= -\sqrt{2}\, \delta_{ab}\, \mathbf{I}_\tau + \frac{i}{\sqrt{2}} \epsilon_{abc}\, \tau_c \;.
\end{aligned}
\tag{3.21}
$$

First, analyze the isospin space part of the amplitude (3.20). The only non-zero contribution is the term proportional to τ_3. The reason for this is due to the factor ϵ_{ab3} coming from the photon-two pion vertex. The isospin-space algebra yields:

$$
\epsilon_{ab3} \left(\delta_{ab} \mathbf{I}_\tau + \epsilon_{bac} \tau_c\right) = -2\tau_3 \;. \tag{3.22}
$$

According to our definitions for the isoscalar and isovector currents, the matrix element proportional to the third Pauli matrix, τ_3, represents the isovector current. The piece proportional to the identity matrix in isospin space is identically zero and therefore no isoscalar current emerges from the two-pion loop diagrams.

In spin space, both scalar (proportional to $\mathbf{I}_\sigma$) and vector (proportional to σ_i) matrix elements contribute. If the nucleon and Δ propagators are equal (i.e. $\Delta \to 0$), the terms proportional to $\mathbf{I}_\sigma$ cancel completely. Thus, the N-Δ mass splitting must be taken into account. In the end, the isovector-scalar matrix element is proportional to $\Delta \sim 1/N_c$. On the other hand, the N-Δ mass splitting can be ignored in the terms proportional to σ_i, since they add together. Then, a relevant piece of (3.20) can be rewritten as:

$$U^\dagger \, 2\,\tau_3 \left(\mathbf{I}_\sigma \, \delta_{nl} \, \frac{-\Delta}{(k^0 + i\epsilon)^2} + \sigma_3 \, \epsilon_{nl3} \, \frac{3i}{2(k^0 + i\epsilon)} \right) U.$$

Due to the angular integration in the definitions of the position-space form factors (3.14), the electric form factor $\widetilde{G}_E$ is determined entirely by the scalar part of the amplitude (proportional to $\mathbf{I}_\sigma$) and only the vector part of the amplitude (proportional to σ_i) contributes to the magnetic form factor $\widetilde{G}_M$.

From the definitions, the electric form factor is obtained by the Fourier transform of the zeroth component of the current (3.14):

$$\begin{aligned}
\widetilde{G}_E^{I=1} &= 8i\Delta \left(\frac{g_A}{2f_\pi} \right)^2 U^\dagger \tau_3 \mathbf{I}_\sigma U \int \frac{\mathrm{d}^3 q}{(2\pi)^3} \, e^{i\vec{q}\cdot\vec{x}} \\
&\qquad \int \frac{\mathrm{d}^4 k}{(2\pi)^4} \left(\frac{\vec{q}}{2} + \vec{k} \right) \cdot \left(\frac{\vec{q}}{2} - \vec{k} \right) \frac{k^0}{(k^0 + i\epsilon)^2} \\
&\qquad \Delta^\pi \left(k + \frac{q}{2} \right) \, \Delta^\pi \left(k - \frac{q}{2} \right) \\
\widetilde{G}_E^{I=1} &\underset{\substack{m_\pi \to 0 \\ r \to \infty}}{=} \frac{1}{2^4 \pi^2} \left(\frac{g_A}{f_\pi} \right)^2 \frac{\Delta}{r^4} \,,
\end{aligned} \tag{3.23}$$

where the normalization $U^\dagger U = 1$ used.

Analogously, the magnetic form factor comes from the spatial components of

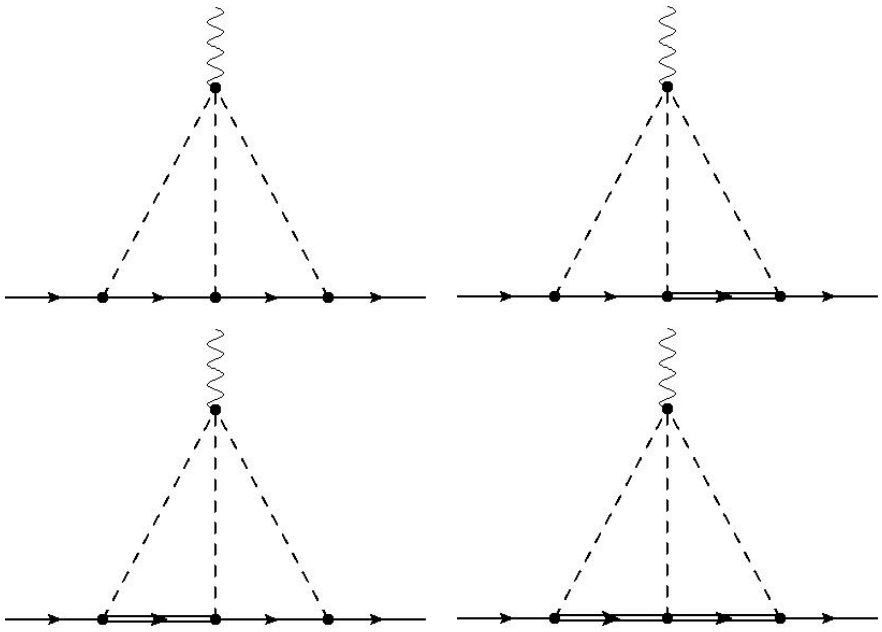

Figure 3.3: Feynman diagrams contributing to the long distance part of the isoscalar form factors (double lines in the intermediate states represent the Δ-isobar).

currents and their Fourier transforms:

$$\begin{aligned}\widetilde{G}_M^{I=1} &= 6\left(\frac{g_A}{2f_\pi}\right)^2 U^\dagger\tau_3\sigma_3 U \int\frac{\mathrm{d}\Omega_x}{4\pi}\int\frac{\mathrm{d}^3q}{(2\pi)^3}e^{i\vec{q}\cdot\vec{x}} \\ &\quad \int\frac{\mathrm{d}^4k}{(2\pi)^4}\,\epsilon_{ij3}\vec{x}_j\vec{k}_i\,\epsilon_{nl3}\left(\frac{\vec{q}}{2}+\vec{k}\right)_l\left(\frac{\vec{q}}{2}-\vec{k}\right)_n \\ &\quad \frac{1}{k^0+i\epsilon}\;\Delta^\pi\left(k+\frac{q}{2}\right)\;\Delta^\pi\left(k-\frac{q}{2}\right) \\ \widetilde{G}_M^{I=1} &\underset{\substack{m_\pi\to 0\\ r\to\infty}}{=} \frac{1}{2^5\pi^2}\left(\frac{g_A}{f_\pi}\right)^2\frac{1}{r^4}. \end{aligned} \tag{3.24}$$

3.3.3 Isoscalar form factors

The calculation of isoscalar form factors is analogous to the calculation of isovector ones; it is, however, more complicated since it involves diagrams with three pions forming two loops. All the relevant Feynman diagrams are summarized in Fig.

3.3. The presence of two loop momenta makes the integrals more complicated from a calculational point of view, but the approach remains the same.

The isoscalar amplitude coming from the diagrams with three pions reads:

$$\begin{aligned} M_{fi} = eA_\mu J^\mu_{I=0} = eA_\mu \frac{i}{2\pi^2 f_\pi^3} \left(\frac{g_A}{2f_\pi}\right)^3 \epsilon_{abc} \int \frac{\mathrm{d}^4k}{(2\pi)^4} \int \frac{\mathrm{d}^4l}{(2\pi)^4} \\ \Delta^\pi\left(k+\frac{q}{2}\right)\ \Delta^\pi\left(k+l\right)\ \Delta^\pi\left(l+\frac{q}{2}\right) \\ \epsilon^{\mu\alpha\beta\gamma}\left(k+\frac{q}{2}\right)_\alpha (-k-l)_\beta \left(l+\frac{q}{2}\right)_\gamma \left(\vec{k}+\frac{\vec{q}}{2}\right)_r \left(-\vec{k}-\vec{l}\right)_s \left(\vec{l}+\frac{\vec{q}}{2}\right)_t \\ U^\dagger \Big(\tau_c^{(NN)}\tau_b^{(NN)}\tau_a^{(NN)}\sigma_t^{(NN)}\sigma_s^{(NN)}\sigma_r^{(NN)}\Delta^N(k)\Delta^N(-l)\ + \\ \tau_c^{(\Delta N)}\tau_b^{(N\Delta)}\tau_a^{(NN)}\sigma_t^{(\Delta N)}\sigma_s^{(N\Delta)}\sigma_r^{(NN)}\Delta^N(k)\Delta^\Delta(-l) + \\ \tau_c^{(NN)}\tau_b^{(\Delta N)}\tau_a^{(N\Delta)}\sigma_t^{(NN)}\sigma_s^{(\Delta N)}\sigma_r^{(N\Delta)}\Delta^\Delta(k)\Delta^N(-l) + \\ \tau_c^{(\Delta N)}\tau_b^{(\Delta\Delta)}\tau_a^{(N\Delta)}\sigma_t^{(\Delta N)}\sigma_s^{(\Delta\Delta)}\sigma_r^{(N\Delta)}\Delta^\Delta(k)\Delta^\Delta(-l)\Big)\ U, \end{aligned} \tag{3.25}$$

where the combinatoric factor 3! is included. The four different combinations of τ and σ matrices come from the four different combinations of intermediate baryons—there are either two nucleons, one nucleon and one Δ, or two Δs. Similarly to (3.21), the product of three matrices can be decomposed to a term proportional to the identity matrix and to terms proportional to Pauli matrices:

$$\begin{aligned} \tau_a^{(NN)}\tau_b^{(NN)}\tau_c^{(NN)} &= i\epsilon_{abc}\,\mathbf{I}_\tau + \delta_{ab}\tau_c - \delta_{ac}\tau_b + \delta_{bc}\tau_a, \\ \tau_a^{(\Delta N)}\tau_b^{(N\Delta)}\tau_c^{(NN)} &= \frac{i}{\sqrt{2}}\epsilon_{abc}\,\mathbf{I}_\tau - \sqrt{2}\delta_{ab}\tau_c - \frac{1}{\sqrt{2}}\delta_{ac}\tau_b + \frac{1}{\sqrt{2}}\delta_{bc}\tau_a, \\ \tau_a^{(NN)}\tau_b^{(\Delta N)}\tau_c^{(N\Delta)} &= \frac{i}{\sqrt{2}}\epsilon_{abc}\,\mathbf{I}_\tau + \frac{1}{\sqrt{2}}\delta_{ab}\tau_c - \frac{1}{\sqrt{2}}\delta_{ac}\tau_b - \sqrt{2}\delta_{bc}\tau_a, \\ \tau_a^{(\Delta N)}\tau_b^{(\Delta\Delta)}\tau_c^{(N\Delta)} &= -i\sqrt{\frac{5}{2}}\epsilon_{abc}\,\mathbf{I}_\tau + \frac{1}{\sqrt{10}}\delta_{ab}\tau_c - 2\sqrt{\frac{2}{5}}\delta_{ac}\tau_b + \frac{1}{\sqrt{10}}\delta_{bc}\tau_a\ . \end{aligned}$$

The ϵ_{abc} factor from the photon-three pions vertex guarantees that only the part proportional to the identity matrix in the isospin space contributes to the

amplitude. The factor $i\epsilon_{abc}\epsilon_{cba}\mathbf{I}_\tau = -6i\mathbf{I}_\tau$ emerges from summing over indices a, b, and c. Recall that in the isovector case, which was discussed in the previous section, only the term proportional to τ_3 was non-zero due to the factor ϵ_{ab3} appearing in the photon-two pion vertex.

In the spin space, the terms proportional to $\mathbf{I}_\sigma$ sum together yielding an overall multiplicative factor $\frac{9}{2}\mathbf{I}_\sigma$. Analogously to the isovector-scalar calculation, the vector terms (proportional to σ) cancel exactly if the N-Δ mass splitting is neglected. Thus, $\Delta \sim 1/N_c$ must be included in the calculation. This observation is in agreement with the work of Broniowski and Cohen [44, 45], who showed that isovector-scalar and isoscalar-vector matrix elements are zero in the leading order in $1/N_c$ expansion.

Continuing exactly as in the isovector form factor calculation, the Fourier transform of the zeroth component of the current gives the electric form factor:

$$\begin{aligned}\widetilde{G}_E^{I=0} = \frac{-27}{2\pi^2 f_\pi^3}\left(\frac{g_A}{2f_\pi}\right)^3 U^\dagger \mathbf{I}_\tau \mathbf{I}_\sigma U \int \frac{\mathrm{d}^3q}{(2\pi)^3}\frac{\mathrm{d}^4k}{(2\pi)^4}\frac{\mathrm{d}^4l}{(2\pi)^4} \\ e^{i\vec{q}\cdot\vec{x}}\left(\epsilon_{rst}\,\vec{k}_r\vec{l}_s\vec{q}_t\right)^2 \Delta^N(k)\Delta^N(-l) \\ \Delta^\pi\left(k+\frac{q}{2}\right)\ \Delta^\pi\left(k+l\right)\ \Delta^\pi\left(l+\frac{q}{2}\right) \\ \widetilde{G}_E^{I=0} \underset{\substack{m_\pi\to 0\\ r\to\infty}}{=} \frac{3^3}{2^9\pi^5}\,\frac{1}{f_\pi^3}\left(\frac{g_A}{f_\pi}\right)^3 \frac{1}{r^9}. \end{aligned} \tag{3.26}$$

The calculation of the isoscalar magnetic (vector-isoscalar) form factor is of the same spirit. However, it is much longer and much more tedious than in the previous three cases, so only a brief summary of the procedure and the result is shown. Recall that the magnetic form factor is fully determined by the spatial components of the baryon current $J^{\mu=i}$. Examining the general formula for the isoscalar current (3.25), one sees that there are three conceptually distinct terms originating in the different

indexings of the four-dimensional Levi-Civita tensor $\epsilon^{i\alpha\beta\gamma}$; either α or β or γ can be 0. Additionally, three ways to arrange products of momenta (how the indices of variables k, l, and q are matched) emerge from the products of three spin-space matrices (3.26). Combined together, there are nine different terms contributing to the isoscalar magnetic form factor. Putting them together and Fourier transforming yield:

$$\widetilde{G}_M \underset{\substack{m_\pi \to 0 \\ r \to \infty}}{=} \frac{3}{2^9 \pi^5} \frac{1}{f_\pi^3} \left(\frac{g_A}{f_\pi} \right)^3 \frac{\Delta}{r^7}. \tag{3.27}$$

3.4 Summary

In this chapter, a particular ratio of long-distance properties of position space nucleon form factors—Eq. (3.1)—was derived in the large N_c variant of chiral perturbation theory. By calculating it directly, the model-independent nature of the proposed relation was shown. It was discussed that the key feature of large N_c physics in this context is the presence of the Δ isobar, which is degenerate with nucleon when $N_c \to \infty$. Attention was also paid to the ordering of limits since, in general, large N_c, chiral, and long distance limits do not commute; this turned out to be the case for the ratio Eq. (3.1).

Chapter 4: Nucleon-nucleon scattering

In this chapter, nucleon-nucleon scattering is analyzed from the point of view of the large N_c limit. In particular, it is shown that the quantity with the well defined N_c scaling is the logarithm of the elastic scattering S-matrix. It is argued that it is proportional to N_c. From this result, several relations for the nucleon-nucleon cross sections are also derived. A majority of results discussed in this chapter is based on the analysis of Refs. [53, 54].

4.1 Motivation

In many ways, the most basic feature of nuclear physics is the interaction of two nucleons. It is necessary to understand this "simple" process first before trying to move to few- and many-body calculations. In the light of the large N_c limit, a key issue is how does one characterize the interaction in a way which yields a well defined large N_c behavior. The most straightforward way is via a nucleon-nucleon potential [55,56]. It follows from the standard counting rules that the strength of the potential is proportional to N_c while the range of the interaction is fixed. However, using a potential in the discussion of the N_c scaling has one conceptual caveat: potentials are not physical quantities. They are merely inputs into a specific formalism

for calculating scattering observables or binding energies—into the formalism of the Schrödinger equation. Naturally, it is important to know the N_c behavior of physical quantities rather than unphysical ones. Thus, the nucleon-nucleon scattering observables are of interest in this analysis.

Nucleon-nucleon scattering process was first analyzed by Witten [2] in the framework of the time-dependent mean-field theory. He made an interesting observation that a smooth large N_c limit is obtained if one takes nucleons' momenta to be of order N_c. In other words, the velocity must be kept fixed since the mass of the nucleon is of order N_c. This regime is called Witten kinematics. More recently, the spin-flavor dependence of the total cross section was discussed [57], and progress in this field continues.

The quantity on which this chapter focuses is the S-matrix for elastic scattering. Despite the fact that the interaction is strong (proportional to N_c), the S-matrix element in any given partial wave clearly cannot be proportional to N_c, since such scaling would violate unitarity if $N_c \to \infty$. It was proposed by Cohen [58] that the correct quantity to study is the logarithm of the S-matrix elements, which scales with N_c:

$$\log\left(S^{NN}_{J;h'h}\right) = 2i\,\delta^{\rm Re}_{J;h'h} - 2\,\delta^{\rm Im}_{J;h'h} \sim N_c\ , \tag{4.1}$$

where J is the total angular momentum and h and h' specify initial and final spin states of colliding nucleons.

In the first part of this chapter, several heuristic arguments are presented in favor of Eq. (4.1). In the second part of this chapter, it is shown that the proposed

scaling of the S-matrix elements has direct consequences for the total cross section of nucleon-nucleon scattering in Witten kinematics. Directly from (4.1), the following formula is derived:

$$\sigma^{\text{total}} = \frac{2\pi \, \log^2(N_c)}{m_\pi^2}\,, \tag{4.2}$$

with corrections of relative order $\log(\log(N_c))/\log(N_c)$. Moreover, it will be shown that the relative fraction of the total cross section corresponding to inelastic processes is exactly 1/8—although one must reinterpret precisely what is meant by "inelastic" in the large N_c world.

4.2 S-matrix elements at large N_c

In this section, several arguments suggesting Eq. (4.1)

$$\log\left(S^{NN}_{J;h'h}\right) = 2i\,\delta^{\text{Re}}_{J;h'h} - 2\,\delta^{\text{Im}}_{J;h'h} \sim N_c \tag{4.3}$$

are presented. Note that none of them are fully rigorous in a mathematical sense. However, when combined they comprise a rather compelling evidence for the validity of Eq. (4.1)

For simplicity and clarity of the presented arguments, the effects of spin and isospin of the nucleons are neglected. It is equivalent to a statement that one works with even N_c; in such case, all quarks are paired and there is no odd quark left to make an overall spin and isospin finite. This simplification is justifiable if one is interested in the leading N_c scaling behavior. It was shown in [53] that the inclusion of finite spin and isospin degrees of freedom does not alter the leading N_c behavior. The logic of the argument is that having finite spin and isospin, the

S-matrix operator is no longer a pure number but rather it is a 4-by-4 dimensional matrix in a spin-isospin space describing all possible transitions between initial and final states. Since the S-matrix is, by definition, unitary, it can be in principle diagonalized. Effectively, the diagonalization turns the problem from four coupled-channels into four uncoupled channels. Each of these channels corresponding to some linear combination of spins and isospins is then treated separately. Since the N_c scaling of all the relevant quantities remains the same—essentially semi-classical nature of the large N_c limit cannot be changed by purely quantum effects of spin and isospin—the result remains the same.

4.2.1 Naive argument from the definition of the S-matrix

To understand why one might expect the logarithm of the S-matrix elements to be proportional to N_c, first look at the formal definition of the S-matrix [59]:

$$\hat{S} = \lim_{t\to\infty} \; e^{i\hat{H}_{(0)}t} \; e^{-2i\hat{H}t} \; e^{i\hat{H}_{(0)}t} \, . \tag{4.4}$$

In (4.4), $\hat{H}$ is the full QCD Hamiltonian that encodes the interaction of hadrons, and $\hat{H}_{(0)}$ is the free Hamiltonian. In the case of nucleon-nucleon scattering (only strong interaction are considered, all electromagnetic effects are neglected since only the effects of large N_c behavior are studied in this dissertation), the free Hamiltonian, by definition, governs the propagation of non-interacting hadrons. It is free—in the sense of lacking inter-particle interaction—at the level of hadrons. However, it is a very complicated object at the level of quarks and gluons—the fundamental degrees of freedom of quantum chromodynamics. Although both $\hat{H}$, and $\hat{H}_{(0)}$ are

fairly complicated objects, some of their properties may be deduced immediately, particularly their behavior at large N_c. According to the standard counting rules [2], both the full Hamiltonian, $\hat{H}$, and the non-interacting Hamiltonian, $\hat{H}_{(0)}$, are linearly proportional to N_c in Witten kinematics (which is the regime of interest). Moreover, their difference $\hat{H}_I = \hat{H} - \hat{H}_{(0)}$ (characterizing the interaction among hadrons) is also of order N_c [2, 56]. Summarizing the knowledge of large N_c behavior of all relevant quantities, one can rewrite the S-matrix into the following form:

$$\hat{S} = \lim_{t\to\infty} \; e^{iN_c\hat{\tilde{H}}_{(0)}t} \; e^{-2iN_c\left(\hat{\tilde{H}}_0+\hat{\tilde{H}}_I\right)t} \; e^{iN_c\hat{\tilde{H}}_{(0)}t} \, . \tag{4.5}$$

If all entries in Eq. (4.5) were ordinary c-numbers and not quantum operators, the overall N_c scaling of the exponent would be obvious and Eq. (4.1) immediately satisfied. The fact that the objects under consideration are quantum operators rather than ordinary c-numbers makes any attempt at a rigorous treatment complicated. Nevertheless, the idea of linear N_c scaling in the exponent of the S-matrix relying only on standard N_c counting properties is at least highly plausible.

The range of the interaction is independent of N_c just as the velocity of scattering nucleons in Witten kinematics. Thus, the time of the collision—i.e. the time in which the difference between full and free Hamiltonians plays a significant role—is also independent of N_c. This observation combined with the fact the the overall strength of the interaction is proportional to N_c, leads to a strong belief that the overall effect of the interaction is also proportional to N_c. Thus, since the interaction effect stands in the exponent of the definition of the S-matrix, it is natural to expect the logarithm of the S-matrix to be proportional to N_c, as postulated in Eq. (4.1).

Obviously, the argument discussed above is more a heuristic suggestion than a rigorous mathematical statement. However its logic is quite clear. Thus, it is very suggestive and encouraging to pursue the idea of logarithmic scaling of the S-matrix.

4.2.2 A toy Hamiltonian model

The second argument in favor of Eq. (4.1) is slightly more rigorous. It is based on Hamiltonian dynamics and the semi-classical approximation. For simplicity, a toy model with only elastic scattering is considered here; the effects of inelastic channels will be discussed later. Recall that the semi-classical regime is natural when working with baryons in the large N_c limit. Additionally, it is also assumed that all of the quantities involved have the same N_c scaling as is expected in large N_c QCD and Witten kinematics. Specifically, the nucleon mass and the strength of the interaction are of order N_c, whereas velocity and range of the interaction are independent of N_c. The only relevant degrees of freedom are the three components of the relative distance and the three components of relative momentum in the center-of-mass frame of reference. Combining these building blocks together, it is easy to see that the Hamiltonian is of the form:

$$H\left(\vec{q},\vec{p}\right) = N_c\,\tilde{H}\left(\vec{q},\tilde{\vec{p}}\right)\ , \tag{4.6}$$

where $p = N_c\,\tilde{p}$. Before proceeding to the quantum analysis, it is useful to analyze the nucleon-nucleon scattering in classical physics first. A typical scattering process is illustrated in Fig. 4.1. The classical canonical equations of motion are:

$$\dot{q}_i = \frac{\partial \tilde{H}}{\partial \tilde{p}_i} \quad , \quad \dot{\tilde{p}}_i = -\frac{\partial \tilde{H}}{\partial q_i}\ . \tag{4.7}$$

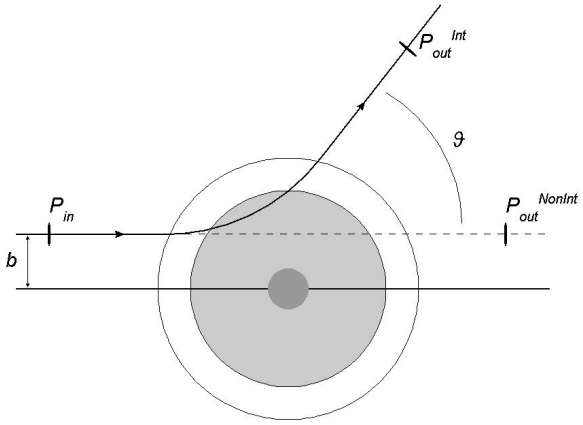

Figure 4.1: A schematic picture of classical scattering.

The crucial thing to realize in Eqs. (4.7) is that the classical equations of motion are independent of N_c. From here, it directly follows that classical trajectories do not depend on N_c in the process of scattering nucleons. The statement holds for fixed initial impact parameter b and momentum $\tilde{p}$ (such as those in Fig 4.1). This restriction, however, does not lead to any loss of generality since it precisely correspond to the standard N_c counting rules. In classical physics, one can calculate the differential cross section:

$$\frac{d\sigma^{\text{classical}}}{d\Omega} = \frac{b(\theta)}{\sin(\theta)}|b'(\theta)|\,. \tag{4.8}$$

In (4.8), $b(\theta)$ is the relation between the scattering angle and the incident impact parameter. This function depends on the specifics of the system's dynamics and can be, in principle, calculated from the equations of motion (4.7). Clearly, the classical differential cross section (4.8) is also independent of N_c.

In quantum mechanics, on the other hand, the differential cross section is determined by the S-matrix which can depend on N_c. Specifically, the N_c dependence

can be (and it will be shown below that it is the case) contained in the phase information that has no classical analogue. In the semi-classical approximation to the Schrödinger equation, the phase information can be obtained by calculating Hamilton's action integral along the classical path.

A suitable form of the classical equation of motion, which determines the classical trajectory, is a partial differential Hamilton-Jacobi equation:

$$H(\vec{q}, \nabla_q S(\vec{q}, \vec{a}) = E_0 \ . \tag{4.9}$$

In (4.9), $\vec{a}$ is a set of constants of motion fixed by initial conditions. For trajectories which solve classical equations of motion, the action is given by the integral along this trajectory

$$S(\vec{q}, \vec{a}(p, b)) = S_0 + \int_{\vec{q}_0}^{\vec{q}_f} \vec{p} \cdot d\vec{q}. \tag{4.10}$$

The initial conditions are (classically) given by an impact parameter b and an initial momentum p; S_0 represents the fact that the action is classically defined up to an additive constant; $\vec{q}_0$, the starting point of the integration, and $\vec{q}_f$, the ending point of the integration are chosen to be well away from the interaction region. An important conserved quantity characterizing the scattering process is the angular momentum, classically defined as $L = b\,p$. Quantum mechanically, on the other hand, the angular momentum corresponds to a specific partial wave. In the partial wave decomposition, the S-matrix is fully determined by a single number—the phase shift δ_L—in each partial wave, $S_L = e^{2i\delta_L}$. In the semi-classical approximation, the phase shifts δ_L are given by the difference between the phase corresponding to the actual motion and the phase corresponding to motion when particles do

not interact, i.e. by the difference between the free and the interacting processes. Doing the formal analysis, paths have to be chosen in such a way that they both begin with particles far away from each other, both correspond to the same impact parameter b and momentum p, and both have the same initial and final distance from the scattering center. Then, the phase shift in one particular angular momentum channel reads:

$$\delta_L = \lim_{R\to\infty} \frac{1}{2} \left(\int_{\hat{n}_0^R R}^{\hat{n}_f^R R} \vec{p} \cdot d\vec{q} - 2\frac{L\,R}{b} \right) , \tag{4.11}$$

where $\hat{n}_0^R$ and $\hat{n}_f^R$ are unit vectors specifying the initial and final directions. Note that each term in Eq. (4.11) diverges as $R \to \infty$ but their difference remains finite.

The semi-classical formula for the phase shifts, δ_L, can be analyzed from the point of view of the large N_c limit too. In Witten kinematics, momentum, p, as well as the angular momentum, $L = b\,p$, are proportional to N_c. Moreover, the range of the interaction, i.e. the region where the actions of interacting and free particles differ is independent of N_c just as are the trajectories. Thus, the N_c scaling factorizes in Eq. (4.11) since neither the impact parameter nor any of the distances depend on N_c:

$$\delta_L = \lim_{R\to\infty} \frac{1}{2} N_c \left(\int_{\hat{n}_0^R R}^{\hat{n}_f^R R} \vec{\tilde{p}} \cdot d\vec{q} - 2\frac{\tilde{L}\,R}{b} \right) . \tag{4.12}$$

The phase shift δ_L occurs in the exponent of the S-matrix elements, $S_L = e^{2i\delta_L}$. Since the phase shift was shown to be proportional to N_c, it directly follows that the logarithm of the S-matrix is also proportional to N_c as postulated in Eq. (4.1).

4.2.3 A toy potential model

In this section, S-matrix elements in a simple model are computed; in this model, the nucleons are treated non-relativistically and their interaction is described by a local central potential. This is a specific incarnation of a general Hamiltonian model discussed in the previous section. The values of phase shifts δ_L are calculated directly from the Schrödinger equation with a central local potential. The N_c scaling of all the relevant quantities is the same as in the large N_c QCD in Witten kinematics:

$$M = N_c\tilde{M}\,,\ V(r) = N_c\tilde{V}(r)\,,\ p = N_c\tilde{p}\,,\ L = N_c\tilde{L}\,, \tag{4.13}$$

where quantities with tilde do not depend on N_c. In non-relativistic scattering, the S-matrix is fully determined by the phase shifts in each individual partial wave:

$$S_L = e^{2i\delta_L}\ . \tag{4.14}$$

To determine the relationship between the scaling of the potential and the scaling of the scattering amplitude one must study the dynamics of the system—solve the Schrödinger equation:

$$\left(-\frac{1}{M}\Delta + V(r)\right)\Psi(\mathbf{x}) = E\Psi(\mathbf{x})\ , \tag{4.15}$$

where the reduced mass is $M/2$. The partial wave decomposition is done using the standard expansion in spherical harmonics $Y_{Lm}(\Omega)$:

$$\Psi(\mathbf{x}) = \sum_L R_L(r)Y_{Lm}(\Omega)\,. \tag{4.16}$$

Since the spherical harmonics are eigenfunctions of the orbital angular momentum $\Delta_\Omega Y_{Lm} = L(L+1)/r^2 Y_{Lm}$, the Schrödinger equation separates to a set of ordinary

differential equations for radial part for each L. The radial part of the Schrödinger equation reads:

$$R_L''(r) + \frac{2}{r}R_L'(r) + \left(k^2 - \frac{L(L+1)}{r^2} - MV(r)\right)R_L(r) = 0\,. \tag{4.17}$$

If one parametrizes the solution of the radial Schrödinger equation as $R_L(r) = e^{i\Phi_L(r)}\psi_L(r)$, it can be shown self-consistently that in the large N_c limit the phase of the wave function—$\Phi_L(r)$—is proportional to N_c whereas the amplitude $\psi_l(r)$ is a slowly varying function. Specifically, for $\Phi_L(r) = N_c\tilde{\Phi}_L(r)$, the leading order part of the radial Schrödinger equation becomes:

$$N_c^2\left(\left(\frac{\mathrm{d}\tilde{\Phi}_L(r)}{\mathrm{d}r}\right)^2 = \tilde{k}^2 - \frac{\tilde{L}^2}{r^2} - 2\tilde{\mu}\tilde{V}(r)\right)\,. \tag{4.18}$$

This decomposition of a wave function to an amplitude and a phase is analogous to the WKB approximation. This observation is consistent with our earlier claim that the large N_c limit is equivalent to the semi-classical regime. The phase of the wave function is given by the integral:

$$\tilde{\Phi}_L(r) = \int_{r_0}^{\infty}\sqrt{\tilde{k}^2 - \frac{\tilde{L}^2}{r^2} - 2\tilde{\mu}\tilde{V}(r)}, \tag{4.19}$$

where r_0 is a classical turning point $r_0 = L/k = \tilde{L}/\tilde{k}$ (note that the turning point is independent of N_c). The phase shift δ_L is given, by definition, as a difference between an actual phase of the wave function obtained with the interaction and a phase of the free wave function obtained without an interaction, i.e. with $V = 0$:

$$\delta_L = N_c\int_{r_0}^{\infty}\left(\sqrt{\tilde{k}^2 - \frac{\tilde{L}^2}{r^2} - 2\tilde{\mu}\tilde{V}(r)} - \sqrt{\tilde{k}^2 - \frac{\tilde{L}^2}{r^2}}\right)\,. \tag{4.20}$$

From Eq. (4.20), it is obvious that the phase shift (i.e. the logarithm of the S-matrix) is proportional to N_c in a non-relativistic potential scattering. This is in agreement with the proposed relation (4.1).

The argument above is valid regardless of the form of the potential, the only requirement (besides analytical properties and fast-enough falloff) is that its strength scales linearly with N_c and its range is independent of N_c. Specifically, it holds in a situation where the potential is complex. Recall that the imaginary part of the potential reflects the fact that the system can undergo a transition to a different channel during the scattering process, for example two nucleons can turn into two nucleons and a pion. If one is able to show that the imaginary part of the nucleon-nucleon potential—i.e. the potential responsible for inelastic processes—is also of order N_c^1, then one has already shown that the scaling of the S-matrix is as proposed in Eq.(4.1) even when the inelasticities are taken into account. The more general discussion of how to incorporate the inelastic processes into the argument will be done in the remainder of this section.

4.2.4 Inelastic scattering I—complex potential

This section deals with the problem that was only touched on briefly in the previous sections—that nucleon-nucleon scattering may lead to inelastic processes. Nucleon-nucleon scattering is inherently a field-theoretical problem; it is possible to create other particles (mesons, mostly pions). This is most easily represented by the use of a complex potential, i.e. a potential with a nonzero imaginary part. On

one hand, the imaginary part in the potential leads to a violation of unitarity and a loss of flux. On the other hand, it is precisely what one expects during inelastic processes—the flux is lost from an elastic channel into other channels (for example a state with nucleons and pions). Since the specifics of the inelastic channels are not important in this analysis, the use of quantum mechanics with a complex potential is sufficient.

A few words should be dedicated to explain what is meant by elastic and inelastic channels. In the large N_c limit, nucleon and Δ are degenerate; more specifically, the whole tower of states with $I = J$ form a ground state multiplet in QCD when $N_c \to \infty$ [4–9]. Thus, the transition from two nucleon state to a two Δ state, for example, requires no extra energy cost since their masses are equal at leading order. On the other hand, the process when new particles (mesons) are created is principally different, since it requires certain energy transfer for new particles to be created. Thus, what is meant by an elastic process is that no additional particles are created—however, the transformation of initial nucleons into other members of the ground state multiplet is allowed.

In the previous section, it was derived that the standard N_c counting rules lead directly to the linear scaling of phase shifts in the framework of the Schrödinger equation. The argument presented above relies critically on the fact that the strength of the potential is proportional to N_c. Note that Eq. (4.20) holds regardless of whether the potential is purely real or whether it has a non-zero imaginary part—as long as they are both proportional to N_c. Although the linear scaling is known to hold for the real part of the potential (the one driving the dynamics of the elastic

processes), the situation for the imaginary part of the potential (the one responsible for inelastic behavior) requires further investigation. Obviously, it is very natural to assume that the imaginary part of the nucleon-nucleon potential follows the same scaling rules as the real part; but a deeper analysis is required to put this belief on a firmer footing. In this section, several arguments based on a meson-exchange reformulation of the potential problem are presented, also, several arguments based on a quark-gluon picture of nucleon scattering that support the claim that the imaginary part of the potential is proportional to N_c are discussed.

It is useful to review some basic principles of meson-exchange picture of the nucleon-nucleon potential. It was argued long ago that, at least at lowest order in a perturbative expansion (Born approximation), the potential between particles is equivalent to an exchange of a particle in the field-theoretical calculation. This way of thinking can be traced back to the 1940s to the work of Hideki Yukawa [60]. It is worth noting that various successful nucleon-nucleon potentials [61–63] are motivated by a meson exchange picture. The forthcoming analysis is done using scalar mesons instead of pseudoscalar ones. The reason for this is the simplicity and clarity of the argument; the basic N_c scaling rules are the same and the algebra is simpler and easier to follow.

The Feynman diagram representing a one-meson exchange is shown in Fig. 4.2. The N_c scaling of this diagram is given by the N_c scaling of the coupling constant in the pion-nucleon-nucleon vertex, which is of order $g \sim N_c^{1/2}$ [2]. There are two vertices in Fig. 4.2, which make the amplitude coming from this diagram to be of order N_c. Note that this is precisely the scaling a nucleon-nucleon potential should

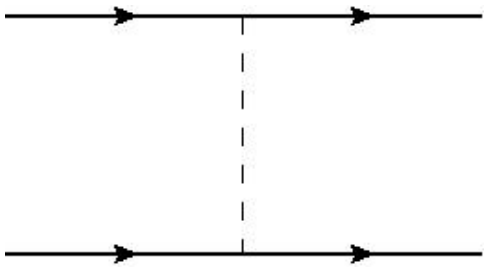

Figure 4.2: Feynman diagram of the one meson exchange part of the potential.

obey according to the standard large N_c counting rules. Note also that for elastic scattering (no energy transfer), kinematics forbid the existence of an intermediate state of two baryons and a meson. Thus, the imaginary part of the amplitude—and also of the potential—is naturally zero for the one-meson exchange diagram.

On the other hand, the situation gets more complicated at the level of two meson exchange. This was discussed extensively in a paper by Banerjee et. al [64]. Relevant diagrams are summarized in Fig. 4.3—the box diagram and the crossed diagram. The naive counting of powers of N_c leads to an overall scaling factor of N_c^2; it is a problem, since the potential should be of order N_c^1. However, a deeper analysis resolves the apparent problem in two steps. First, one observes that the baryon-pole contribution to the amplitude of the box diagram is exactly of the same form as the first iterate of a Lippmann-Schwinger equation with a potential given by one meson exchange from Fig. 4.2. Iterates do not contribute to the potential in order to avoid double counting. Since potential is the quantity that should be of order N_c, the first iterate—which formally contains two powers of potential—is then of order N_c^2, as it should be. In the second step, one is able to show that the meson-pole contribution of the box diagram (the retardation effect) and of the

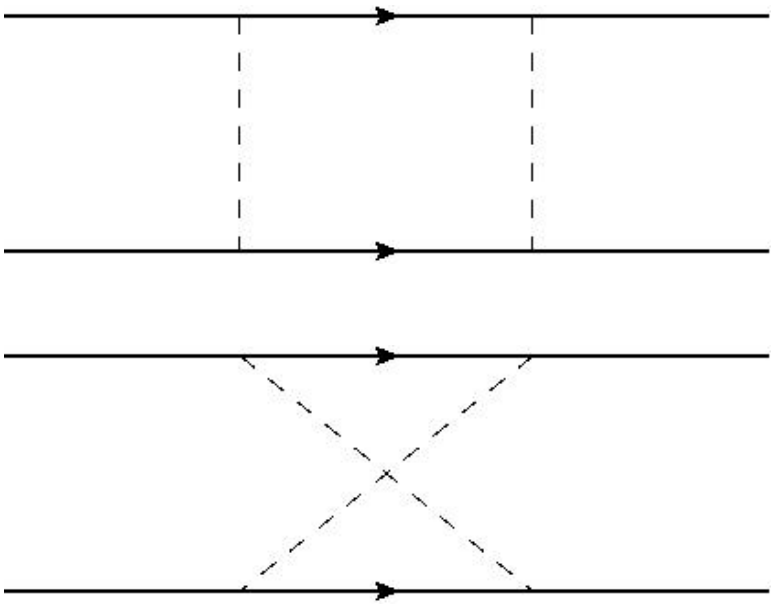

Figure 4.3: Feynman diagrams of the two-meson exchange interaction, one boxed and one crossed.

crossed diagram are equal to each other up to an overall sign at leading order in the $1/N_c$ expansion. Thus, they subtract exactly and the remaining piece, which is not an iterate and therefore genuinely enters the potential, have the desired N_c behavior. However, the exact cancellation in the leading order occurs only in a non-relativistic regime for $v \ll 1$. Consequently, the focus on the non-relativistic dynamics is explained.

In the next step—at the level of three-meson exchange—the connection between the potential picture and the meson-exchange picture becomes much less apparent, as discussed in [65]. However, a sensible definition of the potential can be made so that it scales in a consistent way [66] due to wide cancellations between various diagrams. These cancellations are similar to those between the retardation

Figure 4.4: Feynman diagram of the one meson loop correction to the nucleon propagator.

effects in the box diagram and the crossed diagram at the level of two pion exchange. However, these cancellations are far from obvious and beyond the scope of this dissertation.

In the light of the previous discussion, the imaginary part of the potential emerges naturally. All diagrams in Figs. 4.2 and 4.3 are purely real. However, one can construct a two-meson exchange diagram with a non-zero imaginary part. Thus first order, in which an imaginary part in the potential emerges, is two-meson exchange.

To get an idea of how an imaginary part emerges in the amplitudes, look at the simplest possible one loop diagram: the one meson loop correction to a baryon propagator, which is shown in Fig. 4.4. In the non-relativistic regime, the loop integral reads

$$\begin{aligned} I(k^0 - M) &= \int \frac{\mathrm{d}^4 l}{(2\pi)^4} \frac{i}{l^2 - m_\pi^2 + i\epsilon} \frac{i}{k^0 - M + l^0 + i\epsilon} \\ &= \mathrm{Re}\, I + i\,\pi\,\theta(k^0 - M - m_\pi)\,, \end{aligned} \tag{4.21}$$

where k^0 is the zeroth component of the nucleon four-momentum—i.e. the nucleon energy. One sees directly from (4.21) that the integral acquires an imaginary part when the energy is sufficient to excite a meson—i.e. the total energy exceeds the

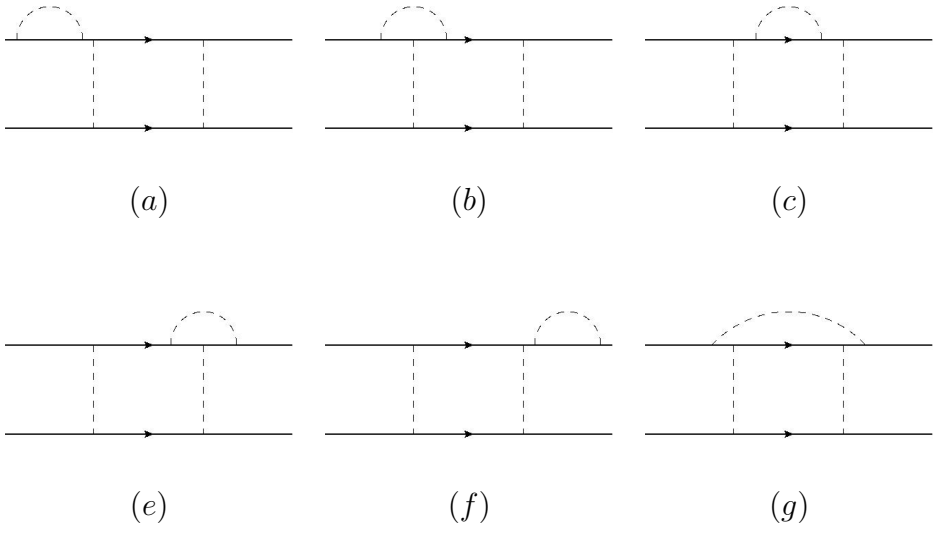

Figure 4.5: A selection of Feynman diagrams with non-zero imaginary part. They represent a renormalization of wave function, propagator, one pion vertex and two pion vertex.

sum of the nucleon and pion masses. It is in agreement with the naive picture of what an imaginary part of the amplitude means—a possibility of creating new particles.

To get a nucleon-nucleon scattering amplitude with a non-zero imaginary part, it is natural to consider two-meson exchange diagrams with the meson loop (which resembles self-energy) on one of the nucleons. A subset of these diagrams is shown in Fig. 4.5—only box diagrams with self-energy correction on the upper nucleon are shown. Each individual diagram is of superleading order—naively, they all are of order N_c^3 since each of them contain six meson-baryon-baryon vertices each of which are of order $N_c^{1/2}$. However, various cancellations of the spirit discussed above, as well as renormalization of mass, vertices, and wave functions occur in order to get the correct form of the leading N_c behavior. These cancellations are highly non-trivial

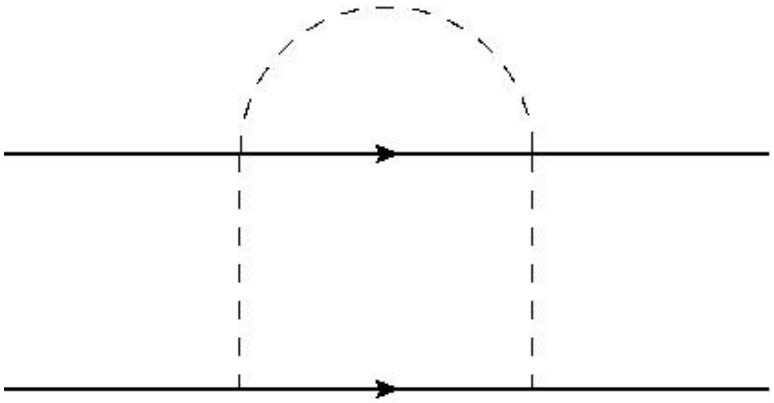

Figure 4.6: Feynman diagram which contributes to the imaginary part of the potential in the leading order.

and beyond the scope of the presented work.

However one can draw a simple diagram that is already of order N_c^1 and which has a nonzero imaginary part. A typical diagram is shown in the Fig. 4.6. By standard Witten counting, it scales as N_c^1. The reason for this is that the meson loop is coupled to the nucleon via a 2-meson-2-baryon vertex (seagull vertex)—the large N_c behavior of this type of interaction is N_c^0. Thus, both the real and the imaginary parts of the potential inferred from this diagram are proportional to N_c. It was shown earlier that a potential which is linearly proportional to N_c (both the real and the imaginary part) directly leads to a phase shift proportional to N_c and thus to Eq. (4.1).

The previous discussion was formulated in the language of mesons and baryons. Next, an argument that the same scaling behavior is also natural at the underlying level of quarks and gluons is presented.

Start by looking at the self-energy diagram containing meson loops such as

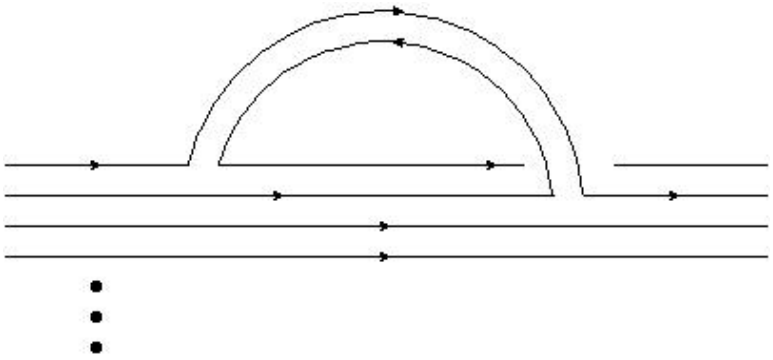

Figure 4.7: A leading order diagram for the nucleon self energy at the level of quarks and gluons.

the one in Fig. 4.7—this diagram is analogous to the one in Fig. 4.4. Again, with appropriate kinematics, the imaginary part emerges. In Fig. 4.8, diagrams analogous to those in Fig. 4.6 are shown. The quark-antiquark pairs, which play the role of the exchanged meson, couple to the same quark line in the upper nucleon in the left diagram, and to a different quark line in the right diagram, respectively. Additionally, the two distinct quark lines in the right diagram must be connected via a gluon to preserve color neutrality. The additional combinatoric factor N_c in the right diagram coming from the fact that the exchanged mesons couple to different quark lines is exactly compensated by an extra factor of $g^2 \sim 1/N_c$ coming from the exchange of a gluon. Thus, both diagrams scale the same way. Overall, it is a simple exercise in N_c counting to verify that both of these diagrams are of order N_c.

Generically, it can be shown that any process with two incoming nucleons and two outgoing nucleons can be drawn as a connected diagram that is of order N_c^1. The most general interaction is illustrated by the "blob" in Fig. 4.9. This "blob" is

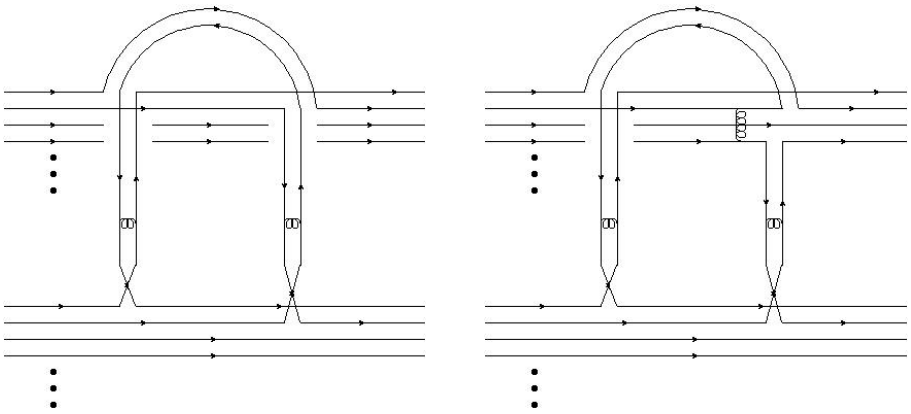

Figure 4.8: Diagrams at the quark-gluon level analogous to Fig. 4.6.

identified with the potential. The argument for the linear N_c scaling comes from the combinatoric properties at the quark-gluon level. Simply, for every additional gluon exchange that is added into the diagram, a combinatoric factor emerges and these two effects cancel exactly. One example of this was discussed above comparing two diagrams in Fig. 4.8. Combining two diagrams in a ladder (as in Fig. 4.10) can be clearly interpreted as an iteration of a potential, if the baryons propagating between "blobs" are nucleons.

A different situation occurs, when one (or both) of the baryons in the intermediate state is not a nucleon but some of its excited states—the situation is illustrated in Fig.4.11, where the non-nucleon in indicated by the zigzag line. It can be shown at a quark level, that any "blob", whose one (or more) leg is not a nucleon is at least $1/\sqrt{N_c}$ suppressed compared with "blob" with only nucleon legs. However, since one is interested in the nucleon-nucleon scattering, in order to have two nucleons in the outgoing state, the process of producing an excited baryon in the first exchange must always be accompanied by a de-excitation in the second exchange. The com-

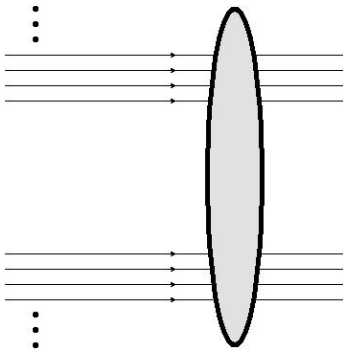

Figure 4.9: A "blob" of general nucleon-nucleon interaction.

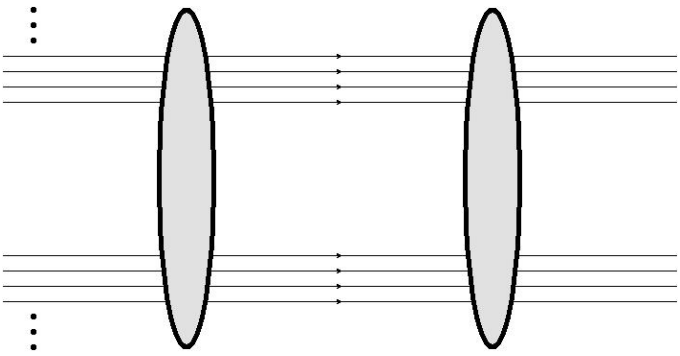

Figure 4.10: A ladder of two consecutive interactions, i.e. the iteration of a potential.

bined process is of order N_c and can be re-absorbed into the original blob of Fig. 4.9. Thus, the scaling of the potential is always of order N_c^1—of both the real and the imaginary part. As was discussed in the previous section, the linear scaling of the potential directly implies the linear scaling of the phase shifts leading directly to Eq. (4.1).

4.2.5 Inelastic scattering II—meson bremsstrahlung

Here, a conceptually different approach towards a nucleon-nucleon scattering in the large N_c limit is presented. Again, the goal is to determine the scaling of

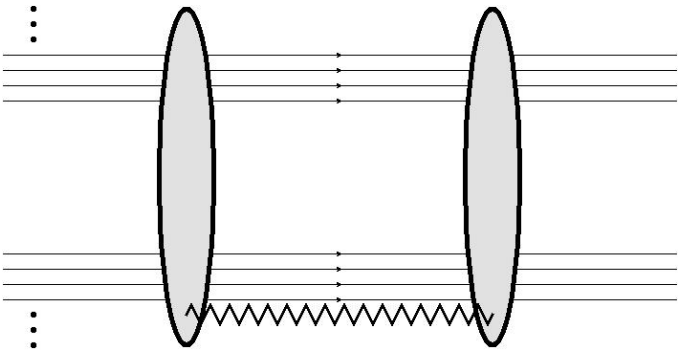

Figure 4.11: A diagram where a baryon in the intermediate state is not a nucleon, but some of its excitations.

the logarithm of the elastic scattering S-matrix; specifically, that it is linearly proportional to N_c (4.1). The argument discussed below is based on the analysis of the energy dissipated into mesons during a typical inelastic process. This process can be viewed as an analog to a classical electromagnetic bremsstrahlung: a process when electron undergoing some accelerated motion emits an electromagnetic radiation. Nucleons undergo an accelerated motion during their collision. Therefore the analogy is relatively straightforward.

Since nucleons are heavy (mass of the nucleon is of order N_c), their motion can be treated classically in a sense that they follow a certain trajectory determined by the equations of motion. Then, a moving nucleon can be viewed as a classical source for a meson field (just as before, the analysis is done with a scalar meson instead of a pseudoscalar, since the technical aspects are simpler and the N_c scaling is the same).

The starting point for the discussion is a Lagrangian for a meson field in the

presence of a classical source:

$$\mathcal{L} = \frac{1}{2}\left(\partial_\mu \phi\right)^2 - \frac{1}{2} m^2 \phi^2 - g\, J(x)\phi \tag{4.22}$$

where the scalar field's coupling to the external current g scales as $N_c^{1/2}$ [2]—this point is crucial for the upcoming analysis. The solution of the equation of motion for the meson field is:

$$\phi = g \int \mathrm{d}^4 x' \Delta_R(x - x') J(x') \ , \tag{4.23}$$

where $\Delta_R(x - x')$ is the retarded Green's function and $J(x')$ represents the classical trajectory followed by the baryon in consideration.

On the classical level, the energy flux is given by the $(0i)^{\text{th}}$ component of the stress-energy tensor (the object equivalent to a Poynting vector for the electromagnetic field):

$$S_i = \dot{\phi}\, \phi_{,i} \, . \tag{4.24}$$

The overall outgoing energy is calculated by integrating over a surface surrounding the area of the collision. The exact formula for the outgoing energy flux is quite complicated since it depends on the specifics of the trajectory followed by the scattered nucleon. However, the N_c scaling can be deduced straightforwardly. The expression for the energy flux S_i (4.24) is quadratic in the meson field ϕ; and meson field ϕ (4.23) is linear in the coupling constant g. The nucleon trajectories are independent of N_c as was discussed more extensively earlier in this chapter, and therefore the coupling constant g is the only N_c dependent variable in the problem. From the

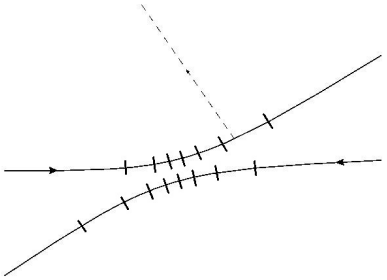

Figure 4.12: A schematic picture representing a classical path of the baryon and an emission of one pion from one segment of the path.

scaling shown above, it directly follows that the energy flux is proportional to N_c:

$$\int_{\Omega} \vec{S} \sim g^2 \sim N_c \,. \tag{4.25}$$

Eq. (4.25) was derived using the classical field theory point of view. The proper quantization of the filed (4.23) is inherently complicated; however, deducing the N_c scaling is possible using the following argument. The total energy carried by the field is of order N_c^1. In Witten kinematics, both the mass and the energy of a meson are of order N_c^0. Thus, in order to get the total energy of mesons emitted by a baryon during accelerated motion to be of order N_c^1, the number of particles must be of order N_c^1.

The next step in the analysis of meson emission is to divide the baryon trajectory into S small segments. These segments are chosen in such a way that the probability of emitting one meson in this segment p is small and the probability of emitting more than one meson is negligible. The schematic picture of this is shown in Fig. 4.12. Since the total number of emitted mesons is of order N_c, the N_c scaling

of S and p must satisfy:

$$N_{meson} = S\,p \sim N_c\,. \tag{4.26}$$

One can parametrize the scaling of quantities S and p in a following way:

$$S \sim (N_c)^{1+\alpha}\ ,\ \ p \sim (N_c)^{-\alpha} \tag{4.27}$$

with α being a positive number. The parameter α must be positive in order to interpret p as a probability in the large N_c limit. Such a choice is also in agreement with the picture of the nucleon trajectory divided into many small segments with a small probability of meson emission in each segment.

The original goal is to get an insight into the elastic process, i.e. the process where no mesons are emitted. Naturally, the probability that no meson is emitted in one segment of the trajectory is $(1-p)$. If one assumes that the attempts to emit a meson in the neighboring segments of the trajectory are uncorrelated, the overall probability that zero mesons are emitted is:

$$P_{el} = (1-p)^S \sim \left(1 - \frac{1}{(N_c)^\alpha}\right)^{N_c^{\alpha+1}} \xrightarrow[N_c\to\infty]{} e^{-N_c}\,. \tag{4.28}$$

From the quantum mechanical point of view, the probability of the process is given by the square of the S-matrix; and

$$\log S \sim \log P_{el} \sim N_c\,. \tag{4.29}$$

This result agrees with a formula postulated in Eq.(4.1) presenting another argument suggesting that the linear N_c scaling of the logarithm of the S-matrix holds.

However, there is a little problem in the picture presented above. What was discussed above is the probability that no meson is produced while nucleons follow

a scattering trajectory for which, on average, N_c mesons are produced. Naturally, the emission or non-emission of N_c mesons significantly changes the trajectory of nucleons due to the back-reaction. Fortunately, this effect does not change the obtained results as was more extensively discussed in Ref. [53].

4.3 Scattering cross section

In this section, another essential quantity characterizing nucleon-nucleon scattering will be analyzed—the scattering cross section. It was shown above that the phase shifts—the logarithms of the S-matrix elements—are proportional to N_c. Here, the consequences of this scaling (4.1) for the scattering cross sections are shown. Specifically, an analytic formula for the total cross section of nucleon-nucleon scattering at large N_c is derived:

$$\sigma^{\text{total}} = \frac{2\pi \, \log^2(N_c)}{m_\pi^2} \, . \tag{4.30}$$

Moreover, it is shown that the fraction of scattering corresponding to inelastic processes is exactly 1/8 in the large N_c limit.

The starting point of the discussion is the observation of previous section that the logarithm of the S-matrix element for the elastic processes is proportional to N_c in the large N_c limit (4.1). It is useful to write it in terms of phase shifts corresponding to respective partial waves:

$$\begin{aligned} S_L &= \exp\left(-2\delta_L^{\text{Im}} + 2i\,\delta_L^{\text{Re}}\right) \\ &= \exp\left(-2N_c\,\tilde{\delta}_L^{\text{Im}} + 2iN_c\,\tilde{\delta}_L^{\text{Re}}\right) \, , \end{aligned} \tag{4.31}$$

where the indices Im and Re indicate the imaginary and the real part of the phase shift, respectively. The convention that quantities with tilde above the letter have the N_c dependence is assumed.

The quantities of interest are inelastic and total cross sections. In the partial wave expansion, they read:

$$\begin{aligned}\sigma_{\text{in}} &= \frac{\pi}{k^2}\sum_L (2L+1)\left(1-|S_L|^2\right) \\ &\approx \frac{\pi}{k^2}\int \mathrm{d}L^2\left(1-|S_L|^2\right)\ , \qquad (4.32)\\ \sigma_{\text{tot}} &= \frac{\pi}{k^2}\sum_L (2L+1)\left(2-2\,\mathrm{Re}\,S_L\right) \\ &\approx \frac{\pi}{k^2}\int \mathrm{d}L^2\left(2-2\,\mathrm{Re}\,S_L\right)\ . \qquad (4.33)\end{aligned}$$

The approximation of the sum by the integral is justified by the fact that the system is in a semi-classical regime where many partial waves contribute. One can see that the formula for the inelastic cross section (4.32) depends only on the imaginary part of the phase shift. The real part of the phase shift leads only to a phase of the S-matrix element whose effect is eliminated by the absolute value in Eq. (4.32). This observation is natural in light of the previous discussion—it is the imaginary part of the potential, or phase shift, that determines the inelastic processes. On the other hand, the total cross section depends on both the real and imaginary parts of the phase shift.

First, consider what happens at a large value of N_c and a finite value of the imaginary part of the phase shift $\tilde{\delta}^{\text{Im}}$. In this case, the value of S_L is exponentially suppressed effectively turning the integrands in (4.32), and (4.33) to a constant,

which makes the integration over L particularly easy. Similarly, the contribution of S_L is negligible if the real part of the phase shift $\tilde{\delta}^{\mathrm{Re}}$ is large. Here, the suppression occurs due to a rapid oscillation of the complex exponential, and the integration is, again, easy since the integrand in (4.33) is effectively constant.

In principle, there is no bound on the Ls that contribute to the integral if N_c is infinity and thus the cross section is also infinity when $N_c \to \infty$. This is expected because nucleons in the extreme large N_c limit in Witten kinematics behave classically. Classical scattering always has infinite cross section (unless the potential has finite support). In other words, there is no forward scattering in classical physics—regardless of how far the particles are, their trajectory is always affected (although only infinitesimally) at all values of impact parameters.

However, quantum mechanically, for any finite value of N_c there is an upper bound on Ls which contribute. The reason for this is that the phase shifts S_L approach zero as $L \to \infty$. The bound is determined by the point where the S-matrix element is neither parametrically suppressed nor approximately unity. It occurs when the full phase shift δ ceases to be of order N_c and becomes of order one—formally $\delta \sim N_c^0$, or equivalently $\tilde{\delta} \sim N_c^{-1}$—then the S_L is neither suppressed nor does it oscillate rapidly. The phase shift in this regime becomes rapidly small making S_L close to unity. Therefore, the integrands in (4.32), and (4.33) rapidly become zero. This effectively sets the upper bound on the integrals. It will be shown below that the contribution to the cross section coming from angular momenta above this bound is negligible; it will also be shown that the effect of certain arbitrariness in the precise choice of the endpoint of the integration plays a subleading role.

The value of angular momentum where the phase shift becomes of order one is, in principle, different for the real and the imaginary parts of the phase shift. Denote the values $L_{\rm Im}$ and $L_{\rm Re}$ for the imaginary and real parts respectively. For the inelastic cross section (4.32), the upper bound is solely determined by the behavior of the imaginary part of the phase shift.

$$\sigma_{\rm in} = \frac{\pi}{k^2} \int_0^{L_{\rm Im}} {\rm d}l^2 = \pi \frac{L_{\rm Im}^2}{k^2} = \pi \; b_{\rm Im}^2 \,, \tag{4.34}$$

where $b_{\rm Im} = L_{\rm Im}/k = \tilde{L}_{\rm Im}/\tilde{k}$ is the impact parameter corresponding to the critical angular momentum. Note that the real part of the phase shift plays no role in the inelastic cross section. In light of the previous discussion, the upper bound for the total cross section (4.33) is given by either $L_{\rm Im}$ or $L_{\rm Re}$, whichever is bigger—i.e. none of the phase shifts may cause the suppression of the S-matrix term in the integrand of Eq. (4.32, 4.33):

$$\begin{aligned} \sigma_{\rm tot} &= \frac{2\pi}{k^2} \int_0^{\max(L_{\rm Im}, L_{\rm Re})} {\rm d}l^2 = 2\pi \, \frac{\max(L_{\rm Im}, L_{\rm Re})^2}{k^2} \\ &= 2\pi \, \max(b_{\rm Im}, b_{\rm Re})^2 \,, \end{aligned} \tag{4.35}$$

where the impact parameter $b_{\rm Re} = L_{\rm Re}/k = \tilde{L}_{\rm Re}/\tilde{k}$ is defined analogously to its imaginary counterpart.

In order to get the values of the cross sections, it is crucial to determine the values of the effective impact parameters $b_{\rm Im}$, and $b_{\rm Re}$. Their derivation is somewhat subtle and relies on several assumptions. Mainly that the relevant dynamics can be treated semi-classically.

Since the total cross section as well as the inelastic cross section are dominated

by the behavior at large partial waves—or equivalently, large impact parameters—one can treat the partial waves semi-classically [67]. In this regime, the phase shifts (4.20) are well approximated by:

$$\tilde{\delta} = -\int_{\tilde{L}/\tilde{k}}^{\infty} \frac{\tilde{\mu}\tilde{V}(r)}{\sqrt{\tilde{k}^2 - \frac{\tilde{L}^2}{r^2}}} \,, \tag{4.36}$$

for the model of Sect. 4.2.3. To be concrete, the short-distance nature of the strong interaction—or equivalently the fact that strong interaction is mediated by massive particles—allows one to consider the potential to be of the Yukawa form $\tilde{V}(r) = \sum_n C_n \frac{\exp(-r/r_n)}{r}$, which correctly captures the longest distance behavior of strong forces. Evaluating the integral, which is dominated by the longest-range contribution to the potential, yields:

$$\tilde{\delta}_L = -\frac{C_0\tilde{\mu}}{\tilde{k}} K_0(b_{\tilde{L}}/r_0) \,, \tag{4.37}$$

where the subscript 0 correspond to the longest range (or equivalently, the lightest intermediate particle) part of the potential. One can invert the relation to obtain the impact parameter:

$$b_{\tilde{l}} = \frac{r_0}{2} W\left(\frac{C^2\tilde{\mu}^2\pi}{\tilde{\delta}^2\tilde{k}^2}\right) \,, \tag{4.38}$$

where W is a Lambert function. As x gets large, $W(x) \to \log(x)$ with the relative corrections of order $\log(\log(x))/\log(x)$. The logarithmic nature of the Lambert function reflects the exponential suppression in the potential which dominates at long distances. At large $\tilde{L}$, the phase shifts become small making the logarithm dominated the by $\tilde{\delta}$. Recall, the goal is to determine the point where the full phase shift δ starts to be of order N_c^0—or equivalently $\tilde{\delta}$ begins to be of order $1/N_c$. For

now, label this point with the index 'cut'; $\tilde{\delta} = \delta_{\rm cut}/N_c$. Thus,

$$b_{\rm cut} = r_0 \log\left(\frac{N_c}{\delta_{\rm cut}}\right) \sim r_0 \log(N_c)\,, \tag{4.39}$$

with relative corrections of order N_c^0. It is apparent that any power law prefactor in front of Yukawa potential does not alter the leading behavior. Note that the precise value picked for $b_{\rm cut}$ is arbitrary but it will be shown below that the exact choice of $b_{\rm cut}$ does not affect the final result. The factor of N_c enters the calculation only through the desired value of the phase shift $\tilde{\delta}$. The range of the interaction r_0 standing in front is a consequence of the exponential which dominates the integral (4.36) at long distances. Note also that the equation (4.36) is linear in the potential. Thus, since the most general complex potential is of the form $V = V_{\rm Re} + iV_{\rm Im}$, the solution is the same for both the real and the imaginary part. The thing that is different for the real and the imaginary part is the value of the longest range of the potential, i.e. the values of $r_{0\,\rm Im}$, and $r_{0\,\rm Re}$.

Before proceeding to the final results, one needs to show that the formulas for the cross sections (4.34), and (4.35) are valid. Specifically, that the corrections to them are suppressed in the large N_c limit. In order to get a more quantitative insight, change the variables in the formula for the inelastic cross section (4.32) into an integral over $\tilde{\delta}$ (the analysis for the total cross section (4.33) would be exactly the same and therefore is not presented here).

$$\sigma^{\rm in} = \pi b_{IM}^2 + \frac{\pi}{\tilde{k}^2} \int\limits_0^{\delta_{\rm cut}/N_c} {\rm d}\tilde{\delta} \left(\frac{{\rm d}\tilde{l}^2}{{\rm d}\tilde{\delta}}\right) \left(1 - |S_l|^2\right)\,, \tag{4.40}$$

where the index 'cut' corresponds to the arbitrarily chosen point where phase shift δ is of order N_c^0, as was discussed more extensively above. Here, it shall be clear

that the arbitrariness in the choice of $\delta_{\rm cut}$ is exactly compensated by the integral in Eq. (4.40). The key observation is that the sensitivity to the particle's mass and to the strength of the potential are contained in the order N_c^0 correction terms to Eq. (4.39). This can be directly traced to Eq. (4.38), where all of these effects are in the argument of the Lambert function W where they are eventually suppressed by the smallness of $\tilde{\delta}$. Moreover, the sensitivity to the choice of the exact value of $\delta_{\rm cut}$ is also contained in the very same N_c^0 order corrections. Note also that the dependence on the choice of $\delta_{\rm cut}$ is compensated by the integral in Eq. (4.40). Since $\delta_{\rm cut}$ is an arbitrary parameter, on which the final result cannot depend, it follows that the integral in Eq. (4.40) must be of the same order as the $\delta_{\rm cut}$ correction coming from the determination of $b_{\rm Im}$, i.e. of order N_c^0. It straightforwardly follows then that the contribution of the integral in Eq. (4.40) to the cross section at large N_c is suppressed. To sum up, Eqs. (4.34), and (4.35) hold with corrections of the relative order $\log(\log(x))/\log(x)$ which follows from the asymptotic behavior of the Lambert function.

Finally, in order to evaluate the inelastic (4.34) and the total (4.35) cross section, the longest-range piece of the real and the imaginary part of the potential need to be identified. The longest range interaction is driven by the lightest particle available in the system, i.e. by the pions—$r_{0\,\rm Re} = 1/m_\pi$. One pion exchange, however, is not able to generate any inelasticity, as was more extensively discussed in the previous section. It was shown earlier that the non-zero contribution to the imaginary part of the potential emerges at the level of two-pion exchange. Thus

$r_{0\,\mathrm{Im}} = 1/(2m_\pi)$. Combining these with Eqs. (4.34), (4.35), and (4.39) gives:

$$\sigma_{\mathrm{in}} = \frac{\pi}{4m_\pi^2} \log^2(N_c)\,, \tag{4.41}$$

$$\sigma_{\mathrm{tot}} = \frac{2\pi}{m_\pi^2} \log^2(N_c)\,. \tag{4.42}$$

The formula for σ_{tot} is identical to the one derived in [58]. The ratio of the inelastic to the total cross section follows directly:

$$\frac{\sigma_{\mathrm{in}}}{\sigma_{\mathrm{tot}}} = \frac{1}{8}\,. \tag{4.43}$$

Note that this ratio does not depend on N_c at leading order.

Naturally, the question of the phenomenological relevance of the obtained formula arises since the real world does not correspond to $N_c = \infty$ but rather to $N_c = 3$. The total cross section predicted by the Eq. (4.42) is $\sigma_{\mathrm{tot}} \approx 150\,\mathrm{mb}$, which is 50% more than the recent observation from LHC [68] at $\sqrt{s} = 7\,\mathrm{TeV}$: $\sigma_{\mathrm{tot}}^{\mathrm{EXP}} \approx 100\,\mathrm{mb}$. Moreover, the total cross section at high energies is dominated by inelastic processes—at LHC, the ratio is approximately 3/4. It is in complete disagreement with Eq. (4.43), which predicts that the dominant portion of the total cross section is the elastic part—the fraction of the inelastic cross section is predicted to be 1/8. The obvious discrepancy between large N_c results and observations is, however, not that surprising. Formally, the relations (4.41 - 4.43) hold in the extreme large N_c limit, specifically for $\log(N_c) >> 1$, which is clearly not the case for $N_c = 3$. Regardless of the phenomenological (in)significance, the ability to calculate the total cross section as well as its inelastic component analytically is very interesting, at least from the point of view of theoretical analysis.

4.4 Summary

In this chapter, several arguments were presented suggesting that the logarithm of the elastic nucleon-nucleon scattering S-matrix element in any given partial wave (i.e. the phase shift) is proportional to N_c in the large N_c limit. None of the arguments are fully rigorous; however, when combined they give a rather compelling picture. The key feature underlying all the reasoning is the fact that the large N_c limit essentially leads to a semi-classical description of nuclear physics. From the scaling of the S-matrix, relations for the total cross section and the inelastic cross section were derived.

Bibliography

[1] G. 't Hooft, Nucl. Phys. B **72**, 461 (1974).

[2] E. Witten, Nucl. Phys. B **160**, 57 (1979).

[3] A. Armoni, M. Shifman and G. Veneziano, p. 353 in *Ian Kogan Memorial Collection: From Fields to Strings: Circumnavigating Theoretical Physics*, World Scientific, 2004.

[4] J.L. Gervais, B. Sakita, Phys. Rev. Lett. **52**, 87 (1984).

[5] J.L. Gervais, B. Sakita, Phys. Rev. D **30**, 1795 (1984).

[6] R.F. Dashen, A.V. Manohar, Phys. Lett. B **315**, 425 (1993).

[7] R.F. Dashen, A.V. Manohar, Phys. Lett. B **315**, 438 (1993).

[8] R.F. Dashen, E.E. Jenkins, A.V. Manohar, Phys. Rev. D **49**, 4713 (1994).

[9] R.F. Dashen, E.E. Jenkins, A.V. Manohar, Phys. Rev. D **51**, 3697 (1995).

[10] F.Gross, T.D. Cohen, E. Epelbaum, R. Machleidt, Few-Body Syst. **50**, 31 (2011).

[11] T.D. Cohen, V. Krejčiřík, JHEP **08**, 138 (2011).

[12] T.D. Cohen, V. Krejčiřík, J. Phys. G: Nucl. Part. Phys. **39**, 055001 (2012).

[13] R. Hagedorn, Nov. Cimen. Suppl. **3**, 147 (1965).

[14] R. Hagedorn, Nov. Cimen. **56A**, 1027 (1968).

[15] K. Huang, S. Weinberg, Phys. Rev. Lett. **25**, 895 (1970).

[16] N. Cabibbo, G. Parisi, Phys. Lett. B **59**, 67 (1975).

[17] T.D. Cohen, Phys. Lett. B **637**, 81 (2006).

[18] Standard result in string theory, see for example: Polchinski J., *String Theory*, Cambridge University Press, 1998.

[19] P. Braun-Munzinger, J. Stachel, Nucl. Phys. A **606**, 320 (1996).

[20] P. Braun-Munzinger, J. Stachel, arXiv:1101.3167[nucl-th] (2011).

[21] W. Broniowski, W. Florkowski, L.Y. Glozman, Phys. Rev. D **70**, 117503-1 (2004).

[22] K. R. Dienes, J.-R. Cudell, Phys. Rev. Lett. **72**, 187 (1994).

[23] W. Broniowski, W. Florkowski, Phys. Lett. B **490**, 223 (2000).

[24] K Nakamura and Particle Data Group 2010, J. Phys. G **37**, 075021 (2010).

[25] Standard result in lattice gauge theory, see for example: Rothe H. J., *Lattice Gauge Theories*, World Scientific Publishing, 2005.

[26] I.I. Kogan, A.R. Zhitnitsky, Nucl. Phys. B **465**, 99 (1996).

[27] B. Sundborg, Nucl. Phys. B **573**, 349 (2000).

[28] O. Aharony, J. Marsano, S. Minwalla, K. Papadodimas, M. van Raamsdonk, Adv. Theor. Math. Phys. **8**, 603 (2004).

[29] O. Aharony, J. Marsano, S. Minwalla, K. Papadodimas, M. van Raamsdonk, Phys. Rev. D **71**, 15018 (2005).

[30] D.J. Gross, Rev. Mod. Phys. **77**, 837 (2005); D. Politzer, Rev. Mod. Phys. **77**, 851 (2005); F. Wilczek, Rev. Mod. Phys. **77**, 857 (2005).

[31] F.J. Ernst, R.G. Sachs, Phys. Rev. **119**, 1105 (1960).

[32] T.D. Cohen, V. Krejčiřík, Phys. Rev. C **86**, 024003 (2012).

[33] T.H.R. Skyrme, Proc. Roy. Soc. Lond. A **260**, 127 (1961).

[34] G.S. Adkins, C.R. Nappi, E. Witten, Nucl. Phys. B **228**, 552 (1983).

[35] A. Pomarol, A. Wulzer, JHEP **03**, 051 (2008).

[36] A. Pomarol, A. Wulzer, Nucl. Phys. B **809**, 347 (2009).

[37] G. Panico, A. Wulzer, Nucl. Phys. A **825**, 91 (2009).

[38] T. Sakai, S. Sugimoto, Prog. Theor. Phys. **113**, 843 (2005).

[39] T. Sakai, S. Sugimoto, Prog. Theor. Phys. **114**, 1083 (2005).

[40] K. Nawa, H. Suganuma, T. Kojo, Phys. Rev. D **75**, 086003 (2007).

[41] H. Hata, T. Sakai, S. Sugimoto, S. Yamato, Prog. Theor. Phys. **117**, 1157 (2007).

[42] K. Hashimoto, T. Sakai, S. Sugimoto, Prog. Theor. Phys. **120**, 1093 (2008).

[43] K. Hashimoto, T. Sakai, S. Sugimoto, Prog. Theor. Phys. **122**, 427 (2009).

[44] T.D. Cohen, W. Broniowski, Phys. Lett. B **292**, 5 (1992).

[45] T.D. Cohen, Rev. Mod. Phys. **68**, 599 (1996).

[46] T.D. Cohen, Phys. Lett. B **359**, 23 (1995).

[47] G.S. Adkins, C.R. Nappi, Nucl. Phys. B **249**, 507 (1985).

[48] A. Cherman, T.D. Cohen, M. Nielsen, Phys. Rev. Lett. **103**, 022001 (2009).

[49] A. Cherman, T.Ishii, Phys. Rev. D **86**, 045011 (2012).

[50] T.D. Cohen, D.B. Leinweber, Comments Nucl. Part. Phys. **21**, 137 (1993).

[51] V. Bernard, N. Kaiser, U.G. Meißner, Int. J. Mod. Phys. E **4**, 193 (1995).

[52] E. Witten, Nucl. Phys. B **223**, 422 (1983).

[53] T.D. Cohen, V. Krejčiřík, arXiv:1308.6771[nucl-th] (2013)

[54] T.D. Cohen, V. Krejčiřík, in preparation.

[55] D.B. Kaplan, M.J. Savage, Phys. Lett. B **365**, 244 (1996).

[56] D.B. Kaplan, A.V. Manohar, Phys. Rev. C **56**, 76 (1997).

[57] T.D. Cohen, B.A. Gelman, Phys. Rev. C **85**, 024001 (2012).

[58] T.D. Cohen, Phys. Rev. Lett. **108**, 262301 (2012).

[59] J. Formánek, *Úvod do kvantové teorie I, II*, Academia, Prague, 2004.

[60] H. Yukawa, Proc. Phys. Math. Soc. Japan **17**, 48, (1935).

[61] R. Machleidt, Phys. Rev. C **63**, 024001 (2001).

[62] V.G.J. Stoks, R.A.M. Klomp, C.P.F. Terheggen, J.J. de Swart, Phys. Rev. C **49**, 2950 (1994).

[63] R.B. Wiringa, V.G.J. Stoks, R. Schiavilla, Phys. Rev. C **51**, 38 (1995).

[64] M.K. Banerjee, T.D. Cohen, B.A. Gelman, Phys. Rev. C **65**, 034011 (2002).

[65] A.V. Belitsky, T.D. Cohen, Phys. Rev. C **65**, 064008 (2002).

[66] T.D. Cohen, Phys. Rev. C **66**, 064003 (2002).

[67] L.D. Landau, E.M Lifshitz, *Quantum Mechanics: Non-relativistic Theory*, Butterworth-Heinemann, Wahington, DC, 1981.

[68] The TOTEM Collaboration et al, EPL **96**, 21002 (2011).